
# Quadrupole Mass Spectrometry under the Influence of Magnetic Field

Thesis submitted in accordance with the requirements of the

University of Liverpool for the degree of

**Doctor in Philosophy**

**by**

**Sarfaraz Uddin Ahmed Hashmi Syed**

Department of Electrical Engineering and Electronics

University of Liverpool

January 2012

# Abstract

A Quadrupole Mass Spectrometer (QMS) is an instrument for measuring concentrations of atoms and molecules by separating atomic and molecular ions according to their mass-to-charge ratios (*m/z*). It consists primarily of an ion source, quadrupole mass filter (QMF) and detector. Generally, QMF resolution can be improved by increasing the number of radio frequency (rf) cycles of the alternating electric field the ion experiences when passing through the mass filter. In order to improve the resolution, the dimensions of the QMF or the operating parameters are to be changed. However geometric modifications to improve performance increase the manufacturing cost and usually the size of the instrument. A low cost method to increase the resolution of a given QMS is the application of magnetic field to the mass filter.

The work is mainly concerned with the performance of a QMS under the influence of magnetic field. Significant improvement in QMS performance was obtained under certain magnetic field conditions, and these have been explained in terms of our theoretical model developed in the University of Liverpool. The theoretical approach assumed in the model is that the QMF contains hyperbolic rods as electrodes and that the magnetic field acts over the full length of the mass filter assembly. This model is capable of accurate simulation of spectra allowing the user to specify different values of mass spectrometer dimensions and applied input signals. The model has been upgraded for better sensitivity, and to simulate the QMF at very high number of rf cycles. Simulation and experimental results were presented for different conditions. This work also demonstrates the modeling of mass spectra of gases using the theoretical model for stability zones 1 and 3. The performance of QMF operating in

stability zones 1 and 3 has been derived and a relationship between maximum obtainable resolution and scan line is obtained.

# Contents

# List of Figures

# Acknowledgements

To start with, I would like to thank God for enabling me to carry out this project, nothing is possible without his will. Then, I would like to express my sincere gratitude to my supervisor **Prof. Stephen Taylor** for providing me with this project. I am grateful to him for his continuous guidance, invaluable advices, and encouragement during the course of this work. He has set before me a tremendous example of drive towards success, and by working under his supervision not only I have gained knowledge in context to research but also I have learned many important ethics of life. It has been a great privilege to work under him.

Thanks to my colleagues from the research group **Dr. Boris Brkic**, **Dr. Neil France** and **Dr. Jeyan Sreekumar** for their whole hearted support and for sharing their PhD experiences with me. Many thanks to **Mrs. Farnoush Salarzaei** and **Mr. Simon Maher** for providing with constructive comments and supplying me with necessary information when needed. Also, thanks to **Mr. Stamatios Giannoukos** for motivation and helpful comments. Big thanks to **Dr. J R Gibson** and **Mr. Thomas Hogan**, for providing me with useful documentation and technical assistance in learning QMS software. I would also like to thank **Dr. Vladimir Leus** for sparing his valuable time, interest, insightful queries, constructive criticism and helpful comments during the course of this project.

I must not forget my friends who made my life sociable, enjoyable and for giving me support whenever needed. **Jai**, **Hassan**, **EzzAldeen**, **Nassim**, **Razzaq**, **Mubeen**, **Imran**, **Ahmed**, **Ibrahim** and all other friends thanks a lot for all the fun and the enjoyment. I thank, from the bottom of my heart, to my sisters **Maimuna** and **Sabrina**, to my brother **Layees**,

and to my lovely friend **Qudsia** for their continual support, love and for all the good times. Also, thanks to my uncle **Mr. M A Hakeem** for his advices and care.

Finally, I would like to thank my father **Mr. Kaleem Syed** and my mother **Mrs. A K Farzana** for their love, support and guidance throughout all my pursuits.

**Sarfaraz Syed**

**Liverpool University**

**January 2012**

# Nomenclature

| | |
|---|---|
| APCI | Atmospheric pressure chemical ionization |
| $a$ | Stability parameter |
| B | Magnetic field intensity expressed in Tesla |
| C | A fixed potential applied to all of the electrodes so as to float the device |
| CI | Chemical ionisation |
| CIT | Cylindrical ion trap |
| DART | Direct analysis in real time |
| dc, DC | Direct current |
| DIOS | Desorption/ionisation on silicon |
| EI | Electron ionisation |
| ESI | Electrospray ionisation |
| $E_z$ | Ion injection energy expressed in $eV$ |
| F | Force acting upon an ion |
| $f$ | Frequency expressed in Hz |
| GUI | Graphical user interface |
| ICR | Ion cyclotron resonance |
| $l$ | Length of the mass filter expressed in mm |
| MALDI | Matrix-assisted laser desorption ionisation |
| MS | Mass spectrometry |
| m, M | Mass of the ion |
| $m/z$ | Mass to charge ratio |
| N | Number of rf cycles experience by the ions in the mass filter |
| QIT | Quadrupole ion trap |
| QMF | Quadrupole mass filter |
| QMS | Quadrupole mass spectrometer |
| $r$ | Electrode/rod radius expressed in mm |
| $r_0$ | Field Radius expressed in mm |
| $q$ | Stability parameter |
| RGA | Residual gas analyzer |
| rf, RF | Radio frequency |
| SIMS | Secondary ion mass spectrometry |

| | |
|---|---|
| $t$ | Time expressed in seconds |
| $U$ | Amplitude of dc supply voltage |
| $u$ | Atomic mass unit |
| $V$ | Amplitude of rf supply voltage |
| $v$ | Velocity of an ion |
| $\omega$ | Angular frequency expressed in radius per second |
| $\Delta M$ | Width of the mass peak measured at 10% of its height |
| $\lambda, \sigma, \gamma$ | Weighting constants for the $x$, $y$ and $z$ coordinates respectively |
| $\xi$ | A dimensionless parameter equal to $\omega t/2$ |

# Chapter 1

# Introduction

## 1.1 Background

"I have described at some length the application of Positive Rays to chemical analysis; one of the main reasons for writing this book was the hope that it might induce others, and especially chemists, to try this method of analysis. I feel sure that there are many problems in Chemistry which could be solved with far greater ease by this than by any other method. The method is surprisingly sensitive - more so even than that of Spectrum Analysis, requires an infinitesimal amount of material, and does not require this to be specially purified:.....", thus expounds J. J. Thomson, the father of the mass spectrometry field in 1913, in his book titled *Rays of positive electricity and their application to chemical analyses* [1].

Decades later, the use of mass spectrometry (MS) has flourished in both industry and for research, with applications ranging from analysis of simple residual gas mixtures to that of complex organic materials. All these form an imposing testimony to the value of this technique [2, 3]. Mass spectrometry is an analytical technique which is used to measure atomic and/or molecular mass and relative composition based on the ionic mass-to-charge ratio. Attributes such as versatility, low-cost, accuracy and mass range have ensured its widespread use. One example, due to the virtues of MS sensitivity and speed, is that it plays a prominent role in many stages of drug discovery [4].

One of the biggest advantages of mass spectrometry is that it is independent of the atomic constitution of the substances being analyzed. This is provided that the substances can be ionised and the mass spectrometer system is configured for the particular mass range under consideration. There are also many other fascinating applications of mass spectrometry such as mass spectrometry-based proteomics; which includes study of protein-protein interactions, mapping of numerous organelles, the concurrent description of the malaria parasite genome and proteome etc [5]. As a result of its enormous utility, it can be said that mass spectrometry will offer many potential applications which have yet to be explored.

## 1.2 Objective and motivation

Of the many different types of mass spectrometer a key instrument is the quadrupole mass spectrometer. First described by W. Paul and H. Steinwedel at the University of Bonn (Germany) in 1953 [6], the linear quadrupole originally developed for mass spectrometry, is now used in many areas as a mass filter, an ion trap, or an ion guide [7].

The performance of a QMS depends on many factors such as sensitivity of the ion source, geometry of the mass filter, the efficiency of the detector. Figure 1.1 shows the physical arrangement of quadrupole mass filter. It may be characterised by two operating properties: the mass range and the resolution [8]. These are dependent upon six basic parameters:

i. length ($l$) of the QMF electrodes
ii. the shortest distance between the electrodes ($2r_0$)
iii. the maximum direct current (dc) supply voltage to the electrodes ($U$)

iv. the radio frequency (rf) supply voltage (*V*) to the electrodes

v. the frequency (*f*) of the rf voltage applied to electrodes

vi. the ion injection energy (*Ez*) into the mass filter

The inter dependence of mass range and resolution to these fundamental instrument parameters is shown in Figure 1.2. The mass range or rather the maximum mass $M_m$ for which an instrument can be tuned is calculated by:

$$M_m = \frac{7\times10^6 V}{f^2 r_0^2} \tag{1.1}$$

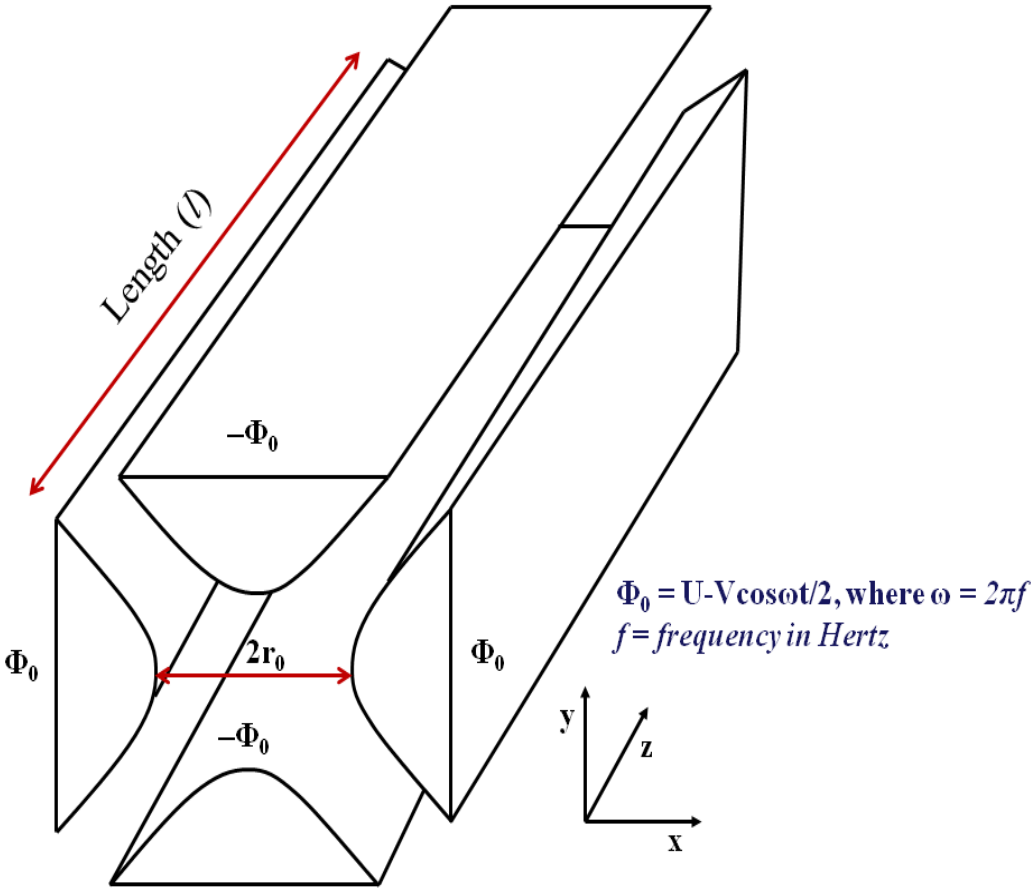


Figure 1.1: Physical arrangement of a quadrupole mass filter.

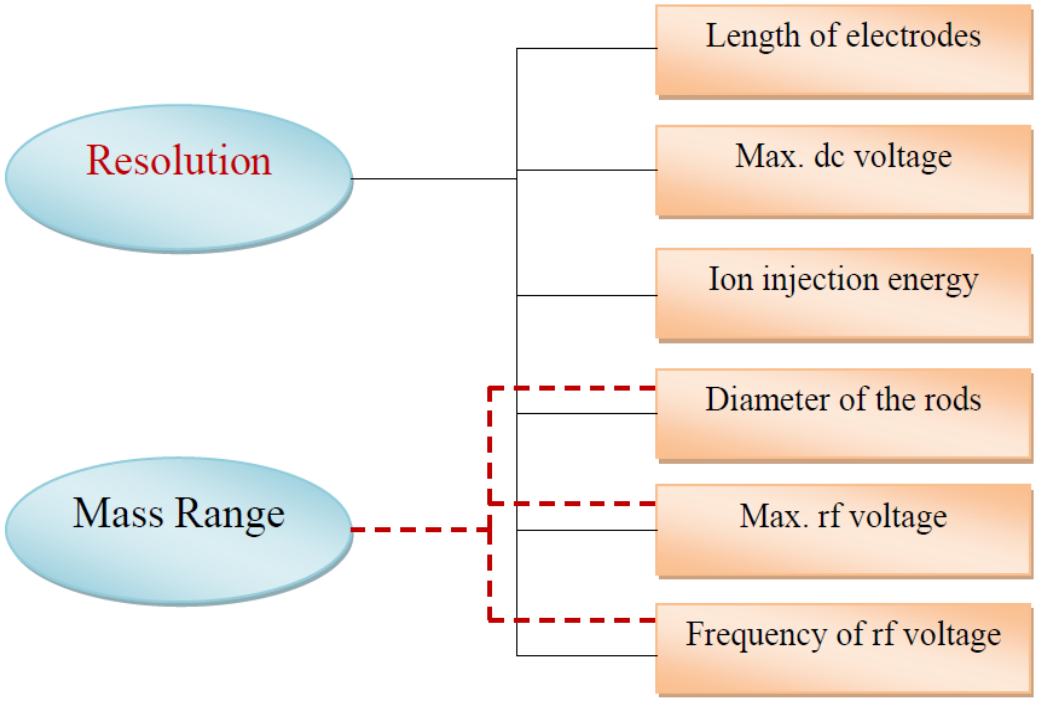


Figure 1.2: Inter relationship of resolution and mass range to instrument parameters.

High resolution QMF is of vital importance in most of the application areas, including process monitoring, especially if two different gases have to be detected with a similar mass number (e.g. CO and $N_2$) or for analysis of low mass isotopes ( e.g. HT and $D_2$ ) [9]. Generally, from the mass spectrum obtained the resolution $R$ can be found by using the equation:

$$R = \frac{M}{\Delta M} \tag{1.2}$$

where $M$ is the mass of the given spectral peak and $\Delta M$ is the width of the mass peak measured at 10% of its height. It is well known that the resolution limit is governed by the

number (*N*) of rf cycles the ion experiences [8]. A good representation of the relationship between resolution (*M/ΔM)* and number of rf cycles is given by:

$$\frac{M}{\Delta M} = \frac{1}{K} N^n \tag{1.3}$$

where *n* is either exactly or closely equal to 2 and *K* is a constant which may be assumed to be 20 for all practical purposes [8, chapter 6]. The precise value of *K* depends on the method used to define $\Delta M$ and inscribed field radius $r_0$ [10]. Given that $N = ft$ where *t* is the time that the ion spends in the quadrupole field, then the relationship between number *N* of rf cycles and the fundamental instrument parameters is given by:

$$N = (f \times l)/\sqrt{(\frac{2eEz}{m})} \tag{1.4}$$

where e is the ionic charge and *m* is the mass.

In order to improve the resolution, the dimensions of the QMF or the operating parameters are to be changed, and this will normally increase the manufacturing cost and usually the size of the instrument. An alternative and cost effective method to increase the resolution of a given QMF is the application of magnetic field to the mass filter, and is the motivation behind this study. Previously, very little work has been done in relation to the application of magnetic field to the QMF. For stability zone 1, Tunstall *et al* found experimentally that the application of static magnetic field to the mass filter of QMS increases the resolution by reducing the long tail on low mass side of the mass spectra [11].

Later work showed the effect of static transverse magnetic field on ion trajectories and resolution [12].

The aim of this project is to study the performance of QMS under the influence of magnetic field for operation in the Mathieu stability zone 1 and zone 3. The effect of magnetic field in both the axial and transverse directions is explained in detail in terms of the theoretical model. Simulation and experimental results are presented for each of the different operating conditions. This work is also concerned with the study of factors influencing the resolution of the QMF operating in Mathieu stability zones 1 and 3.

### 1.3 Outline of the thesis

The structure of the thesis is as follows: Chapter 2 gives a literature review of the advances made in the field of mass spectrometry since construction of the first instrument; it was first constructed by J. J. Thomson in 1913, (called then: 'a parabola spectrograph') [1]. Chapter 2 also includes a review of the work undertaken by different researchers to study the performance and behaviour of the QMS using numerical simulation techniques.

Chapter 3 gives the general explanation of the action of mass spectrometry and the effect of individual component parts. Chapter 3 also explains in detail the description of the QMF and its theory of operation.

Chapter 4 gives a detailed description of the simulation software used in this work. It also presents the information regarding the features incorporated in the software and how the

results are processed, and what alterations has been made to software to undertake the simulations reported.

Chapter 5 considers the case of a QMS operating in stability zone 1 under the influence of magnetic field. It also describes for which values of operating parameters an enhancement of the instrument resolution is achieved when magnetic field is applied in either axial or transverse direction, where possible experimental and simulation results are presented.

Chapter 6 gives the detail of the behaviour of a QMS in the third stability zone with magnetic field applied. The work presented in the chapter also presents an ultra high resolution QMF for identification of low mass isotopes via application of a transverse magnetic field, which are not achievable using present day commercially available instruments.

Chapter 7 describes QMS simulation techniques for design and performance of a QMF for operation in stability zones 1 and 3. The investigation considers the factors which limit the maximum resolution ($\boldsymbol{R_{max}}$) for a particular value of scan line that can be obtained for a given QMF.

The thesis will conclude with chapter 8, which also presents the future work to be done.

## References


1. Thomson, J .J. *Rays of positive electricity and their application to chemical analyses*, Longmans green and co. 1913.
2. Reynolds, J. H. High sensitivity mass spectrometer for noble gas analysis. *Review of Scientific Instruments*. 1956. 11. 928-934.
3. VanLear, G.E; McLafferty, F.W. Biomedical aspects of high-resolution mass spectrometry. *Annual Review of Biochemistry*. 1969, 38, 289-322.
4. Glish, G.L.; Vachet, R.W. The basics of mass spectrometry in the twenty-first century. *Nature*. 2003, 2, 140-150.
5. Aebersold, R.; Mann, M. Mass spectrometry-based proteomics. *Nature*, 2003, 422, 198-207.
6. Paul, W.; Raether, M. Das elektrische massenfilter. *Zeitschrift fur Physik*. 1955. *40*, 262-273.
7. Douglas, D.J. Linear quadrupoles in mass spectrometry. *Mass Spectrometry Reviews*. 2009, *28*, 937-960.
8. Dawson, P.H. *Quadrupole mass spectrometry and its applications*, Elsevier: Amsterdam 1976.
9. Sreekumar, J.; Hogan, T.J.; Taylor, S.; Turner, P.; Knott, C. A Quadrupole Mass Spectrometer for Resolution of Low Mass Isotopes. *J. Am. Soc. Mass Spectrom.* 2010, *21*, 1364–1370.
10. Holme, A.E.; Thatcher, W.J.; Leck, J.H. An investigation of the factors determining maximum resolution in a quadrupole mass spectrometer. *Journal of Physics* ***E:*** *Scientific Instruments.* 1972, *5*, 429-433.

11. Tunstall, J.J.; Taylor, S.; Vourdas, A.; Leck, J.H.; Batey, J. Application of static magnetic field to the mass filter of a quadrupole mass spectrometer. *Vacuum*, 1999, *53*, 211-213.
12. Srigengan, B.; Gibson, J.R.; Taylor, S. Ion trajectories in quadrupole mass spectrometer with a static transverse magnetic field applied to mass filter. *IEE Proc-Sci. Meas. Technol*. 2000, 147 (6), 2000, 274-278.

# Chapter 2

## Literature Review

First constructed by J. J. Thomson in 1913, a mass spectrometer (then called a parabola spectrograph) [1], is used to separate ions by their different parabolic trajectories in electromagnetic fields. Ions are detected upon striking a fluorescent screen or photographic plate. Figure 2.1 shows J. J. Thomson and a cathode ray tube used to perform some of the first *m/z* measurements; as seen from it, deflection of the electrons was observed once the electric field was turned on.

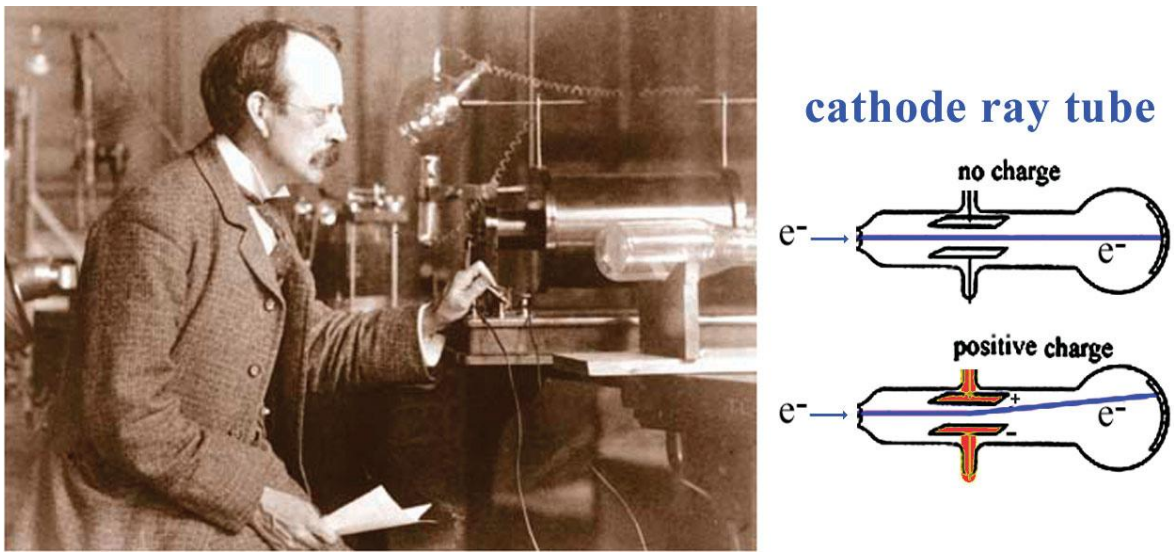


Figure 2.1: J. J. Thomson and a cathode ray tube used to perform some of the first *m/z* measurements. Deflection of the electron was observed once the electric field was turned on, diagram taken from [4].

Later, Thomson's protégé, Francis W. Aston designed a mass spectrometer with resolution improved by an order of magnitude, allowing applications to isotopic analysis [2]. At the same time, A. J. Dempster also improved the resolution with a magnetic analyzer and developed the first electron impact source, which ionises volatilized molecules with a beam of electrons [3]. Thomson, Aston, and Dempster provided a strong foundation for MS instrument design and theory for those who followed to develop instruments capable of meeting the demands of chemists and biologists. One of the crucial issues, particularly for chemists was the need of an instrument with improved accuracy for the analysis of elements and small organic molecules [4]. This question led to the development of four different types of MS intrument: magnetic sector double focusing [5], time-of-flight (TOF) [6], quadrupole [7], and Fourier transform ion cyclotron resonance (FT-ICR) [8] mass analyzers.

Nier at the University of Minnesota developed the high-mass-resolution double-focusing instrument during World War 2 to perform isotopic analysis and separate $^{235}U$ from $^{238}U$. This played a major role in the development of the first nuclear bomb [5]. Applications such as this generated tremendous interest, resulting in further development of new kinds of mass spectrometers in the years to follow. Moreover, mass spectrometry as a microanalytical technique was able to obtain characteristic information of the analytes. In the mass spectrometric process some form of energy is transferred to the analyte molecules to effect ionisation. If an electron ionisation technique is used as an ion source, the molecular ions of the analyte are converted into a variety of lower mass fragment ions. The resulting fragmentation pattern together with residual molecular ions results in a mass spectrum which can be used as a "finger print" to characterize the analyte [9]. In this way the application of mass spectrometers became wide spread in the study of kinetic reactions, biological analysis, drug analysis [10], biochemistry [11, 12, and 13], explosives, and other industrial

applications, particularly in the petroleum industry. There are also medical applications like the detection of urea breath test for the Helicobacter pylori [14, 15, 16, and 17].

The use of a quadrupole field for MS dates back to the pioneering work of Wolfgang Paul and co-workers in the 1950's [18], and is widely used as a mass filter in a QMS, an ion guide or a linear ion trap [19]. Since then much research has been undertaken by different researchers to study the performance and behaviour of the QMS by either experimental methods or by numerical simulation techniques. In 1962, Von Zahn, a member of the Paul group constructed a mass filter of 5.82 m in length and reported a resolution of the order of 16000, for high-precision mass measurements [20]. Brubaker and Tull, investigated the transmission efficiency and resolution of a QMF as a function of ion source exit aperture and frequency of excitation; the ion source exit aperture defines the area of illumination of the QMF and is usually a fraction of the inscribed QMF field radius ($r_0$) [21]. It was concluded that higher resolution is obtained with small aperture size and higher frequency.

Some workers constructed a simple mass spectrometer; the electrodes used were shaped by hand from a coarse stainless steel mesh [22]. Despite the inaccurate shape of the electrodes, the mass spectrometer was reported to have a resolution of 75 measured at 50% peak height. The device is a three dimensional quadrupole, or ion trap type of mass spectrometer. In 1971, Holme *et al* performed a series of experiments to investigate the factors which determine the resolution of a QMF under normal operating conditions [23]. During this same period some workers designed an rf quadrupole mass spectrometer for the study of positive or negative ions in flames burning at atmospheric pressure [24]. Richards *et al* described a new operating mode for the QMF by using a rectangular time varying function applied to the electrodes for excitation other than the commonly used combined dc and rf

signals [25]. It was shown that when such a time varying potential function is chosen the device is freed of some of the technological limitations which hamper its usefulness in high precision applications; and the need to maintain the *U/V* ratio constant is replaced by the requirement of keeping timing parameters steady, making the latter technologically simpler. However, rectangular time varying functions when chosen reduces the sensitivity of the QMS dramatically when compared to sinusoidal waveforms [26]. For this reason sinusoidal waveforms are still preferred over rectangular time varying functions.

Other workers designed a small analytical QMS to meet the requirements of an analytical instrument for use in high and ultra high vacuum systems [27]. It was shown that the performance of the QMS was adequate for the measurement of partial pressures down to and below $10^{-11}$ torr; and was achieved with constant sensitivity over the range 0-200 *amu* with a resolution adequate to separate completely individual peaks up to 50 *amu.* Later Lefaivre and Marmet showed that the absolute transmission of QMF is improved when ions are bunched and injected at the proper phase into the instrument [28]. In 1976, Wittmaack successfully used a quadrupole mass spectrometer for the operation of scanning ion microscope by combining an ion microprobe with the quadrupole equipped secondary ion mass spectrometer. It was reported that by operating the microprobe in raster scanning mode, ion images with a lateral resolution of about 10 μ could be obtained [29]. Dylla and Jarrell showed experimentally that by using an entrance aperture which spatially separates the rf and direct current (dc) fringe fields in a QMF, transmission-resolution characteristics can be improved [30].

Dawson used linear algebra (matrix) methods to calculate ion transmission for various scan lines and various apertures both with and without fringing fields, based on maximum ion

displacements for mass filters [31]. In later research (1976) the design and performance of the mass filter is described in detail, and it was mentioned that resolution can be represented by $\mathbf{R} = N^n/K$, where *n* is either or exactly equal to 2 and *K* is a constant which is assumed to be 20 for all practical purposes [32]. In 1977, Magee *et al* described a quadrupole-based secondary ion mass spectrometer for depth profiling which combines ultrahigh vacuum construction with high sputtering rate, detection sensitivity, depth resolution, mass spectral purity, and abundance sensitivity [33]. It was reported that impurities such as B and Al implanted in Si can be profiled to levels below one part per million atomic (ppma).

Mao and Leck described in detail the characteristics of the quadrupole mass filter designed for use as a residual gas analyzer (RGA) in vacuum systems [34]. It was suggested that the QMS system should be small, inexpensive and simple to operate. Quantitative data can be obtained using a QMS provided care is taken in operation, in particular, in setting-up appropriate calibration facilities for each application. In 1991, Hiroki *et al* performed separation of helium and deuterium peaks with a quadrupole mass spectrometer by using the second stability zone in the Mathieu diagram [35]. A resolution of 320 measured at 50% peak height was reported. In 1995, some workers used membrane inlet mass spectrometry for the continuous measurement of gases and volatiles in the headspace gas of fermenters and for components dissolved in the fermentation liquid [36]. During the same period some workers have successfully performed quadupole mass spectrometry using ion traps. In U.S. Patent 5,420,425 [37], the Thermo Finnigan linear ion trap (LIT) was described by Schwartz and co-workers as a two-dimensional mass spectrometer in which mass-selective ion ejection from the LIT occurs radially [38]. Later the MDS SCIEX LIT mass spectrometer was disclosed in 2001 in a U.S. patent 6,177,668 [39]. Hager described the LIT as a new method for confinement of ions and to mass selective ion ejection. In the MDS SCIEX LIT instrument,

trapped ions are axially mass selectively ejected by taking advantage of the mixing of degrees of freedom induced by fringing fields and other anti-harmonics in the vicinity of the end lens [40]. Later, Patterson *et al* reported a miniature cylindrical ion trap (CIT) mass spectrometer, which is of great interest because it can be used outside the laboratory [41]. In 2005, the rectilinear ion trap (RIT) was first disclosed publicly in U.S. patent 6,838,666 [42]. Ouyang and his team described the ion trap mass spectrometer as a totally new ion trap with rectilinear geometry and high trapping capacity. It can be operated to provide the mass analysis in mass-selective stability mode as well as mass-selective instability mode. In addition, arrays of multiple ion traps allow combination of multiple gas phase processes to be applied to the trapped ions to achieve high sensitivity and selectivity. In 2009, Brkic *et al* presented a prototype design of a quadrupole mass filter with hyperbolic electrodes fabricated using digital light processing, a low cost and light weight 3D rapid prototyping technology [43].

There have been many analytical predictions of the behaviour of QMS. In 1987, Batey presented a detailed review of quadrupole gas analyzers and showed that some features of the behaviour of the QMS could be predicted by tracing the motion of ion through the mass filter [44]. Later in 1993, Konenkov investigated the influence of fringing fields on the acceptance of a QMF in the separation mode of the intermediate stability region [45]. Other workers presented a powerful numerical method which can be adequately used for mass independent optimization of the performance of the quadrupole pre-filters [46]. It was reported that in the numerical method neither the effects of fringe fields nor those of initial transverse velocities were taken into consideration, however it was shown that a good agreement with the measured transmission data was obtained. Muntean used the matrix method to develop a computer simulation program to model ion transmission through the

filter by calculating ion trajectories in rf only quadrupoles [47]. More examples of such types of analytical work include the modeling of ion transmission through the filter by calculating ion trajectories in exactly determined hyperbolic quadrupole fields [48]; the effects of rf frequency, phase and magnitude on the performance of QMS [49]; and the effects of initial ion energy and quadrupole electrode length on transmission percentage of ions through the mass filter along with the effects of aperture parameters [26].

Titov used numerical simulation techniques to study in detail the ion separation in imperfect fields of the QMF, by taking various aspects into consideration [50, 51, 52, and 53] and verified the predictions experimentally [54]. Later work provided a detailed study of QMF operating within first, second and third stability zones [55]. Tunstall *et al* described the development of a computer program designed to simulate the performance of the mass filter in an ideal QMS. Their simulation program provides flexible input parameters to allow the user to investigate the ion trajectories and transmission efficiency for different operating conditions. It operates by solving the Mathieu equation in two dimensions using a 4th-order Runge–Kutta iteration routine [56]. Gibson and Taylor have also developed computational methods to determine the trajectories of large number of ions in the QMS; their computer program generates large number of ions (at least $10^5$ ions injected into the quadrupole model at each point on the mass scale) thus providing a detailed computer simulation for both hyperbolic and circular rods [57, 58]. Du *et al* theoretically modeled peak structures for a QMF operating in zone 3 [59]; it was suggested that to improve the peak structures changes in ion inlet optics or changes to ion detection geometry are required. Douglas *et al* examined the effect of displacement of QMF electrodes with circular rods on spatial harmonics, and it was concluded that the data can be useful in designing quadrupole mass filters [60]. Later, Douglas and Konenkov have used numerical calculations to investigate the influence of

electrode radius $r$ to field radius $r_0$ which is referred to as $(r / r_0)$ on the peak shape for a linear QMF constructed with round electrodes [61]. Some workers have used commercially available software tools, such as SIMION 3D, to compute field conditions and ion trajectories of a commercial QMS with a number of imperfections, as compared to ideal hyperbolic geometry [62]. Other workers have used computer simulation of ion motion in a QMS to examine the effect of ion entry acceptance conditions on the performance of a quadrupole mass spectrometer operated in upper and lower stability regions [63].

Hogan and Taylor performed computer simulation with a large number of ions ($10^8$) to investigate the operation of QMF in first and third stability zones, and it was concluded that QMF operation in zone 3 of the Matthieu stability diagram provides an improved immunity from the effects of the variation in the value of $(r / r_0)$ compared to zone 1 [64]. Later work showed the effect of mechanical tolerances on QMF performance for operation in zone 3 [65]. Some workers have performed elemental analysis with quadrupole mass filters operated in higher stability regions, and it was concluded that there is an increase in resolution when QMF is operated in higher stability regions [66]. Sreekumar *et al* performed simulations with a large number of ions ($>10^7$) to determine the required resolution for the qualitative and quantitative identification of low mass isotopes in the mass range 1-6 *amu* [67]. More recently, Ahn and Park provided with computer simulations of electron and ion trajectories in electron-impact ion sources of a QMS; and it was shown that computer simulation of electron and ion trajectories can be utilized for the characterization and optimization of the electron-impact ion source [68].

Magnetic fields have long been used in quadrupole ion sources, magnetic sector instruments [69], and in ion traps [70] to increase the performance or the resolution.

However, surprisingly little work has been done in relation to the application of magnetic field to the QMS mass filters to increase the resolution. This aspect is a key feature of the work of this thesis.

**References**


1. Thomson, J .J. *Rays of positive electricity and their application to chemical analyses*, Longmans green and co. 1913.
2. Aston, F.W. *Isotopes*, Arnold, London. 1922.
3. Dempster, A.J. *A new method of positive ray analysis*. Physical Review. 1918, *11(4)*, 316–325.
4. Borman, S; Russell, H; Siuzdak, G. Mass spec timeline. *Chemistry chronicles*. 2003, 47-49.
5. Nier, A. O. Nat. Bur. Stand. Circ. (U.S.). 1953,*522*, 29–36.
6. Wiley, W.C.; McLaren, I.H. Time-of-flight mass spectrometer with improved resolution. *The review of scientific instruments*, 1955, *26*, 1150-1157,
7. Paul, W.; Reinhard, H.P.;Von, Z.U. Das elektrische massenfilter asl massenspektrometer and isotopentrenner. *Z Phys*. 1958, *152*, 143-182.
8. Cumisarow, M.B.; Marshall, A.G. Fourier transform ion cyclotron resonance spectroscopy. *Chemical physics letters*, 1974, *25(2)*, 282-283,
9. Herbert, C.G; Johnstone, R.A. *Mass spectrometry basics*. Boca Raton; London, CRC Press (c2003).
10. Glish, G.L; Vachet, R.W. The basics of mass spectrometry in the twenty-first century. *Nature*, 2003, *2*, 140-150.

11. Doherty, A.J.; Ashford, S.R.; Subramanya, H.S.; Wigley, D.B. Bacteriophage t7 dna ligase. Overexpression, purification, crystallization, and characterization. *Journal of Biological Chemistry* 1996, *271(19),* 11,083–11,089.
12. Rose, M.; Johnstone, R.A.W. *Mass spectrometry for chemists and biochemists*. Cambridge University Press, Cambridge. 1982.
13. Siuzdak, G. *Mass spectrometry for biotechnology*. Academic Press, San Diego. 1996.
14. Dooley, C.P.; Cohen, H.; Fitzgibbons, P.L.; Bauer, M.; Appleman, M.D.; Perez-Perez, G.I.; Blaser, M.J. Prevalence of helicobacter pylori infection and histologic gastritis in asymptomatic persons. *New England Journal of Medicine.* 1989, *321(23),* 1562–1566.
15. Nachamkin, I.; Skirrow, M.B. Campylobacter, arcobacter and helicobacter. Systematic Bacteriology 9th Ed. *2*. 1998.
16. Peterson, W.L. Helicobacter pylori and peptic ulcer disease. *New England Journal of Medicine 324(15),* 1043–1048. 1991.
17. Versalovic, J.; Fox, J.G. Helicobacter. *Manual of Clinical Microbiology*. 1999, 727–738.
18. Paul, W.; Raether, M. Das elektrische massenfilter. *Zeitschrift fur Physik*. 1955. *40*, 262-273.
19. Douglas, D.J. Linear quadrupoles in mass spectrometry. *Mass Spectrometry Reviews*. 2009, *28*, 937-960.
20. Von Zahn, U. Prazisions-massenbestimmungen mit dem elekrischen massenfilter. *Zeitschrift fur Physik.* 1962. *168*, 129-142.
21. Brubaker, W.M.; Tuul, J. Performance studies of a quadrupole mass filter. *The review of scientific instruments*. 1964. *35 (8)*, 1007-1010.

22. Dawson, P.H.; Hedman, J.W.; Whetten, R.N. A simple mass spectrometer. *The review of scientific instruments*. 1969. *40 (11),* 1444-1450.
23. Holme, A.E.; Thatcher, W.J.; Leck, J.H. An investigation of the factors determining maximum resolution in a quadrupole mass spectrometer. *Journal of Physics E: Scientific Instruments.* 1972. *5*, 429-433.
24. Hayhurst, A.N.; Mitchell, F.G.R.; Telford, N.R. A quadrupole mass spectrometer designed for flame ionization studies. *International Journal of Mass Spectrometry and Ion Physics*. 1971. 7, 177-187.
25. Richards, J.A.; Huey, R.A; Hiller, J. A new operating mode for the quadrupole mass filter. *International Journal of Mass Spectrometry and Ion Physics*. 1973. 12, 317-339.
26. Voo, A.C.C; Ng, R.; Tunstall, J.J.; Taylor, S. Transmission through the quadrupole mass filter: The effect of aperture and harmonics. *J. Vac. Sci. Technol. A.* 1997, *15 (4),* 2276-2281.
27. Holme, A.E.; Thatcher, W.J.; Leck, J.H. A small analytical quadrupole mass spectrometer designed for operation in high and ultra high vacuum systems. *Vacuum.* 1973, 7-11.
28. Lefaivre, D.; Marmet, P. Optimizing ion injection phase in quadrupole mass filters. *Rev. Sci. Instrum.* 1974. 45 (9), 1134-1137.
29. Wittmaack, K. Successful operation of a scanning ion microscope with quadrupole mass filter. *Rev. Sci. Instrum.* 1976. 47 (1), 157-158.
30. Dylla, H.F.; Jarrell, J.A. Transmission-resolution curves for a quadrupole mass spectrometer with separated rf and dc fields in the entrance aperture. *Rev. Sci. Instrum.* 1976. *47 (3),* 331-333.

31. Dawson, P.H. A detailed study of quadrupole mass filter. *International Journal of Mass Spectrometry and Ion Physics*. 1974, *14*, 317-337.
32. Dawson, P.H. *Quadrupole mass spectrometry and its applications*, Elsevier: Amsterdam, 1976.
33. Magee, C.W.; Harrington, W.L; Hoing, R.E. Secondary ion quadrupole mass spectrometer for depth profiling-design and performance evaluation, *Rev. Sci. Instrum*. 1978, *49 (4)*, 477-485.
34. Mao, F.M; Leck, J.H. The quadrupole mass spectrometer in practical operation. *Vacuum.* 1987, *37(8)*, 669-675.
35. Hiroki, S.; Abe, T.; Murakami, Y. Separation of Helium and Deuterium Peaks with a Quadrupole Mass Spectrometer by Using the Second Stability Zone in the Mathieu Diagram. *Rev. Sci. Instrum.* 1992, *63*(8), 83874–3876.
36. Bohatka, S.; Futo, I.; Gal, I.; Gal, J.; Langer, G.; Molnar, J.; Paal. A.; Pinter, G.; Simon, M.; Szekely, Z.; Szilagyi, J.; Quadrupole mass spectrometer system for fermentation monitoring. *Vacuum*. 1993, *44 (4-7)*, 669-671.
37. Schwartz, J.C.; Senko, M.W.; Syka, J.E.P. U. S. Patent 5,420,425, 1995.
38. Schwartz, J.C.; Senko, M.W.; Syka, J.E.P. A two-dimensional quadrupole ion trap mass spectrometer. *J Am Soc Mass Spectrom*. 2002, *13*, 659–669.
39. Hager, J.W. U. S. Patent 6,177,668, 2001.
40. Hager, J.W. A new linear ion trap mass spectrometer. *Rapid Commun. Mass Spectrom*. 2002, *16*, 512-526.
41. Patterson, G. E.; Guymon,A. J.; Riter, L. S.; Everly, M; Griep-Raming, J.; Laughlin, B. C.; Ouyang, Z.; Cooks, R. G. Miniature cylindrical ion trap mass spectromete, *Anal. Chem., Vol. 74, no. 24*, 6145-6153, 2002.
42. Ouyang, Z.; Cooks, R.G.; U. S. Patent 6,838,666, 2005.

43. Brkic, B.; France, N.; Clare, A.T.; Sutcliffe, C.J.; Chalker, P.R.; Taylor, S. Development of quadrupole mass spectrometry using rapid prototyping technology. *J Am Soc Mass Spectrom*. 2009. *20*, 1359-1365.
44. Batey, J.H. Quadrupole gas analyzers. *Vacuum*. 1987, *37*, 659-668.
45. Konenkov, N. V. Influence of fringing fields on the acceptance of a quadrupole mass filter in the separation mode of the intermediate stability region. *Internation Journal of Mass Spectrometry and Ion Processes. 123*. 101-105. 1993.
46. Trajber, C.; Simon, M.; Bohatka, S.; Futo, I. A mass independent pre-filter arrangement for quadrupole mass spectrometer. *Vacuum*. 1993, *44 (4-7)*, 653-656.
47. Muntean, F. Transmission study for r.f – only quadrupoles by computer simulations. *International Journal of Mass Spectrometry and Ion Processes*, 1995, *151*, 197-206.
48. Reuben, A.J.; Smith, G.B.; Moses, P.; Vagov, A.V.; Woods, M.D.; Gordon, D.B.; Munn, R.W. Ion trajectories in exactly determined quadrupole fields. *International Journal of Mass Spectrometry and Ion Processes*. 1996, *154*, 43-59.
49. Ma, F.M.; Taylor, S. Simulation of ion trajectories through the mass filter of a quadrupole mass spectrometer. *IEE Proc-Sci. Meas. Technol.* 1996, *143 (1)*, 71-76.
50. Titov, V. V; Ion separation in imperfect fields of the quadrupole mass analyzer Part 1: Ion beam dynamics in the phase space. *International Journal of Mass Spectrometry and Ion Processes. 1995. 141*. 13-26.
51. Titov, V. V; Ion separation in imperfect fields of the quadrupole mass analyzer Part 2: Ion beam dynamics in the phase space of the fringing field. *International Journal of Mass Spectrometry and Ion Processes.* 1995. *141*. 27-35.
52. Titov, V. V; Ion separation in imperfect fields of the quadrupole mass analyzer Part 3: Transmission and option ion injection. *International Journal of Mass Spectrometry and Ion Processes.*1995, *141*. 37-43.

53. Titov, V. V; Ion separation in imperfect fields of the quadrupole mass analyzer Part 4: Theoritical applications. *International Journal of Mass Spectrometry and Ion Processes.* 1995, *141*. 45-56.

54. Titov, V. V; Ion separation in imperfect fields of the quadrupole mass analyzer Part 5: Esperimental verifications. *International Journal of Mass Spectrometry and Ion Processes.* 1995, *141*, 57-65.

55. Titov, V. V. Detailed study of the quadrupole mass analyzer operating within first, second, and third (intermediate) stability regions. 2 transmission and resolution. *J Am Soc Mass Spectrom*. 1998, *9*, 70-87.

56. Tunstall, J.J.; Voo, A.C.C.; Taylor, S. Computer simulation of the mass filter for a finite length quadrupole. *Rapid Commun. Mass Spectrom*, 1997, *11*, 184–188.

57. Gibson, J.R.; Taylor, S.; Leck, J.H.; Detailed simulation of mass spectra for quadrupole mass spectrometer systems. *J. Vac. Sci. Technol. A.* 2000, 18(1), 237-243.

58. Gibson, J.R.; Taylor, S. Prediction of quadrupole mass filter performance for hyperbolic and circular cross section electrodes. *Rapid Commun. Mass Spectrom*, 2000, *14*, 1669–1673.

59. Du. Z.; Douglas, D.J.; Glebova, T.; Konenkov, N.V.; Peak structure with a quadrupole mass filter operated in the third stability region. *International Journal of Mass Spectrometry*. 2000, *197*, 113–121.

60. Douglas, D. J.; Glebova, T. A.; Konenkov, N. V.; Sudakov, M. Yu. Spatial harmonics of the field in a quadrupole mass filter with circular electrodes. *Technical Physics*. 1991, *44 (10)*. 1215-1219.

61. Douglas, D.J.; Konenkov, N.V. Influence of the $6^{th}$ and $10^{th}$ harmonics on the peak shape of a quadrupole mass filter with round rods. *Rapid Commun. Mass Spectrom*. 2002, *16*, 1425-1431.

62. Blaum, K.; Geppert, Ch.; Muller, P.; Nortershauser, W.; Otten, E.W.; Schmitt, A.; Trautmann, N.; Wendt, K.; Bushaw, B.A. Properties and performance of a quadrupole mass filter used for resonance ionization mass spectrometry. *International Journal of Mass Spectrometry*. 1998, *181*, 67–87.
63. Turner, P. Gibson, J.R.; Taylor, S. Effect of ion entry acceptance conditions on the performance of a quadrupole mass spectrometer operated in upper and lower stability regions. *J. Vac. Sci. Technol*. 2005, *23(3)*, 480-487.
64. Hogan, T.J.; Taylor, S. Performance Simulation of a Quadrupole Mass Filter Operating in the First and Third Stability Zones. *IEEE*. 2008, *57 (3)*, 498-508.
65. Hogan, T.J.; Taylor, S. Effect of mechanical tolerances on QMS performance for operation in stability zone 3. *IEEE*. 2010, *59 (7)*, 1933-1940.
66. Du, Z.; Douglas, D. J.; Konenkov N. Elemental Analysis with Quadrupole Mass Filters Operated in Higher Stability Regions. *J. Anal. At. Spectrom.* 1999, *14*(8), 1111–1119
67. Sreekumar, J.; Hogan, T.J.; Taylor, S.; Turner, P.; Knott, C. A Quadrupole Mass Spectrometer for Resolution of Low Mass Isotopes. *Journal of the American Society for Mass Spectrometry*. 2010.
68. Ann, J.R; Park, C.J.; Computer simulations of electron and ion trajectories in electron-impact ion sources of a quadrupole mass spectrometer. *Nuclear Instruments and Methods in Physics Research A*, 2011, *645*, 345–349.
69. Gooden J.K.; Rempel D.L.; Gross, M.L. Evaluation of Different Combinations of Gated Trapping, RF-Only Mode and Trap Compensation for In-Field MALDI Fourier Transform Mass Spectrometry. *Journal of the American Society for Mass Spectrometry*. 2004, *15*, 1109-1115.

70. Desiderio, D.M.; Nibbering, N.M. *Mass Spectrometry: Instrumentation, Interpretation, and Applications*. Wiley (2008)

# Chapter 3

# Mass Spectrometer

A mass spectrometer essentially consists of three fundamental components namely: the ionisation source, the mass analyzer and the detector [1, 2]. Figure 3.1 shows the schematic diagram of a mass spectrometer.

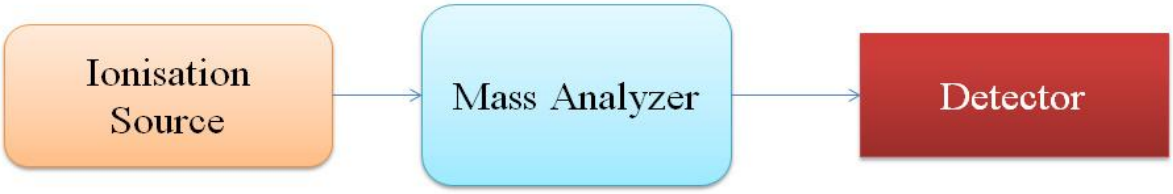


Figure 3.1: Schematic diagram of a mass spectrometer.

## 3.1 Ionisation Source

The first step in the mass spectrometric analysis of compounds is the production of gas-phase ions of the compound. The atoms or molecules are usually ionised through electron ejection, electron capture, protonation, deprotonation, the transfer of a charged species from a condensed phase to the gas phase. For example a molecule (M) is ionised to produce an $M^+$ ion. A variety of ion sources are available and each has its own advantages and disadvantages [3]. The choice of ion source for a particular application depends on the nature of the sample and the type of information desired as no one ion source is ideally suited to all applications.

Electron ionisation (EI) [4, 5] and chemical ionisation (CI) [6] are suitable for gas-phase ionisation and thus their use is limited to compounds that are sufficiently volatile and thermally stable. Electrospray ionisation (ESI) and Matrix- assisted laser desorption ionisation (MALDI) are used for many application involving bio-organic compounds due to their softer character and only produce molecular species. Other types of ionisation technique include glow discharge, field desorption (FD), desorption/ionisation on silicon (DIOS), thermospray, fast atom bombardment (FAB), secondary ion mass spectrometry (SIMS), atmospheric pressure chemical ionisation (APCI), direct analysis in real time (DART), spark ionisation and thermal ionisation [7].

### 3.2 Mass Analyzer

Once the ions are created, they are accelerated into the mass analyzer by an electric field. The mass analyzer separates these ions according to their *m/z* value. The selection of mass analyzers depends upon resolution, mass range, scan rate and detection limits required for an application [1]. For this purpose, there are many different types of analyzers available. Scanning analyzers include quadrupole mass filters and magnetic sectors. These analyzers are similar to a filter used for optical spectroscopy. These analyzers transmit a single selected *m/z* to the detector system and the mass spectrum is obtained by scanning the analyzer so that different mass to charge ratio ions are detected.

Although mass analyzers are generally scanning devices, some allow the transmission of all ions, such as the time-of-flight mass analyzers, the ion trap, and the dispersive magnetic analyzers.

### 3.3 Detector

The final part in the mass spectrometric system is detector. The beam of ions passes through the system and is then detected and transformed into a suitable detector. The detector records the ion current, amplifies it and the signal is transmitted to the data system which will produce a mass spectrum, a record of ion as a function of mass-to-charge ratios. Different types of detectors exist and can be classified into two categories. The photographic plate and the Faraday cup allow a direct measurement of the charges that reach the detector, whereas detectors such as electron and photon multipliers and array detectors increase the ion intensity of the signal [1, 2].

### 3.4 Quadrupole Mass Filter

The geometry of the quadrupole mass filter is shown in Figure 3.2a. The usual arrangement consists of a parallel array of four rods mounted in square configuration as shown in Figure 3.2b [8]. The hyperbolic shape shown in Figure 3.2a is difficult to produce; consequently circular electrodes as shown in Figure3.2b are widely used and provide good approximation of the quadrupole field. The field within the analyzer is produced by coupling opposite pairs of electrodes together and applying dc and rf potentials. Upon injection of ions within the array, the ions describe complex trajectories. The ions with unstable trajectories are lost, for example collision with electrodes, whereas, the ions with stable trajectories are successfully transmitted through the analyzer to the detector.

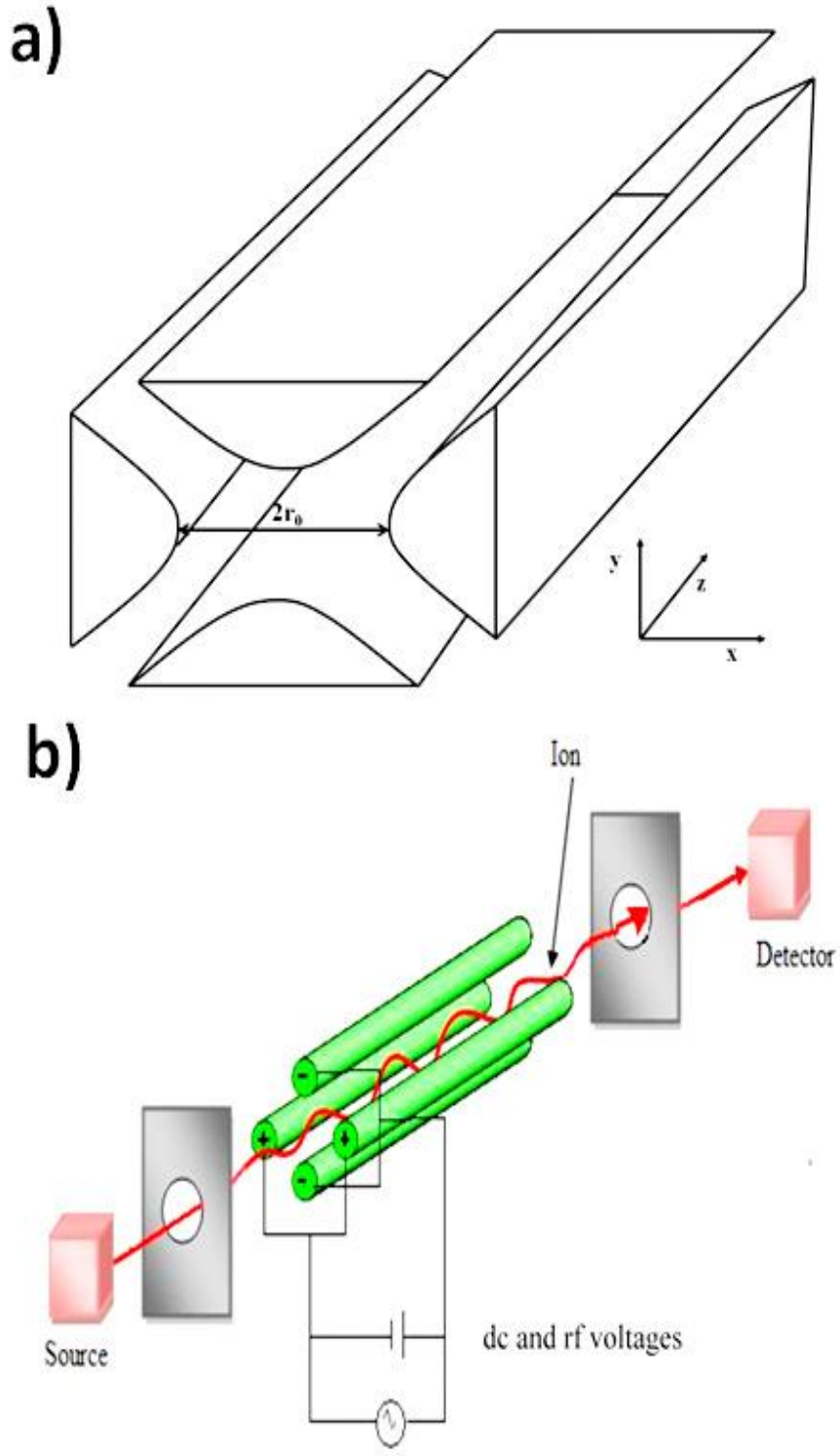


Figure 3.2: The quadrupole mass spectrometer (a) arrangement of four electrodes with hyperbolic geometry which serve to create a cylindrical symmetric field, (b) Schematic arrangement of the quadrupole mass spectromter.

For a given inter-electrode spacing $2r_0$, the path stability of an ion with a particular value of *m/z* depends on the amplitude of rf voltage (*V*), the magnitude of its frequency ω, and the *U/V* ratio. When $U = 0$, a wide range of *m/z* values are transmitted, and as the ratio *U/V* is increased, the resolution increases and at the stability limit only a single value of *m/z* corresponds to a stable trajectory, resulting in decrease in sensitivity and transmission, and collection of ions of a single *m/z* ratio.

### 3.5 Theory of quadrupole devices

A QMF consisting of a parallel array of four electrodes mounted in square configuration produces a central electric field whose strength increases linearly with increasing displacement from the central axis and is independent in *x* and *y* (ideal quadrupole field) [2, 8]. In a quadrupolar device described with reference to the rectangular coordinates, the potential $\emptyset_{x,y,z}$ at any given point can be expressed as

$$\emptyset_{x,y,z} = A(\lambda x^2 + \sigma y^2 + \gamma z^2) + C \tag{3.1}$$

where A is a term independent of *x*, *y*, and *z* that includes the electric potential applied between the electrodes of opposing polarity, C is a fixed potential applied to all of the electrodes so as to float the device, and $\lambda, \sigma,$ and $\gamma$ are weighting constants for the *x*, *y* and *z* coordinates respectively.

In an electric field, it is essential that the Laplace condition $\nabla^2 \emptyset_{x,y,z} = 0$ be satisfied. This means that $A(2\lambda + 2\sigma + 2\gamma) = 0$

Clearly, A is nonzero; therefore

$$(\lambda + \sigma + \gamma) = 0 \tag{3.2}$$

An infinite number of combinations of $\lambda, \sigma,$ and $\gamma$ exist which satisfy the above equation. However, the simplest combination that has generally been chosen in practice for the two-dimensional quadrupole mass filter and linear ion trap (LIT) is given below

$$\lambda = -\sigma = 1 \quad \gamma = 0$$

Substituting the values in equation 3.1 gives

$$\emptyset_{x,y} = A(x^2 - y^2) + C \tag{3.3}$$

where for the x pair of rod electrodes $x^2 - y^2 = r_0^2$ and for y pair of electrodes $x^2 - y^2 = -r_0^2$

The quadrupolar potential $\emptyset_0$ is given by the difference between the potentials applied to *x* pair and *y* pair of electrodes

$$\emptyset_0 = 2Ar_0^2 \tag{3.4}$$

Therefore $A = \emptyset_0/2r_0^2$

Hence equation 3.3 becomes $\emptyset_{x,y} = (\emptyset_0/2r_0^2)(x^2 - y^2) + C$

At the origin C=0, therefore above equation reduces to

$$\emptyset_{x,y} = (\emptyset_0/2r_0^2)(x^2 - y^2) \quad (3.5)$$

To examine the motion of an ion when subjected to the potential given in the above equation, considering first the component of motion in *x* direction by putting *y*=0 in equation 3.5 gives

$$\emptyset_{x,0} = (\emptyset_0/2r_0^2)(x^2) \quad (3.6)$$

So that electric field at the point (*x*, 0) is

$$(d\emptyset/\, dx)_y = (\emptyset_0 x/r_0^2)$$

As a result, the force acting on an ion, $F_x$, at a point (*x*, 0) is given by

$$F_x = -e(d\emptyset/\, dx)_y = -e(\emptyset_0 x/r_0^2) \quad (3.7)$$

where negative sign is an indication that the force is acting in the opposite direction to increasing *x*, since force is given by mass×accelaration, from equation 3.7, the following equation is obtained

$$m\left(\frac{d^2x}{dt^2}\right) = -e(\emptyset_0 x/r_0^2) \quad (3.8)$$

Let us now consider a real system in which

$$\emptyset_0 = (U - Vcos\omega t) \tag{3.9}$$

Where *V* is the amplitude of rf voltage peak-to-peak, ω is the magnitude of its frequency; *U* is the amplitude of dc voltage.

Substituting equation 3.9 in 3.8

$$m\left(\frac{d^2x}{dt^2}\right) = -e(U - Vcos\omega t)\, x/r_0^2 \tag{3.10}$$

This may be expanded to

$$\left(\frac{d^2x}{dt^2}\right) = -(eU/m - eVcos\omega t/m)\, x/r_0^2 \tag{3.11}$$

The commonly accepted form of Mathieu equation is given by

$$\frac{d^2u}{d^2\xi} + (a_u - 2q_u cos2\xi)u = 0 \tag{3.12}$$

Where $u$ represents the displacement and, $\xi$ is the dimensionless parameter equal to $\omega t/2$ such that ω must be a frequency of the potential $\phi_0$ applied to the electrode and $t$ the time.

From the relation $\xi = \omega t/2$ equation 3.12 reduces to

$$\frac{d^2u}{dt^2} = -\left(\frac{\Omega\omega^2}{4}a_u - 2 \times \frac{\Omega\omega^2}{4}q_u cos\omega t\right)x \quad (3.13)$$

From equations 3.11 and 3.13, the dimensionless quantities $a_u$ and $q_u$ are given by

$$a_u = a_x = -a_y = \left(\frac{4eU}{mr_0^2\omega^2}\right) \quad (3.14)$$

$$q_u = q_x = -q_y = \left(\frac{2eV}{mr_0^2\omega^2}\right) \quad (3.19)$$

The dimensionless quantities $a_u$ and $q_u$ are particularly interesting because they are functions of the magnitude of either the dc voltage or the rf voltage applied to a quadrupolar device, the rf frequency, the mass/charge ratio and the size of the device; that is, the stability parameters are functions of the instrumental parameters that govern the operation of a quadrupole device [8].

### 3.6 Regions of stability of the QMF

For the mass filter, the condition for simultaneous stability in both *x* and *y* directions can therefore be represented as shown in Figure 3.3 and Figure 3.4 These composite stability diagrams are obtained by superimposing two separate stability diagrams which differ by a factor of -1. The area, which is pointed in the inset of Figure 3.3, is generally used for mass filter operations, and is termed zone1.

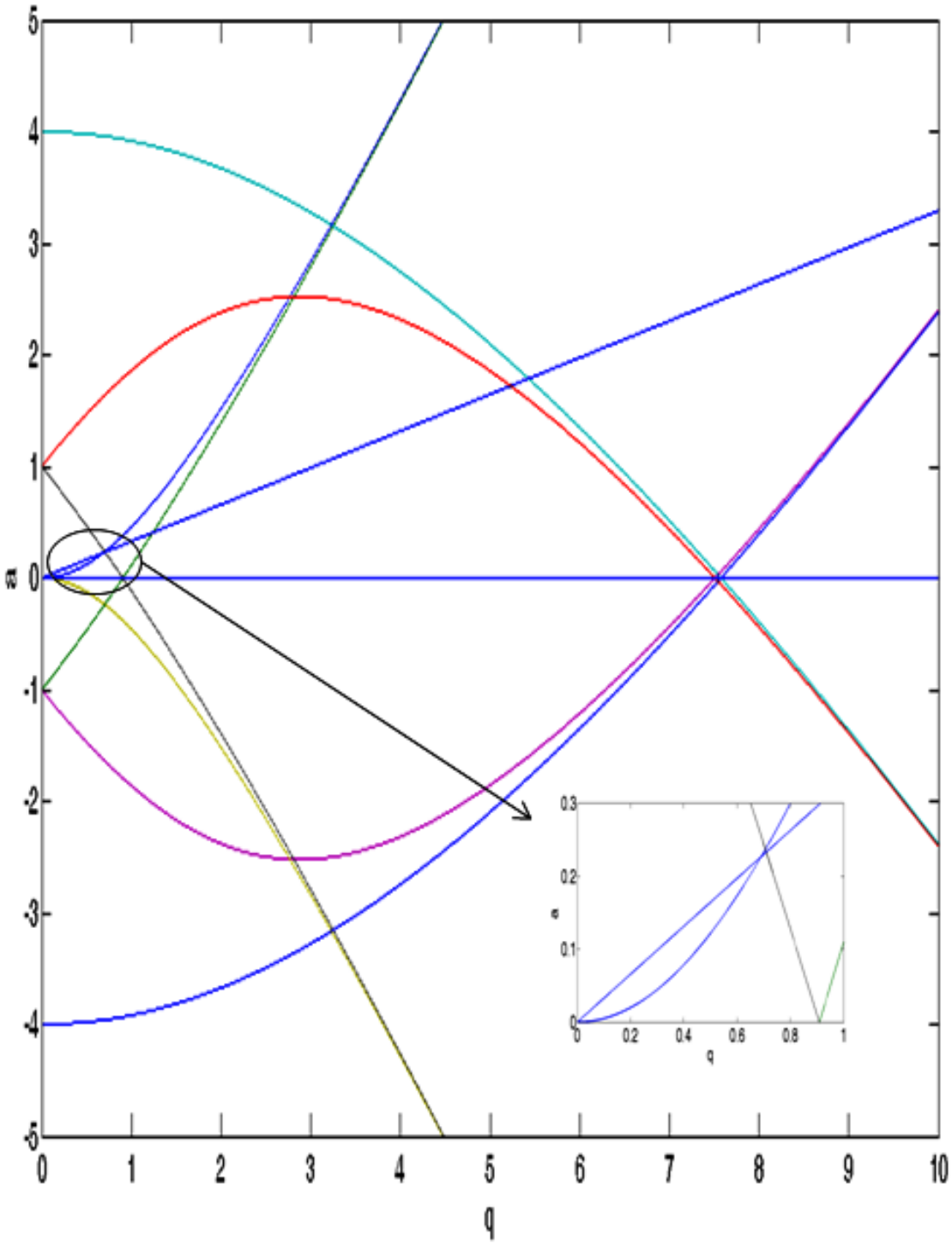


Figure 3.3: The Mathieu stability diagram for the mass filter showing the regions of simultaneous stability in the *x* and *y* directions.

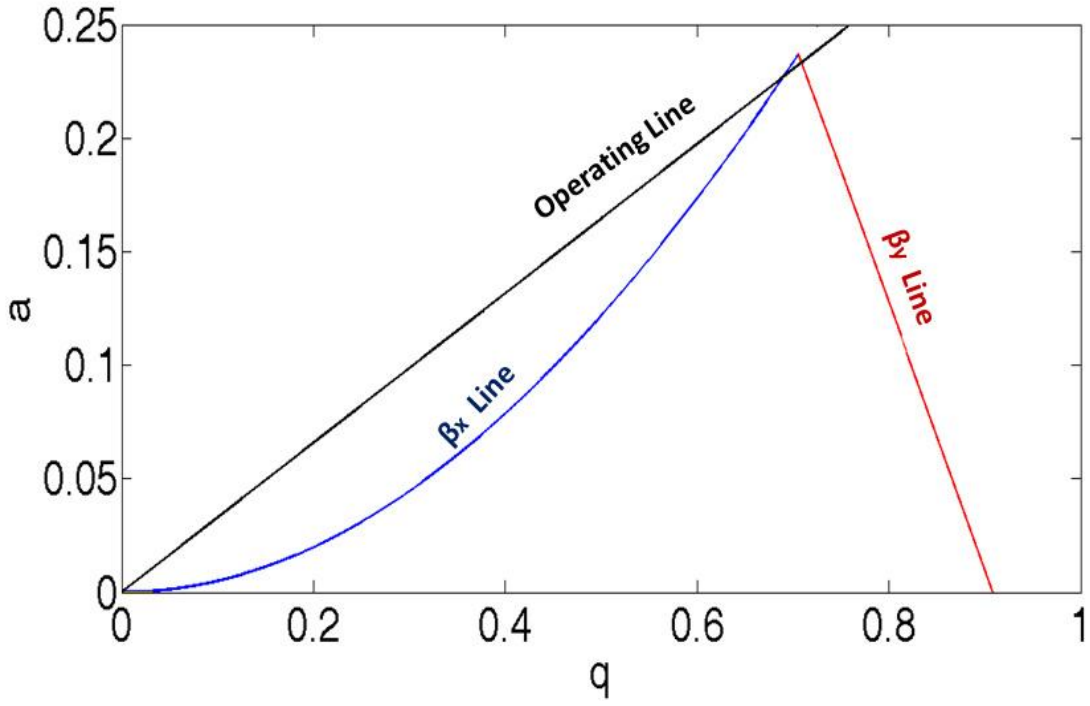


Figure 3.4: The lower stability region normally used in mass filter operation showing iso-$\beta$ lines for the x and y directions and a typical operating line.

For fixed values of $r_o$ $\omega$, $U$, and $V$, all ions of the same $m/z$ possess the same operating point ($a$, $q$) in the stability diagram. Since $a/q$ is equal to $2U/V$ and does not depends upon $m/z$ the operating points of all the ions lie on the same line of constant $a/q$, passing through the origin of the stability diagram. The ratio of the voltages $U$ and $V$ controls the QMF resolution setting and the voltage $V$ sets the mass scale. Varying $V$ and therefore $U$ (while keeping the ratio of $U$ to $V$ constant) this changes the mass value that can successfully pass through the filter. This variation of the voltages is called the mass scan line. When $a \neq 0$ only those ions with operating points lying between the intersections of the mass scan line with $\beta_y = 0$ and $\beta_x = 1$ will have stable trajectories in both $x$ and $y$ directions and only those ions will pass through the mass filter to the detector. By increasing the $U/V$ ratio the sensitivity goes on decreasing and the resolution increases up to a certain value of $U/V$ ratio and then decreases. With increase in the $U/V$ ratio, the mass scan line approaches to the tip of the stable region

and only a narrow range of *m/z* values will be associated with stable trajectories, thus resolution increases and detection sensitivity decreases. Ions of lower mass will be stable in *x* direction and ions of higher mass will be stable in *y* direction [2].

**References**


1. Hoffmann, E.D.; Stroobant, V. *Mass spectrometry principles and applications*. Wiley, 2007.
2. Dawson, P.H. *Quadrupole mass spectrometry and its applications*. Elsevier, Amsterdam, 1976.
3. Ashcroft, A.E. *Ionisation Methods in Organic Mass Spectrometry* .Cambridge: Royal Society of Chemistry, 1997.
4. Brunis, A.P. Mass spectrometry with ion sources operating at atmospheric pressure. *Mass spectrometry reviews*. 1991, *10(1)*, 53–77.
5. Bleakney, W. A new method of positive ray analysis and its application to the measurement of ionisation potentials in mercury vapour. *Phys. Rev*. 1929, *34*, 157.
6. Nier, A.O. A mass spectrometer for routine isotope abundance measurement. *Rev.Sci. Instrum*. 1940. 18, 212-216.
7. Todd, J.F.J. Recommendations for nomenclature and symbolism for mass spectroscopy. *International Journal of Mass Spectrometry and Ion Processes*, 1995, *142(3)*, 209–240.
8. March, R.E.; Todd, J.F.J. *Quadrupole Ion trap Mass Spectrometry*,Wiley, 2005.

# Chapter 4

# Software

A custom software program (QMS-hyperbolic) developed in Visual C++ environment is used in this thesis. The program calculates ion trajectories by solving the Mathieu equations using a fourth order Runge-Kutta algorithm. It operates by dividing the ion trajectories into small time steps and assuming that over the steps the ion motion in three directions *x*, *y*, and *z* is uncoupled. Mass scans are computed by ramping the values of *U* and *V* with fixed *U*/*V* ratio, which sets the resolution of an instrument. An option of introducing magnetic field ( i.e. Magnetic flux density '**B**', also known as the magnetic field **B**) in all the three directions *($B_x$, $B_y$, $B_z$)*, along the whole length of the mass filter is also incorporated. The original model [1, 2] has been upgraded since it was unable to simulate the QMF at large number of rf cycles. For the work of this thesis the model has been modified for better sensitivity (using a larger number of steps along the mass scale), to include large number of ions at each point on the mass scale, and to simulate a QMF at very high number of rf cycles. The new version of the model developed has a pointer to a block of memory, i.e. the program uses dynamic memory which significantly increases its performance.

A second program (IonSrc) allows entry conditions for large number of ions (typically $10^8$), to be specified, which are subsequently supplied to the mass filter calculation engine to simulate individual trajectories in each case. The IonSrc file assumes a uniformly illuminated ion distribution across a user defined ion source exit radius. Each ion is injected into the QMF with random phase with respect to the rf at the time of entry. This chapter gives a

detailed description of the simulation software used in this thesis and it also presents the information regarding the features incorporated in the software.

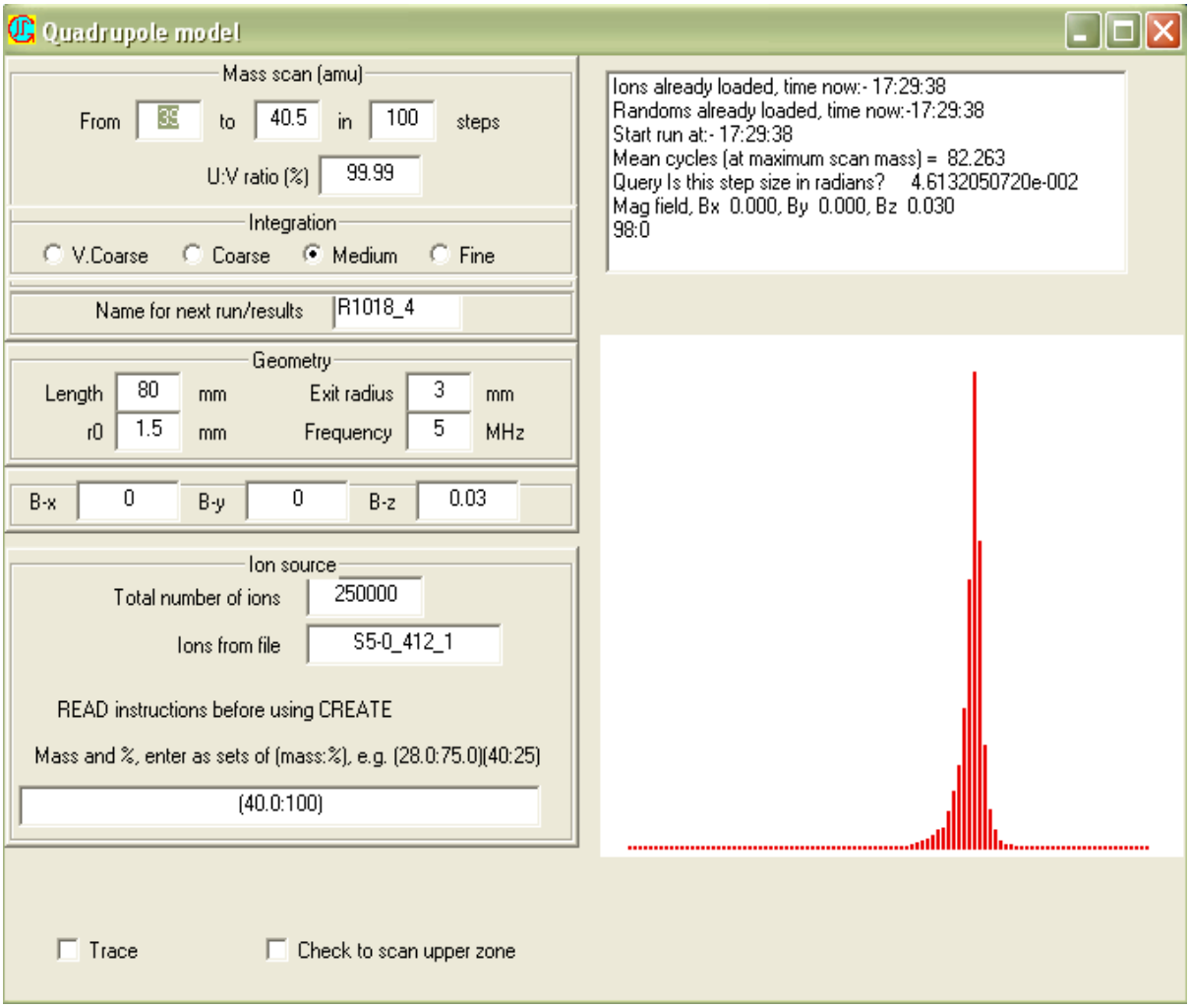


Figure 4.1: QMS-Hyperbolic GUI.

### 4.1 QMS-hyperbolic

The software consists of a graphical user interface (GUI) which is divided into number of control groups enabling the user to easily control the operating parameters. The range of mass scan, voltages, geometry of the filter can be set into the software interface. Figure 4.1 shows

QMS hyperbolic GUI; whereas, Figure 4.2 shows a schematic of the QMS and how each parameter in the model is related to QMS.

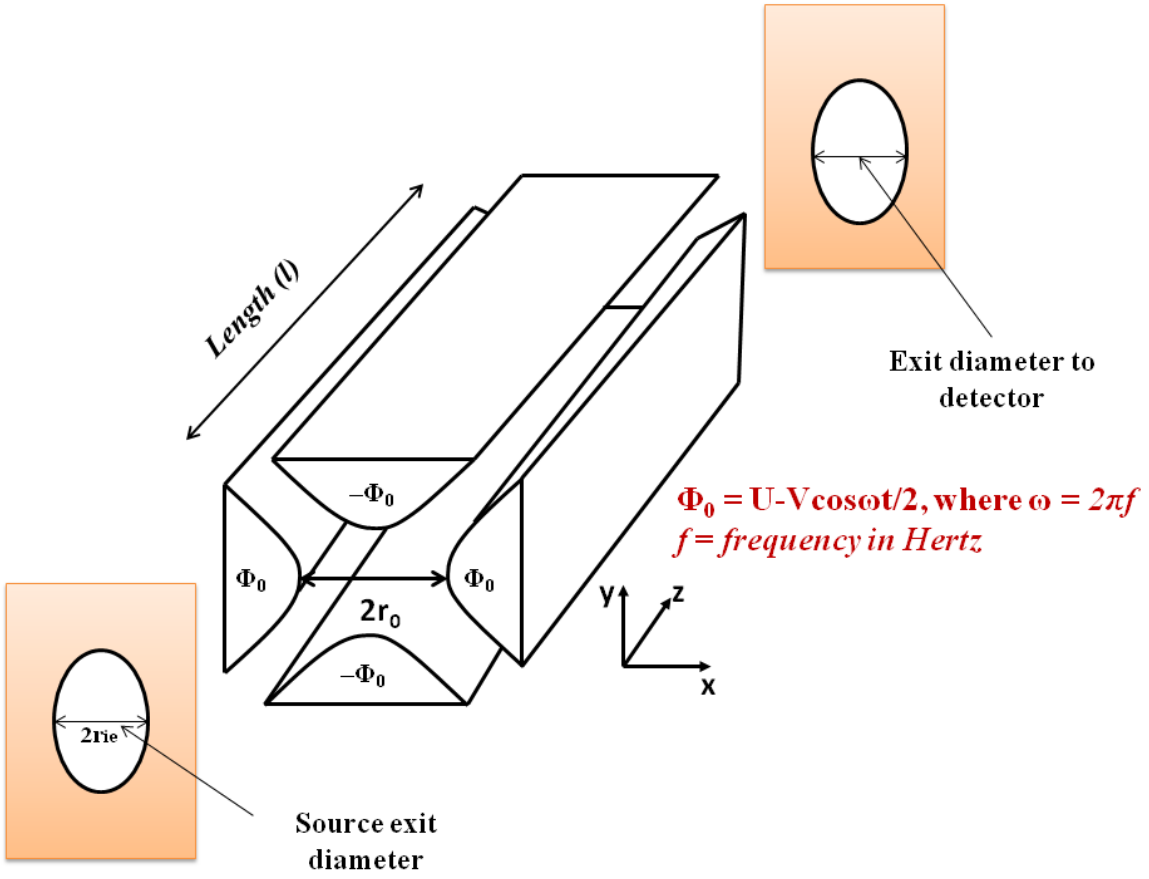


Figure 4.2: Schematic of the QMS showing different geometrical and operating parameters.

### 4.1.1 Mass Scan

It is used to control the *m/z* range of a mass scan simulation, it is provided with text boxes such as mass start range and stop range and number of steps along the mass scale. The integer values of mass start range, stop range and number of steps along a mass scan can be set in their respective boxes.

### 4.1.2 *U/V*

For a given mass-to-charge ratio the values of the voltages *U* and *V* can be calculated for particular points on the *a*-*q* plane, as shown in the Figure 4.3.

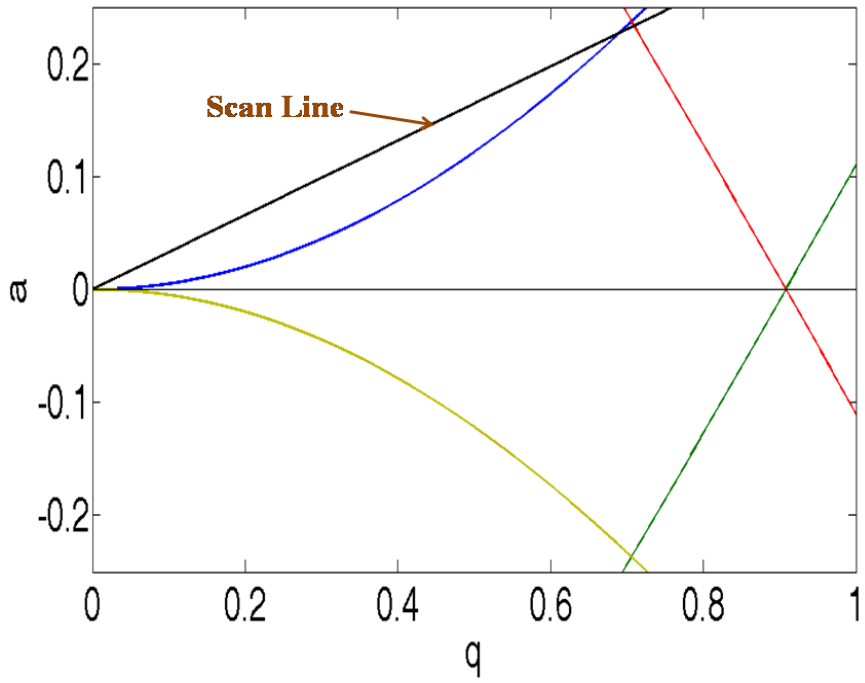


Figure 4.3: Stability region Zone 1.

The mass scan line shown in the figure represents one possible set of values. As the slope of the scan line increases, the line approaches the tip of the stable diagram and the range of mass-to-charge ratios that pass successfully through the filter decreases, the resolution increases and the sensitivity decreases. Conversely as the scan line slope decreases, the range of mass-to-charge ratios that are passed successfully increases, the resolution decreases with a corresponding increase in sensitivity. The scan line determines the resolution of the scan. It is assumed in the model that the QMF control setting *U/V*=100%

corresponds to the peak of the stability diagram (i.e., $a$ = 0.23699 and $q$ = 0.706 for zone 1). Making $U/V$ <100% increases the passband.

### 4.1.3 Integration

The QMS hyperbolic interface is provided with an integration section with four radio switches which are used to control Runge-Kutta step size. Runge-kutta integration is generally an extension of Euler integration that improves accuracy by a considerable amount without increasing the computational burden. The basic principle involved is to step into the interval and evaluate derivatives. This is similar to shortening of time step in Euler integration, but provides more accuracy with less increase in computation time.

The four radio switches includes V Coarse, Coarse, Medium and Fine. V Coarse is suitable for a quick check; the remainder switches provides increasingly accurate ion trajectories. Fine is suitable for highest accuracy but increases the time steps.

### 4.1.4 Geometry

The physical characteristics of the QMF to be simulated can be introduced in the Geometry section of the QMS hyperbolic interface. It is provided with different text boxes to define the length of the QMF, the field radius, the detector radius and the rf excitation frequency.

**Filter**

| | |
|---|---|
| Length | Length of the QMF in mm |
| $r_0$ | Field radius in mm |

| | |
|---|---|
| Frequency | rf excitation frequency in MHz. |
| Exit Radius | Detector radius mm |

### 4.1.5 Magnetic Field

An option of introducing magnetic field in all the three directions *($B_x$, $B_y$, $B_z$)*, is also incorporated in the QMS-Hyperbolic interface. The numerical model assumes that the magnetic field penetrates along the full length of the filter. The strength of the magnetic field is described in Tesla.

### 4.1.6 Ion Source Program

This is run by clicking the Ion Create button of the main QMS program; when clicked the screen shown in Figure 4.4 should appear. The program chooses its own name for the output. After the ion files are produced and exit is pressed the return to the main program is automatic and the correct name should appear in the box for ion file name. There will be two files left in c:\QMS\, one with extension .INS and the other with extension .ARC

The use of the values the text boxes is obvious. Generally energy spread and angular spread have a very minor effect on results unless extreme values are used. They produce approximately Gaussian distributions which are truncated. The peaked distribution check box gives a distribution that is slightly peaked to the centre. If required a feature to offset the source to check the effects of mis-alignment can be added. Again the program remembers the last values used so it is easy to perform several runs changing only one value.

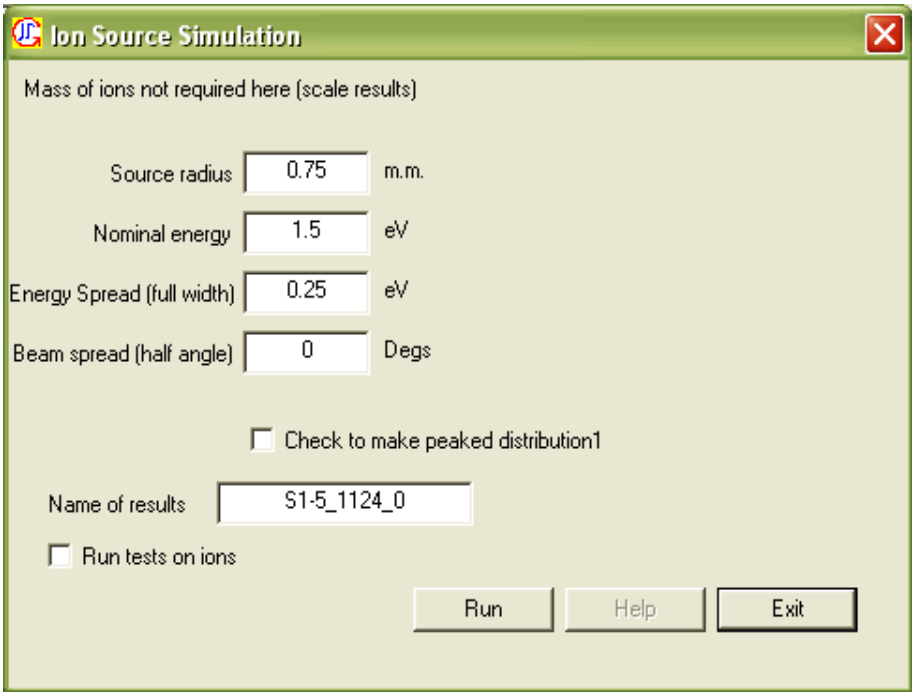


Figure 4.4: The Ion Source Program.

### 4.1.7 Number of Ions and Mass Specification

Number of ions: Integer value for the number of ions to simulate at each mass scan point.

Ion Mass: It defines the *m/z* value(s) for the ion(s) entering the QMF.

Specification: Requires the following format

(*m/z* value: percentage)

i.e.

(40:100) Entered value

40*m/z* ion

100% indicates all ions of this type

If parameter number of ions = 100,000 then 100,000 ions of *m/z* = 40 would be simulated at each mass scan point.

(20:25)(32:75) Entered value

20 *m/z* ion

25% indicates a quarter of the ions are this type

32 *m/z* ion

75% indicates three quarters of ions are this type

If parameter number of ions = 100,000 then 25,000 ions of *m/z*=20 would be simulated at each mass scan point and 75,000 ions of *m/z* = 32 would be simulated at each mass scan point.

### 4.1.8 Stability Zone

Selects the required stability zone. The text box check to scan upper stability zone if checked selects zone 3. For stability zone 3 the operating point at 100% corresponds to the *U/V* ratio at $q$ = 3.0 and $a$ = 2.8 which is near the centre of the stability zone 3. With increasing *U/V* ratio the scan line approaches the upper left tip of stability zone 3.

### 4.1.8 Ion Trajectories

The simulation program includes a trace facility and this allows many details of individual ions to be recorded. The check box trace, if checks computes individual ion trajectories at each point on the mass scale.

### 4.2 QMS-hyperbolic simulations results

The main objective of this section is to show the mass spectra of gases modelled using QMS-hyperbolic program by setting different values of the mass spectrometer dimensions and applied input signals. These test simulations will enable the use of the QMS-Hyperbolic program to model the mass spectra of different gases for later research studies described in this thesis.

#### 4.2.1 Modelling of mass spectrum of Argon Gas

To model a spectrum of argon gas the simulation used 300 steps across the mass range, with $1 \times 10^6$ ion trajectories run at each mass step on the peak. The length of the mass filter was chosen as 300 mm. The inscribed radius of the QMF was taken to be 0.9 mm. The frequency of the rf voltage used in the simulation was 3.685 MHz and the ion energy was chosen as 5 *eV*. The ion source radius ($r_{ie}$ ) was selected as 0.5 mm. The operating point (*U/V* ratio) was selected as 99.998%, where 100% corresponds to the intersection of the scan line with the peak of the Mathieu stability diagram at *U/V* = 0.168. The number of rf cycles N was calculated as 226.

Figure 4.5 shows a model of a mass spectrum for $^{40}Ar^{+}$ obtained using QMS-Hyperbolic, *M* is the mass of the given spectral peak and $\Delta M$ is the width of the mass peak measured at 10% of its height. The resolution *R* can be found by using the equation $R=M/\Delta M$, and for this particular peak it is found to be approximately 2934.

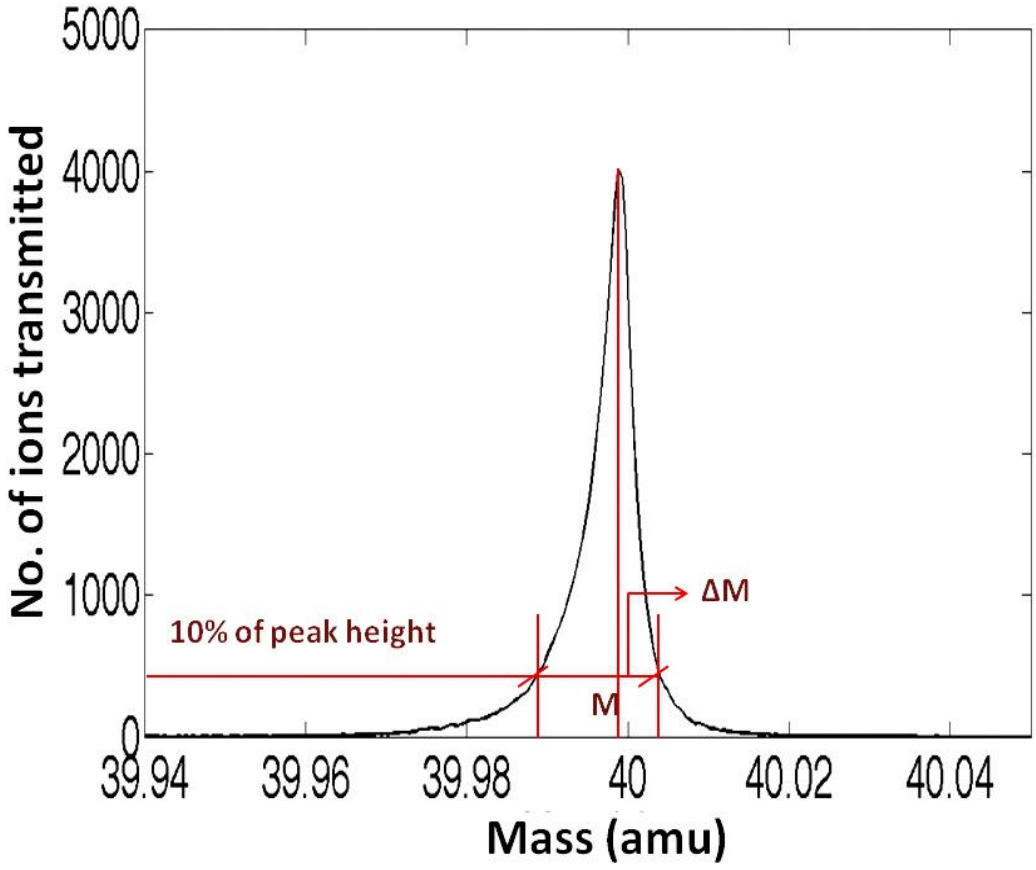


Figure 4.5: A model of a mass spectrum for $^{40}Ar^{+}$.

### 4.2.2 Modelling of the Von Zahn QMF

Using the QMS2-hyperbolic the 5.82 meters long QMF reported by Von Zhan [3] was simulated. At an operating point for stability zone 1 with a *U/V* ratio of 99.998%, and *N*= 415 an instrument resolution of around 17000 at 50% peak width definition was predicted using the QMS2 model which matches well the reported experimental results.

The simulation used 300 steps across the mass range, with $1 \times 10^6$ ion trajectories run at each point on the peak. The inscribed radius of the QMF was taken to be 35 mm. The

frequency of the rf voltage used in the simulation was 471 KHz and the ion energy was chosen as 30 *eV*. The ion source radius ($r_{ie}$ ) was selected as 1 mm. Figure 4.6 shows a model of a mass spectrum for $^{132}Xe^{+}$ obtained using QMS-Hyperbolic.

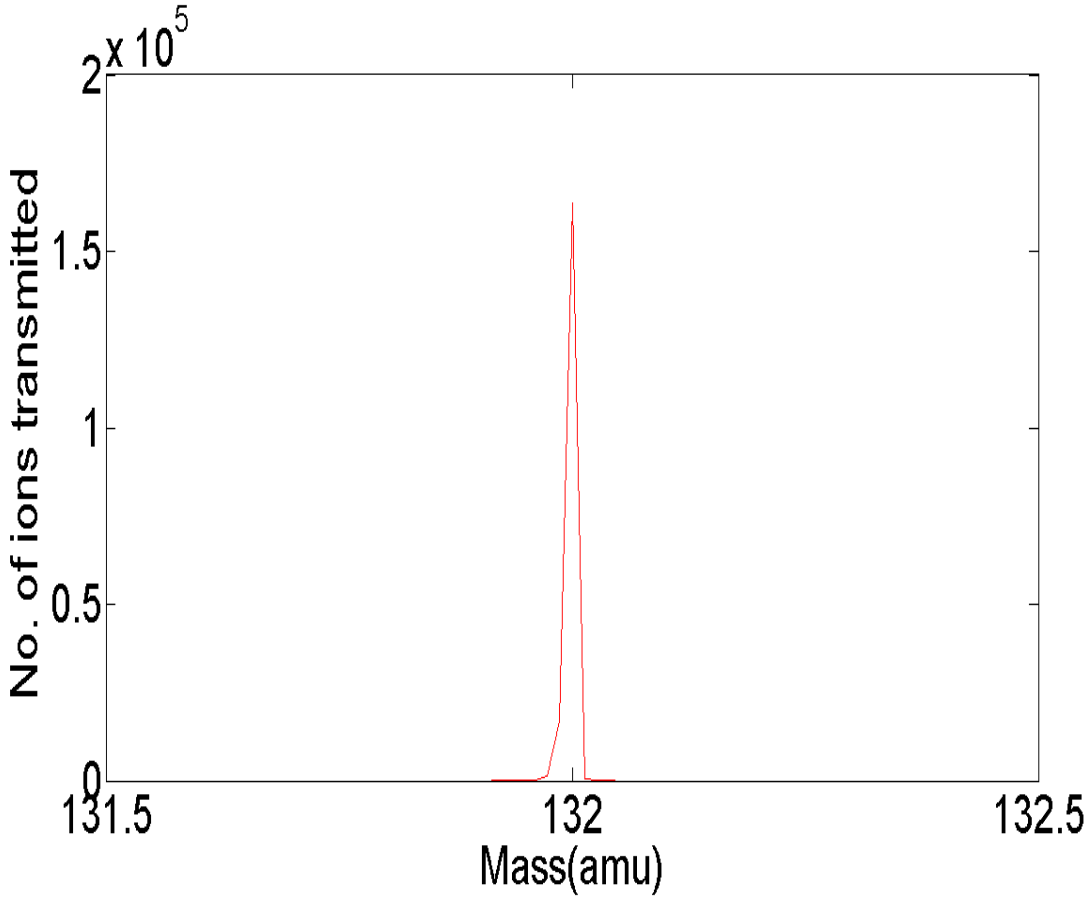


Figure 4.6: Simulated mass spectrum for $^{132}Xe^{+}$ for Von Zahn QMF.

### 4.2.1 Modelling of mass spectrum of Air

The layer of gases surrounding the planet Earth and retained by the Earth's gravitational field is called the Air or Earth atmosphere. Dry Air contains about 78% of nitrogen, 20% of oxygen, 1% of argon, 0.33% of carbon dioxide, and 0.67% of other rare gases [4]. The four main components were modelled using QMS hyperbolic.

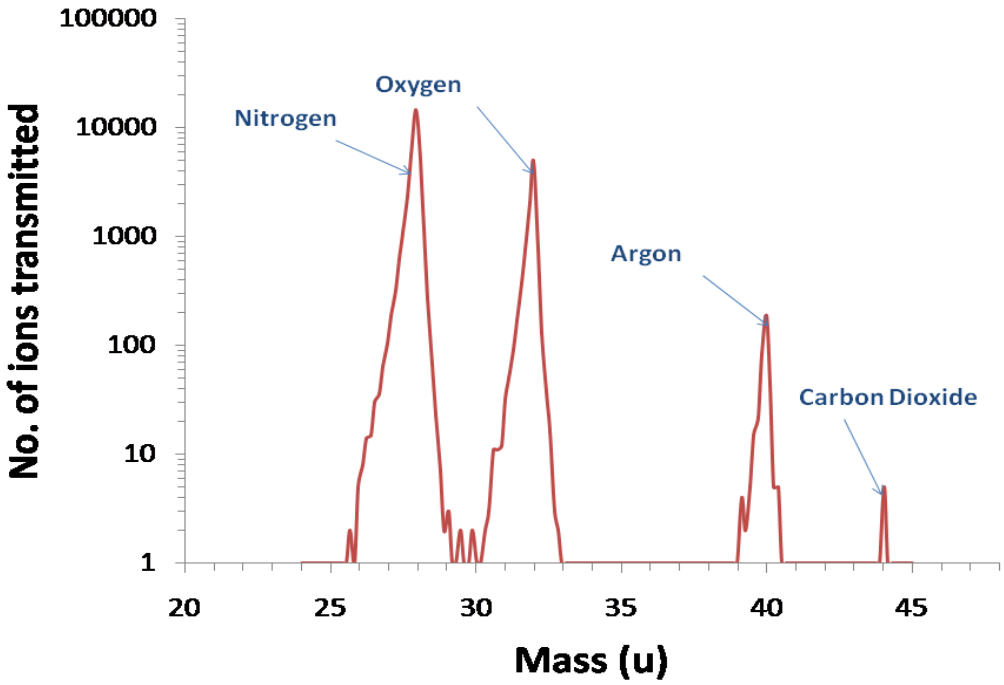


Figure 4.7: Simulated mass spectrum of Air showing four main gases.

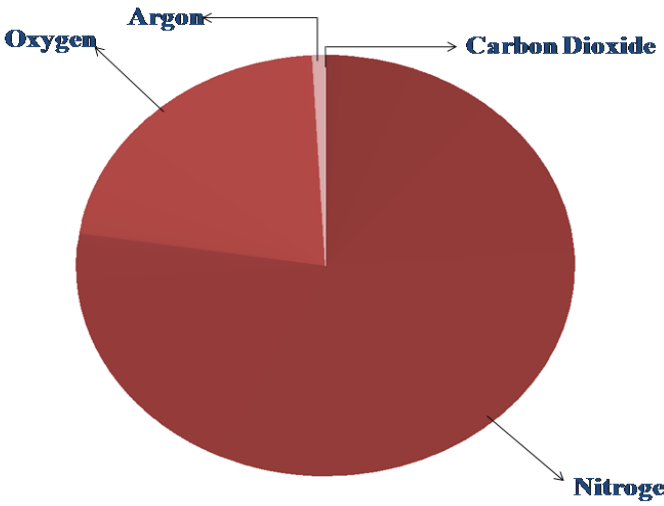


Figure 4.8: Proportional volume of gases comprising dry air.

Figure 4.7 shows a log plot of simulated mass spectrum of dry air mixture with four main gases in context to composition: nitrogen (28), oxygen (32), argon (40) and carbon dioxide (44). The other trace gases are not taken into consideration as their relative composition is quite low. Figure 4.8 shows the proportional volume of gases comprising dry air, obtained from the simulated mass spectrum using QMS-hyperbolic.

## 4.3 Conclusions

A detailed description of the simulation software used in this thesis is given. The software can model the very large number of ions (> $10^8$), which cannot be generated in other ion optics packages (e.g.) SIMION [5]. In the following chapters the use of the QMS model to simulate QMF performance under different operating conditions is described.

## References


1. Tunstall, J.J.; Taylor, S.; Vourdas, A.; Leck, J.H.; Batey, J. Application of static magnetic field to the mass filter of a quadrupole mass spectrometer. *Vacuum*, 1999, *53*, 211-213.
2. Srigengan, B.; Gibson, J.R.; Taylor, S. Ion trajectories in quadrupole mass spectrometer with a static transverse magnetic field applied to mass filter. *IEE Proc-Sci. Meas. Technol*. 2000, 147 (6), 2000, 274-278.
3. Von Zahn, U. Prazisions-massenbestimmungen mit dem elekrischen massenfilter. *Zeitschrift fur Physik.* 1962. *168*, 129-142.
4. Hemat, R. A.S. *Air*. Urotext. Black Rock, IRL. 2006

5. Gibson, J.; Taylor, S.; Leck, J.H. Detailed simulation of mass spectra for quadrupole mass spectrometer systems. *Journal of Vacuum Science and Technology A: Vacuum, Surfaces and Films.* 2000, *18(1)*, 237–243.

# Chapter 5

# Quadrupole Mass Spectrometer in the First Stability Zone with Magnetic Field Applied

## 5.1 Introduction

Two of the main operating descriptors of a quadrupole mass filter are the mass range and the resolution. The resolution and mass range are dependent upon six parameters: the length, the shortest distance between the electrodes, the maximum dc supply voltage to the electrodes, the rf frequency applied to the quadrupole electrodes, the rf supply voltage and the ion injection energy. In order to improve the resolution, the dimensions of the QMF or the operating parameters can be changed. However geometric modifications to improve performance can increase the manufacturing cost and usually the size of the instrument. A low cost method to increase the resolution of a given QMF is the application of magnetic field to the mass filter [1, 2].

Magnetic fields have long been used in ion traps, quadrupole ion sources and magnetic sector instruments; however little work has been done in relation to the application of magnetic field to the QMS. Poritsky and Gerrard [3] provide an exact analytical solution for the case of electron motion in a quadrupole electric field with a static magnetic field applied in the direction of the z-axis. However, in their case the electric field was not time varying as is the general case for the QMS. In an analytical study Pavlenko and Toporoba [4] considered ion motion in a homogeneous magnetic field. They showed that by varying the

magnetic field resolution could be improved, and this is true for any of the stable regions of the Mathieu stability diagram. Some workers have described an rf-only ion trap mode of operation, with high magnetic fields applied to overcome problems such as the low charge state of ions and ion focusing [5]. This method has been used for in-field matrix-assisted laser desorption ionisation Fourier transform mass spectrometry. It was found that for a larger ion trap a high value of applied magnetic field increases the resolution. Tunstall *et al* found experimentally that the application of static transverse magnetic field to the mass filter of QMS increases the resolution by reducing the long tail on low mass side of the mass spectra [1]. Later work explained the effect of a static magnetic field in terms of computed ion trajectories. Simulations showed that an applied transverse magnetic field in the *x*-direction has no effect on ion motion in the *x*-direction; however, ion motion in the *y*-direction is both displaced and increased in amplitude resulting in increased rejection of unwanted ions and improved resolution [2].

In this chapter therefore we extend the previous work and present new theoretical and experimental results for a QMS operating under a static magnetic field along the length of the mass filter. The numerical model used in the simulation assumes that the QMS contains hyperbolic electrodes and that the magnetic field penetrates along the full length of the filter.

## 5.2 Magnetic field

First discovered by Oersted in 1819, a magnetic field is produced whenever there is electric charge in motion [6, 7 and 8]. For example, if two parallel metal wires are brought near to each other and steady currents flow through them, there is a force between the two wires as shown in Figure 5.1. If the currents are in same direction the force is attractive, and if the

currents are in opposite direction the force is repulsive. Magnetic field is also produced by a permanent magnet. In the case of a permanent magnet there are no electric currents; however, there are the spins of electrons and orbital motions within the permanent magnet material which lead to magnetization within the material and a magnetic field outside. The magnetic field exerts a force on both current-carrying conductors and other permanent magnets; the latter also causes forces to act on wires carrying currents. If a wire carrying a current is suspended between the poles of a permanent magnet, then it experiences a force perpendicular to the direction of the current and is deflected. If the direction of the current is reversed then the deflection of the wire reverses also. A wire with a steady current flow through it and a permanent magnet both have the same effect on another wire carrying a current.

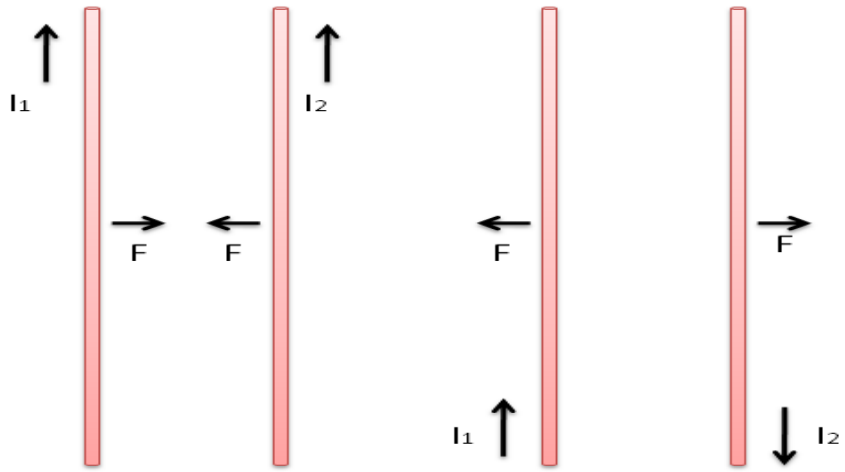


Figure 5.1: The forces between parallel wires carrying currents. Currents in the same direction cause attraction, currents in the opposite direction cause repulsion.

Figure 5.2 shows a uniform magnetic field between the pole faces of a permanent magnet; whereas Figure 5.3 shows the force on a positively charged particle moving in a

uniform magnetic field. The force **F** on charged particles moving in the gap between parallel pole faces or parallel metal wires carrying steady currents is proportional to the speed of the particle, its charge $\boldsymbol{q}$ and to the sine of the angles between vectors **v** and **B**. The units of magnetic field are defined by choosing the constant of proportionality to be unity, leading to

$$\boldsymbol{F} = \boldsymbol{qv} \times B \tag{5.1}$$

This equation is known as the *Lorentz force law*. The direction of the force is shown in Figure 5.4. In a Cartesian coordinate system the components of force F are:

$$F_x = q(v_y B_z - v_z B_y)$$

$$F_y = q(v_z B_x - v_x B_z)$$

$$F_z = q(v_x B_y - v_y B_x)$$

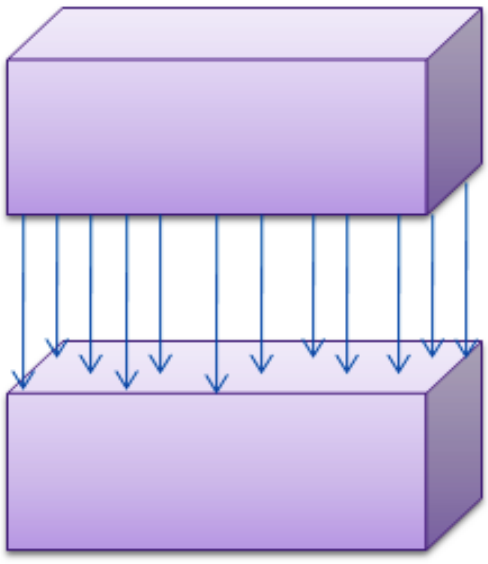

Figure 5.2: A uniform magnetic field between the pole faces of a permanent magnet.

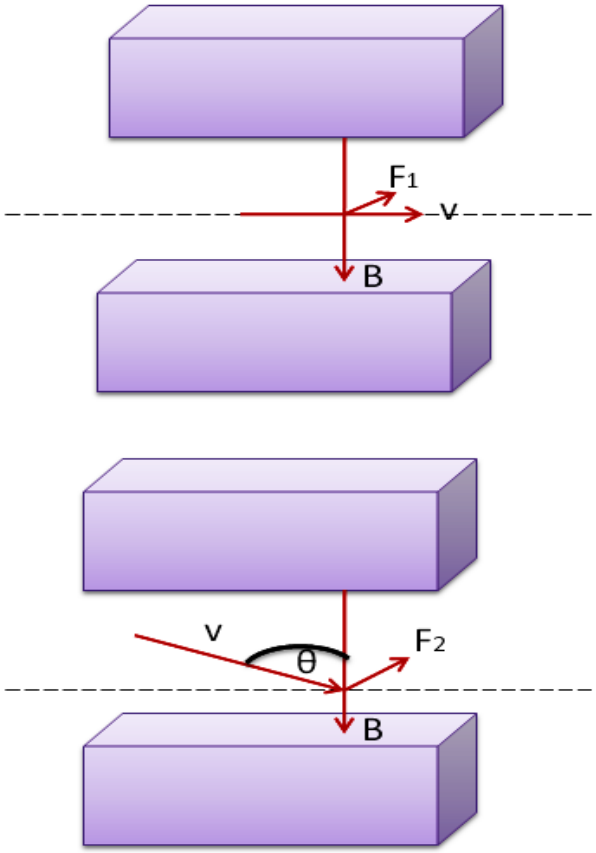


Figure 5.3: The force on a positively charged particle moving in a uniform magnetic field. If the particle moves parallel to the pole faces, as shown in the top diagram, the magnitude of the force $\mathbf{F_1}$ is proportional to the product *vB*. If the particle makes an angle Θ with the direction of the field *B* the magnitude of the force $\mathbf{F_2}$ is $vB\sin\Theta$.

If an electric field **E** is present as well as a magnetic field, the charged particles experiences an additional force $\boldsymbol{qE}$ and the total force is given by

$$\boldsymbol{F = q(E + v \times B)} \tag{5.2}$$

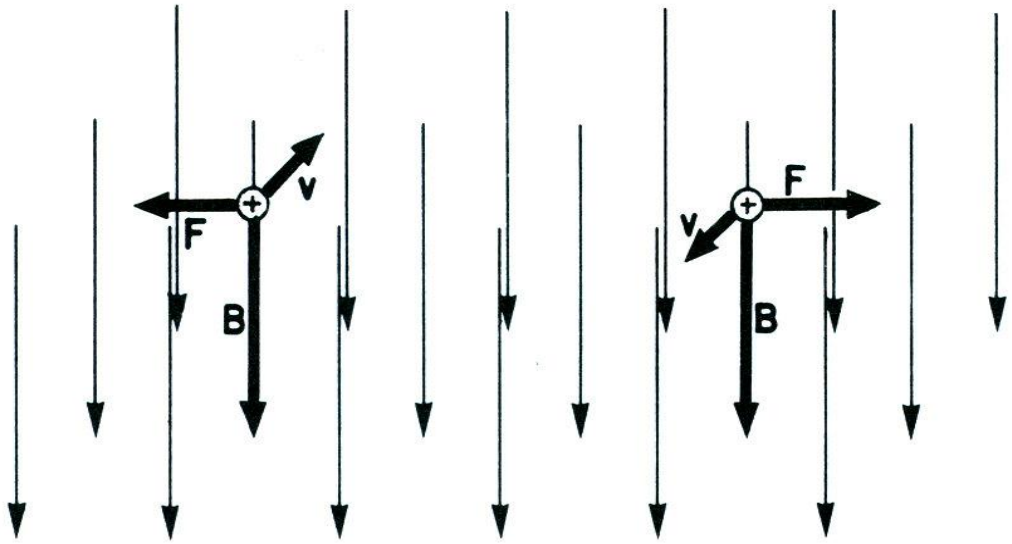


Figure 5.4: The direction of force on a positively charged particle moving in a magnetic field, diagram taken from [8].

An efficient way to produce uniform magnetic fields from a conductor is to use a long thin solenoid with a current passing through it. Figure 5.5 shows the field which is nearly uniform inside the solenoid. Solenoids allow electrically controlled magnetic fields [8, 9].

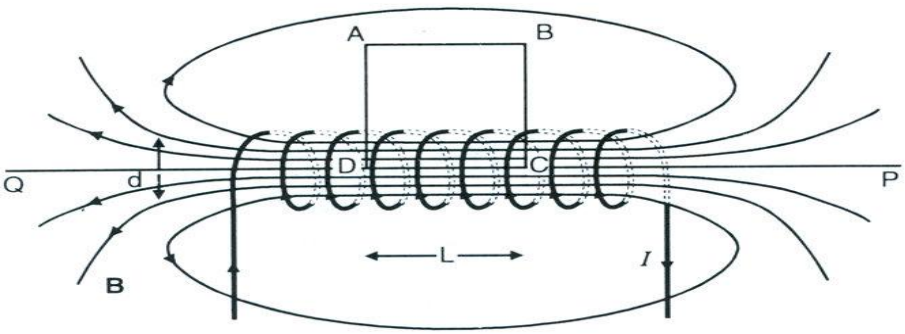


Figure 5.5: The field of long Solenoid carrying a current, diagram taken from [8].

### 5.3 Theory of a QMS under the influence of magnetic field

Ions oscillating tangentially to a magnetic field will therefore experience a Lorentz force. If the electric field is given by conventional quadrupolar potential where *U* is the amplitude of dc potential applied to electrodes, *V* the amplitude of rf potential, $f$ the frequency of the sinusoidal field and $r_0$ the inscribed radius of the electrodes, for a general field $\boldsymbol{B} = (B_x, B_y, B_z)$ the coupled equations of motion are given by:

$$\frac{d^2x}{d^2\xi} = -x\,(a - 2qcos2\xi) + (\frac{dy}{d\xi}b_3 - \frac{dz}{d\xi}b_2) \tag{5.3}$$

$$\frac{d^2y}{d^2\xi} = y(a - 2qcos2\xi) + (\frac{dz}{d\xi}b_1 - \frac{dx}{d\xi}b_3) \tag{5.4}$$

$$\frac{d^2z}{d^2\xi} = (\frac{dx}{d\xi}b_2 - \frac{dy}{d\xi}b_1) \tag{5.5}$$

In the numerical model the above equations have been written in a dimensionless form where the only dimension that appears is that of length displacement. The time *t* has become $t = 2\xi/\omega$ where $\omega$ is the angular frequency equal to $2\pi f$. In the absence of an applied magnetic field the direct potential *U* and alternating potential *V* are related to *a* and *q* as

$$a = (\frac{4eU}{mr_0^2\omega^2}) \tag{5.6}$$

$$q = (\frac{2eV}{mr_0^2\omega^2}) \tag{5.7}$$

The components of the ***B*** field are

$$(b_1, b_2, b_3) = (\frac{2eB_x}{m\omega}, \frac{2eB_y}{m\omega}, \frac{2eB_z}{m\omega}) \quad (5.8)$$

It can be seen from equations (5.3 – 5.5) that if the magnetic field is taken to be zero the coupled differential equations reduce to the familiar Mathieu equations for a linear quadrupole. Solving numerically the coupled differential equations gives the trajectories of the ions through the mass filter. From the trajectories it is feasible to determine the conditions which give successful ion transmission for a given mass to charge ratio. This depends on the values of direct potential *U*, the rf potential *V*, the rf voltage frequency *f*, the inscribed radius of the quadrupole rods $r_0$, the magnetic field ***B***, the initial velocity, initial phase and the ion position. The first four parameters appear as the variables of *a* and *q* in the Mathieu equation for (*B*=0). For ***B*** non-zero there will be a further dependence of *a* and *q* upon the magnetic field [4].

## 5.4 Effect of an axial magnetic field on the performance of a Quadrupole Mass Spectrometer

This section considers the case of a quadrupole mass spectrometer in which a static magnetic field is applied axially in the *z*- direction along the length of the mass filter. The theoretical approach assumed in the model is that the QMS contains hyperbolic rods as electrodes and that the magnetic field acts over the full length of the mass filter assembly. The analysis also predicts for which values of operating parameters an enhancement of the instrument

resolution is achieved when an axial magnetic field is applied. Initial experimental results with Argon and Helium for a low resolution instruments confirm the predicted theoretical trends.

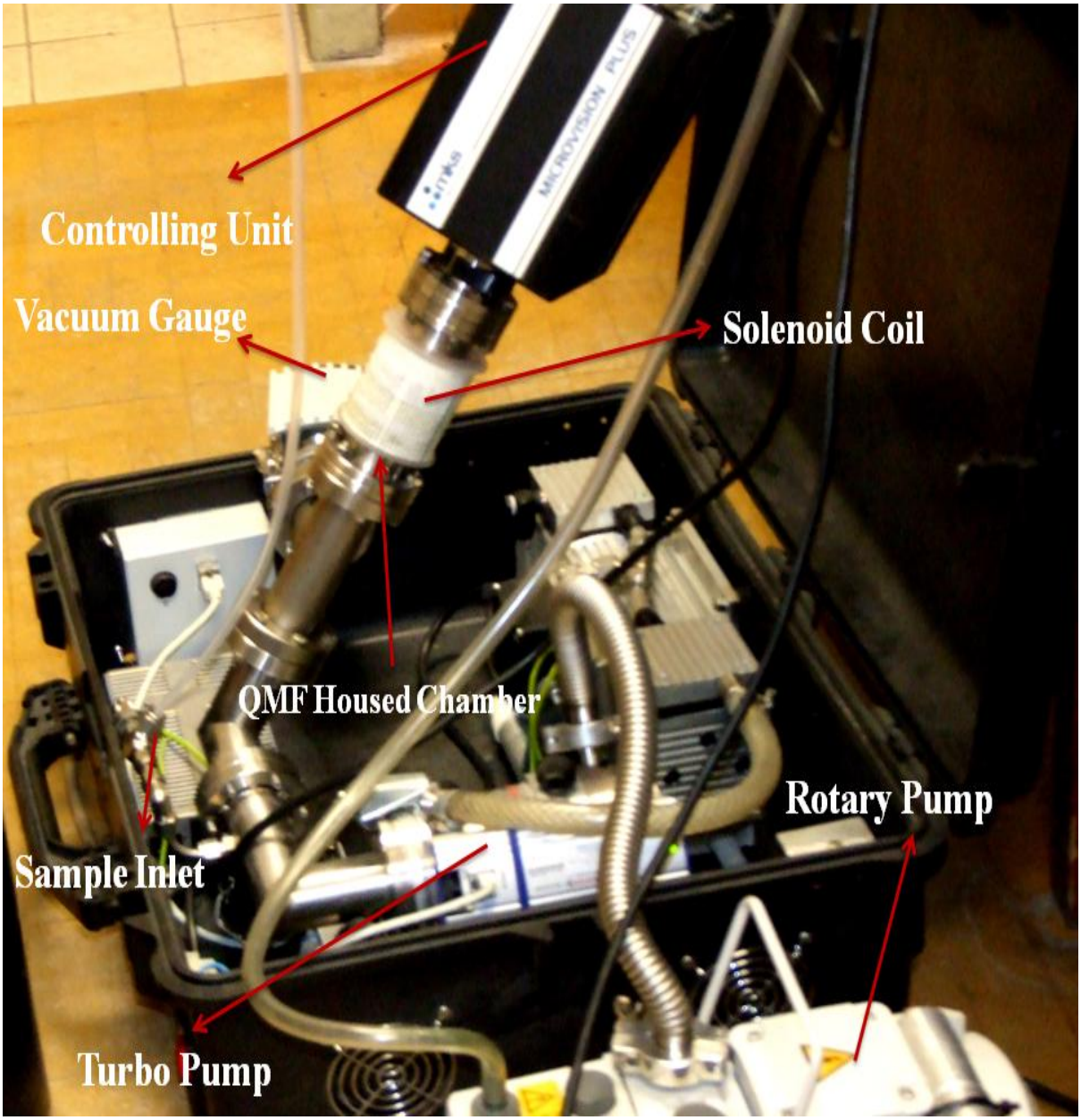


Figure 5.6: MKS Microvision Plus and vacuum system.

### 5.4.1 Experimental results

#### 5.4.1.2 MKS Microvision Plus

Reported here are the experimental mass peaks for $^{40}Ar^{+}$ and $^{4}He^{+}$ ions with and without an applied magnetic in the *z*- direction. A conventional single filter QMS instrument supplied by MKS Spectra Products (UK) was used as shown in Figure 5.6. The QMF length was 100mm with an electrode diameter of 6.35 mm and field radius of 2.76 mm, excited at 1.8342 MHz. The instrument was operated in Faraday only mode and in this configuration typically used as a Residual Gas Analyzer. The QMS was housed in a stainless steel chamber pumped by a turbo pump, backed by a rotary backing pump. A residual gas pressure of $2 \times 10^{-6}$ torr was achieved. After admitting the sample gas into the vacuum chamber the working pressure was raised to about $1 \times 10^{-4}$ torr.

An axial magnetic field is applied in the *z*- direction of the mass filter by passing a direct current through a solenoid coil wrapped on the stainless steel chamber housing the QMF exterior to the electrode length. The magnetic field is generated by applying a fixed value of current from a dc supply and measured using Hall Effect sensor. The value of magnetic field B was adjusted to 0.015 T for experiments with Argon, whereas for the case with Helium it was set to 0.007 T. The resolution was adjusted by setting ion energy to a value of 4.5 *eV*, this also gives an easily measurable ion current. The emission current was adjusted as 0.5 mA and the electron energy in the QMS ion source was set to 70 *eV*. The magnetic field extended 80% of the length of QMF.

The QMS used the Microvision plus software with a fully automated high stability data acquisition electronic drive unit for fast dynamic scanning of the mass filter electrode voltages. The start mass, end mass (range), number of steps, sweep rate and averaging were user selected. A visual display of each mass scan was displayed in real time on the PC.

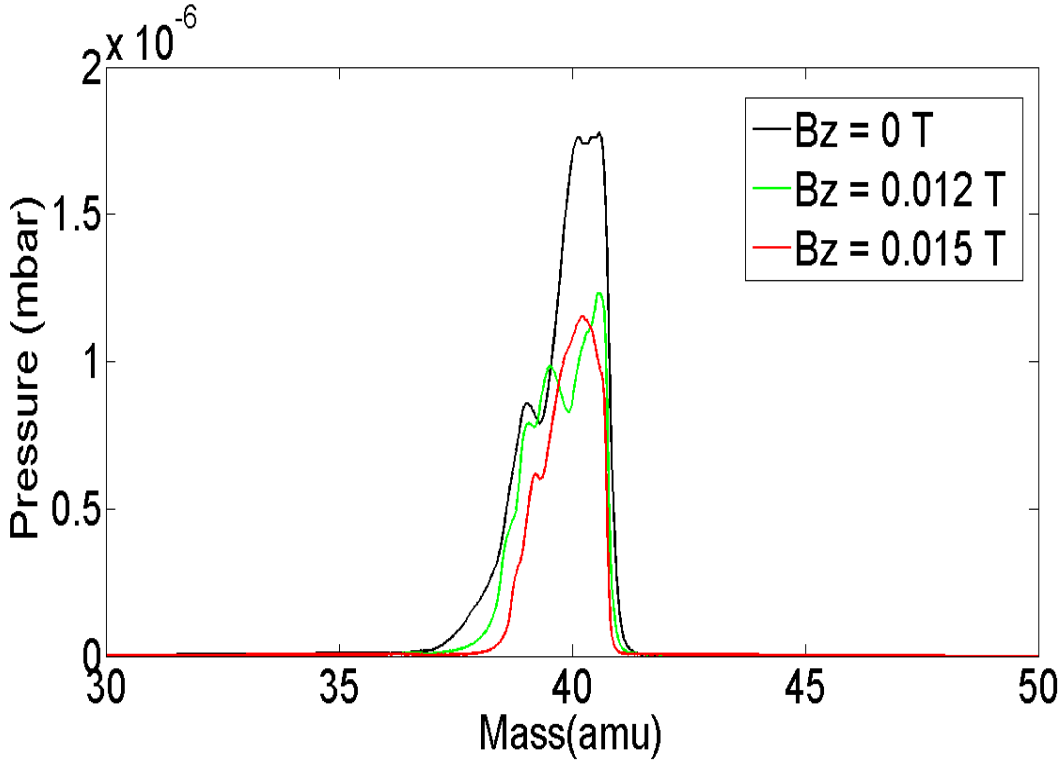


Figure 5.7: Experimental mass peaks for $^{40}Ar^{+}$ with and without an axial magnetic field applied obtained using MKS Microvision plus.

To demonstrate the effect of magnetic field in the *z*- direction on resolution of the QMF, $^{40}Ar^{+}$ and $^{4}He^{+}$ mass peaks with an expanded mass scale were obtained with and without the magnetic field $B_z$ applied. Figure 5.7 shows typical mass peaks obtained experimentally from the QMS for $^{40}Ar^{+}$, whereas Figure 5.8 shows mass peaks obtained experimentally for $^{4}He^{+}$. From both figures it can be seen that there is a clear improvement in resolution at 10% peak height with magnetic field applied, from approximately R = 13 to R =

19 (*Bz* = 0.015T) for the case with Argon and from R = 4.1 to R = 6.1 (*Bz* = 0.007 T) for the case with Helium.

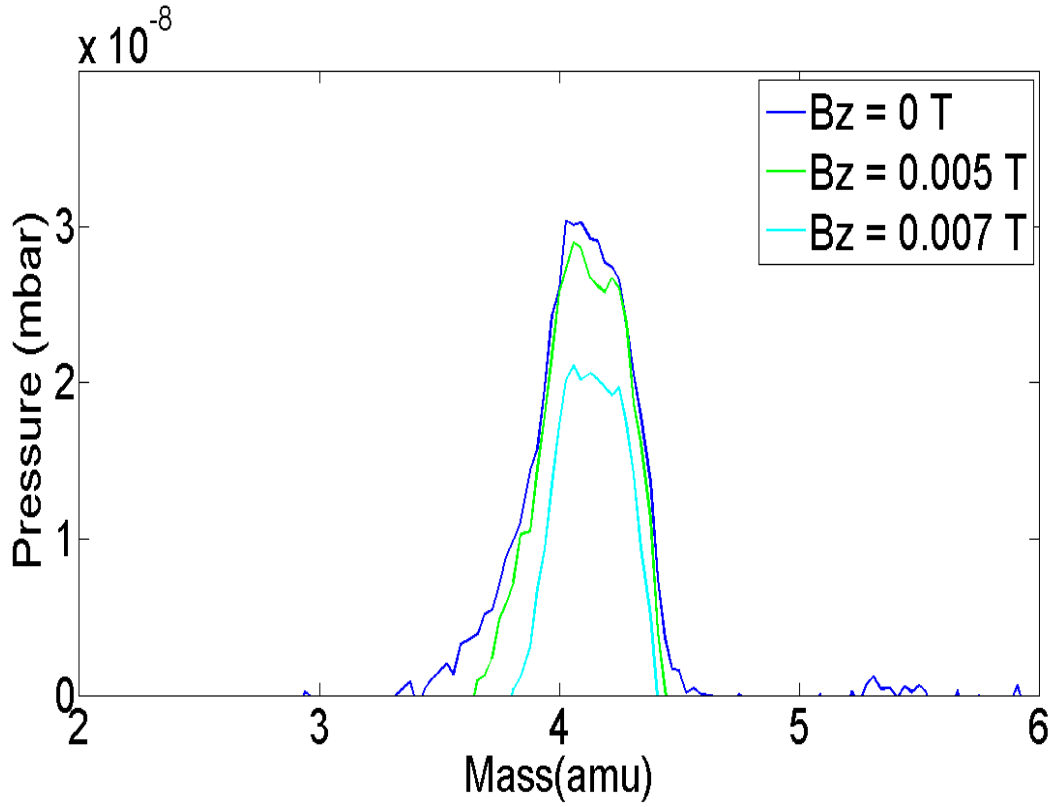


Figure 5.8: Experimental mass peaks for $^{4}He^{+}$ with and without an axial magnetic field applied obtained using MKS Microvision Plus.

Although such instrument resolutions are low in comparison with more sophisticated instruments (e.g. triple filter QMFs), this experimental result clearly illustrates the resolution enhancement provided by an axially applied magnetic field. Figure 5.9a shows the behaviour of the resolution, measured at 10 % peak height as a function of magnetic field for $^{40}Ar^{+}$ ions; whereas, Figure 5.9b shows the behaviour of the resolution as a function of magnetic field for $^{4}He^{+}$ ions. For the magnetic field in *z*- direction the resolution increases with increasing *Bz*, however the resolution will not increase indefinitely since as *Bz* increases peak height decreases.

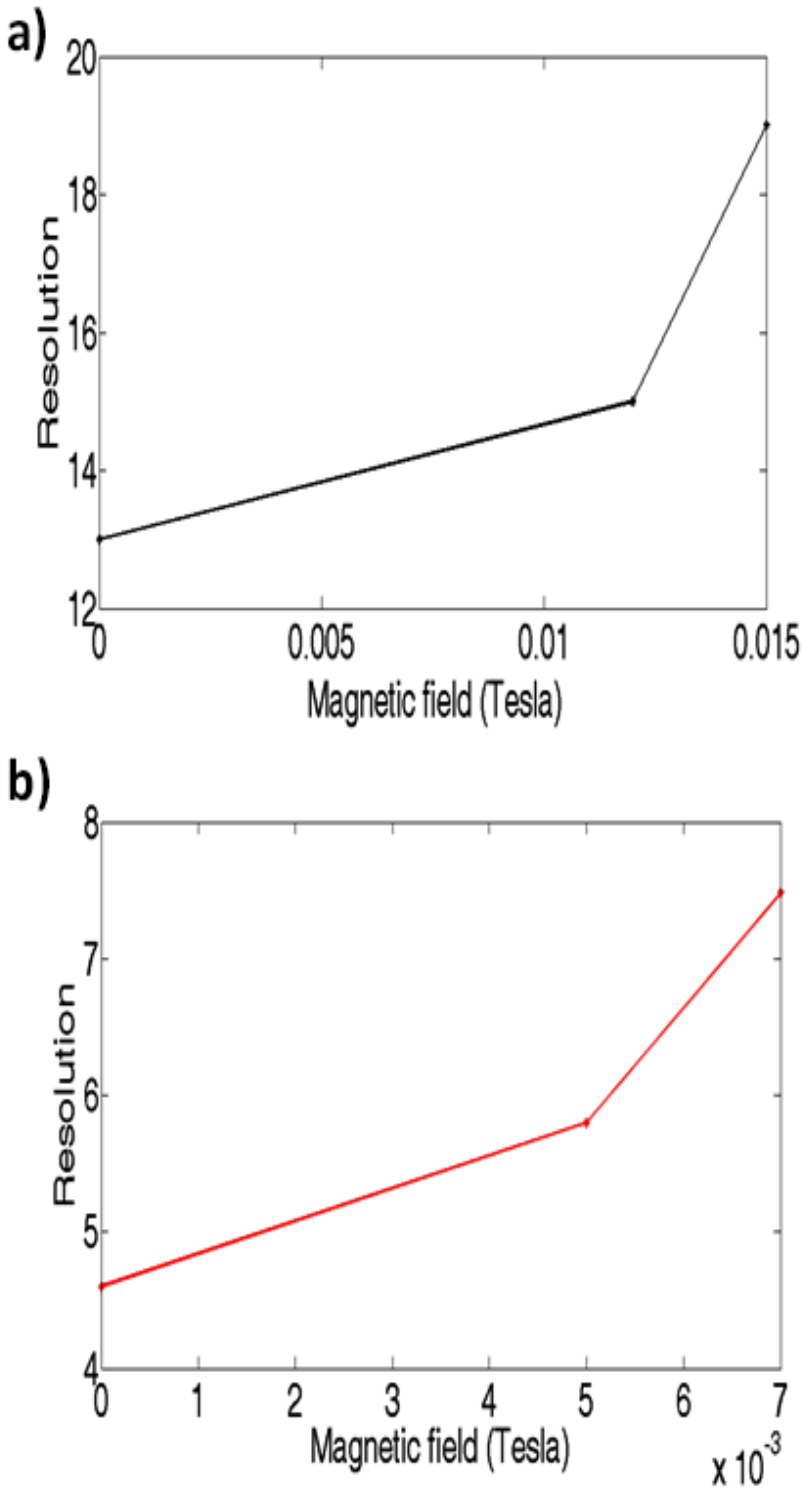


Figure 5.9: (a) The effect of magnetic field on resolution applied in z- direction for $^{40}Ar^{+}$ ions

(b) The effect of magnetic field on resolution applied in z- direction for $^{4}He^{+}$ ions.

### 5.4.1.2 Pfeiffer type QS422 QMS

The effect of an axial magnetic field upon QMS performance was also investigated for another instrument to confirm the effect. A Pfeiffer type QS422 QMS installed in a portable vacuum system provided by European Spectrometry Systems Ltd was used for this experiment. A rotary pump was used to improve vacuum stability and replaced the original diaphragm pump. A Pfeiffer PKR 251 pressure gauge was installed to ensure constant pressure conditions. Where possible the system remained under vacuum, otherwise a minimum stabilisation time of 24 hours was allowed before each set of measurements. The filaments were switched on 24 hours prior to measurements to ensure that filament effects on the resultant spectrum was minimised. A final base pressure of $7.3\times10^{-7}$ torr was achieved. On opening the inlet an operating pressure of $5\times10^{-5}$ torr is obtained. The QMF length was 100mm with a field radius of 5.33 mm, excited at 2.2 MHz. The ion energy was fixed to 5 *eV*. Figure 5.10 shows the Pfeiffer type QS422 QMS installed in a portable vacuum system.

The axial magnetic field is generated as before by applying a fixed value of current through a solenoid coil wrapped on the stainless steel chamber housing the QMF from a dc supply. All data were collected in analogue mode, and the mass range was set according to the mass of the gas under consideration. To demonstrate the effect of magnetic field in the *z*-direction on resolution of the QMF, $^{4}He^{+}$ mass peaks were obtained with and without the magnetic field $B_z$ applied. Figure 5.11 shows mass peaks obtained experimentally for $^{4}He^{+}$ using Pfeiffer type QS422 QMS. From Figure 5.11 it can be seen that there is an improvement in resolution at 10% peak height with magnetic field applied, from approximately R = 3.8 to R = 4.65 (*Bz* = 0.04T), a 30% increase in resolution.

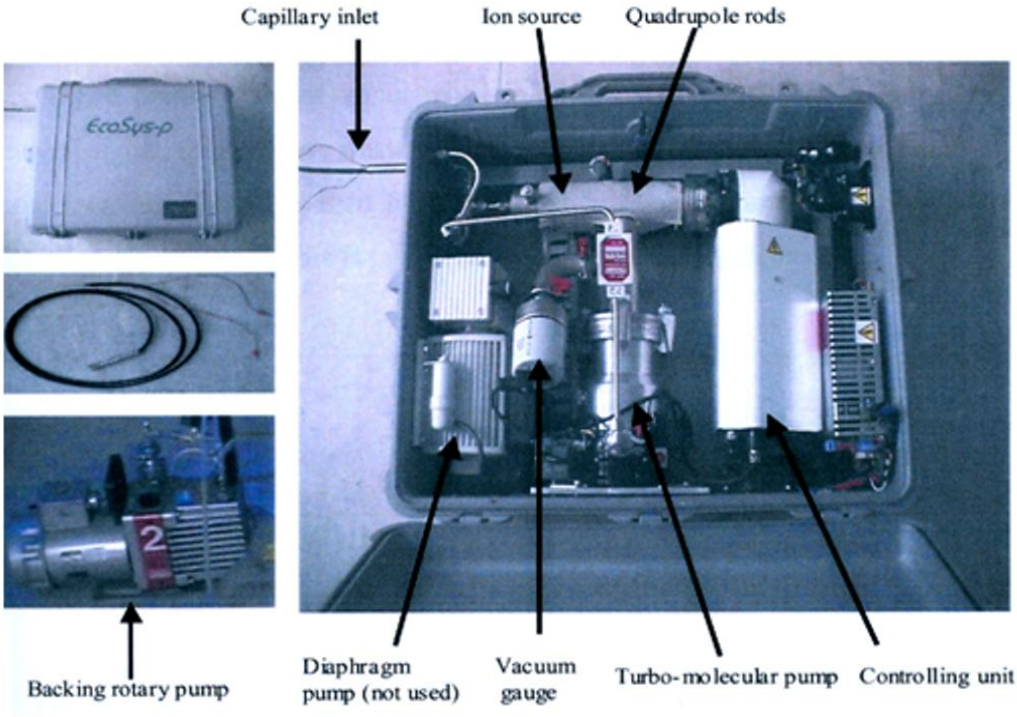


Figure 5.10: Pfeiffer type QS422 QMS installed in a portable vacuum system.

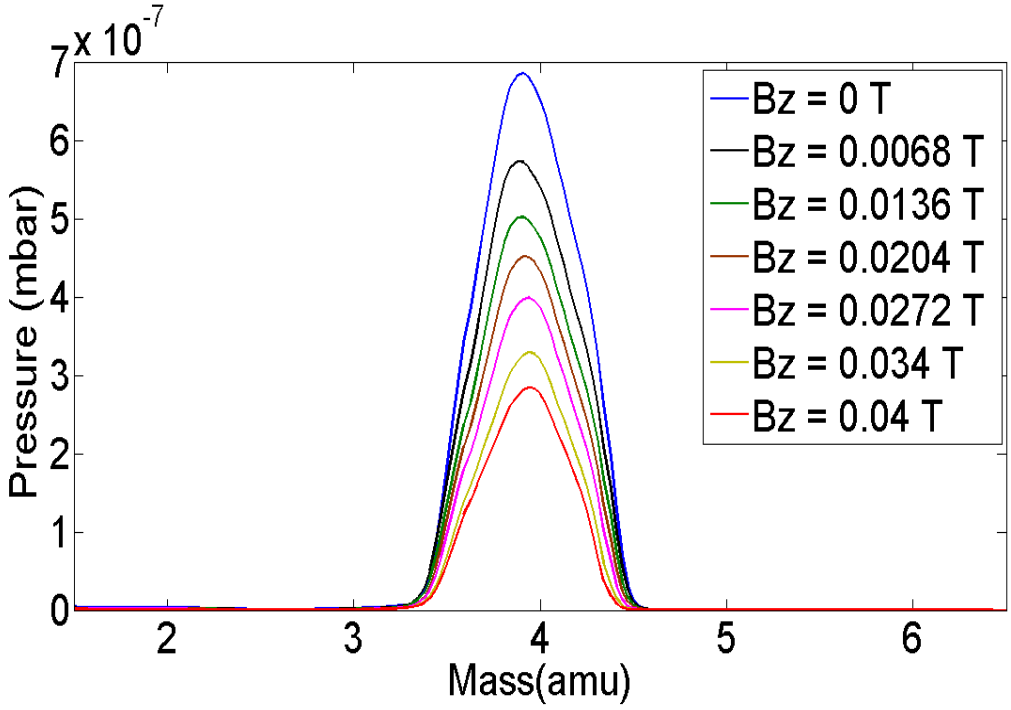


Figure 5.11: Experimental mass peaks for $^4He^+$ with and without an axial magnetic field applied obtained using Pfeiffer type QS422 QMS.

Figure 5.12 shows typical mass peaks obtained experimentally from the QMS for $Ar^+$ at different values of magnetic fields. Due to the EI, the parent atom breaks apart which is commonly known as the cracking/fragmentation pattern. This fragmentation pattern forms the mass spectrum, which aids identification of the gas atom. According to the cracking patterns for different gases, there will be different peaks (isotopes) displayed on the mass-to-charge ratio scale for different gases. For example, another Argon peak can be seen at *m/z* 20 from Figure 5.12.

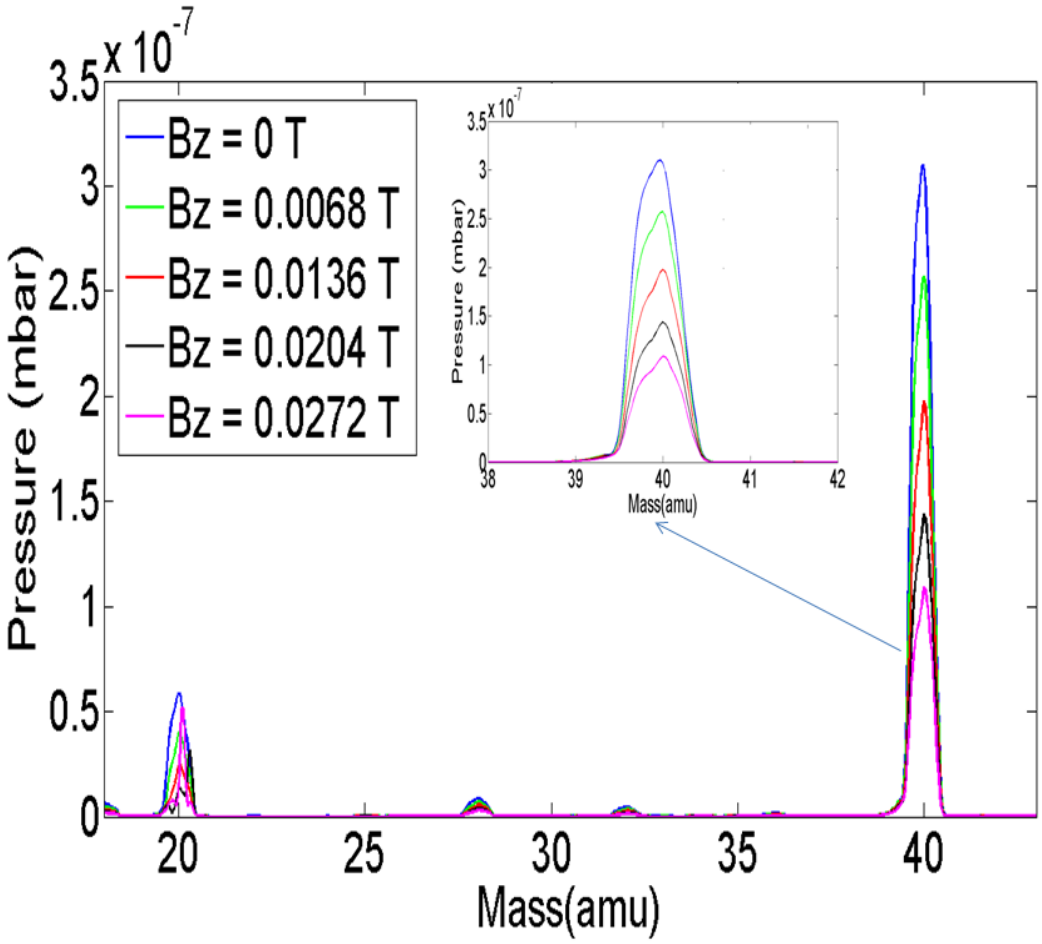


Figure 5.12: Typical mass peaks obtained for $Ar^+$ in the mixture with and without an axial magnetic field applied obtained using Pfeiffer type QS422 QMS.

During EI a majority of single ionized parent argon gas atoms ($Ar^{+}$) are created and there is a lower chance of doubly charged *Ar* atoms ($Ar^{++}$) being created. Thus, $Ar^{+}$ and $Ar^{++}$ form the mass spectrum of argon gas. In the mass spectrum shown in Figure 5.12, the *x*-axis displays mass to-charge ratio. $Ar^{+}$ is displayed at a mass-to-charge ratio of 40/+1 = 40 and $Ar^{++}$ is displayed at a mass-to-charge ratio of 40/+2 = 20. Inset shows typical mass peaks obtained for $^{40}Ar^{+}$ in the mixture at different values of magnetic fields. The maximum increase in resolution for $^{40}Ar^{+}$ was found to be approximately 10%. The resolution increase obtained for $^{40}Ar^{+}$ is lower than $^{4}He^{+}$ (approximately 30%). It should be noted that higher the mass of the ion, higher the value of magnetic field is required for same percentage increase in resolution. This dependency will be explained later in the chapter using the numerical model.

### 5.4.2 Simulation results

#### *5.4.2.1 The effect of magnetic field in the z- direction on ion trajectories*

The simulation program discussed in Chapter 4 includes a trace facility and this allows many details of individual ions to be recorded. Figure 5.13 shows typical behaviour of the ion trajectories calculated using the theoretical model for ions transmitted with and without the axial magnetic field applied. All the simulations were carried out in stability zone 1 (i.e., $a$ = 0.23699 and $q$ = 0.706). The corresponding traces shown in the figure are for the same ion injected into the mass filter at the same point in time (rf phase) and space and at the same point on the mass scale ($m$ = 39.96 *amu*). The upper trace of the figure is for the case with no field applied and lower trace with $B_z$ of 0.03 T.

Ion motion in Figure 5.13 originates at $x = 2.45 \times 10^{-4}$ *m* and $y = 7.70 \times 10^{-6}$ *m* with initial velocity of $4.90 \times 10^{3}$ *m/s*. In the lower trace, due to the Lorentz force provided by $B_z$, the amplitude of ion trajectory along *y*- direction increases and the amplitude of the trajectory oscillations in the *x*- direction decreases. The application of magnetic field therefore displaces the ion in the *y* direction so that the ion is lost through impact with the electrodes. It should be noted that ion motion in **both** the *x* and *y* directions is affected if the magnetic field is applied in the *z*- direction. This is in contrast to the case of magnetic field application in the *x*- direction, where ion motion only in *y*- direction is affected [5].

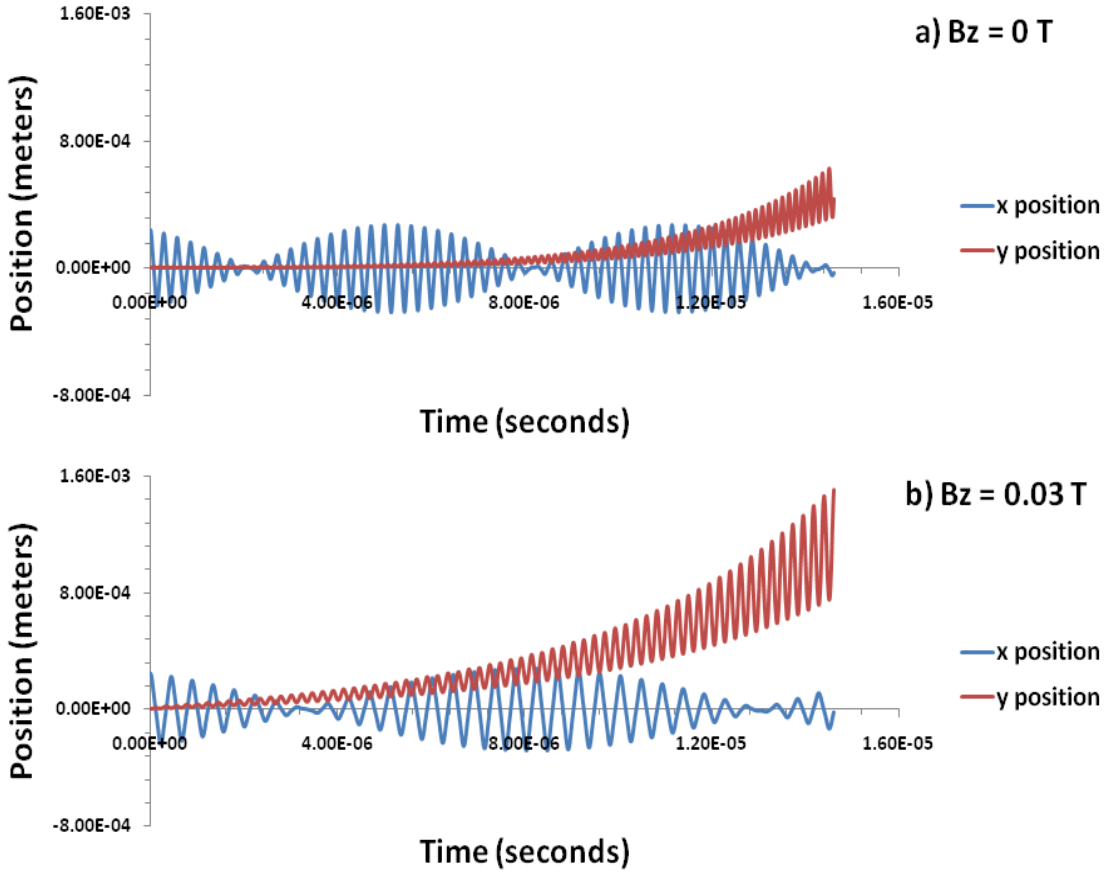


Figure 5.13: Numerical simulation of ion trajectories in x and y directions for $^{40}Ar^{+}$ with a) Bz = 0 T (upper trace) and b) Bz = 0.03 T (lower trace).

### *5.4.2.2 The effect of magnetic field in z- direction on the resolution of QMF*

The simulated mass peaks for $^{40}Ar^{+}$ ions using the computer software are shown in Figure 5.14. All the simulations used 200 steps across the mass range, with $1.5 \times 10^5$ ion trajectories run at each point on the peak. Mass peaks for $^{40}Ar^{+}$ are generated for a hyperbolic quadrupole mass filter with length ($l$) of 100 mm. The inscribed radius of the QMF was taken to be 1.5 mm. The frequency of the rf voltage used in the simulation was 5 MHz and the ion energy was chosen as 5 *eV*. The ion source radius ($r_{ie}$ ) was selected as 0.5 mm and the exit radius was chosen as 3 mm. The operating point (*U/V* ratio) was selected as 99.99%, where 100% corresponds to the intersection of the scan line with the peak of the Mathieu stability diagram at *U/V* = 0.168. Figure 5.14a shows the behaviour of the resolution, measured at 10 % peak height as a function of axial magnetic field for three different lengths of QMF. For *l*=100mm the resolution increases as *Bz* is varied between 0 - 0.035 T and then decreases as it is varied between 0.035 - 0.06 T, indicating that the QMF resolution will not increase indefinitely with *Bz*. This is because as *Bz* increases, the peak shape eventually degrades. A similar effect is seen for shorter and longer QMF: resolution rises with applied *Bz* reaching a maximum value, then decreases. In the case of *l*=200 mm the predicted value of resolution is in excess of 3000 which if achieved in practice would allow specialist high resolution RGA applications

Figure 5.14b shows a set of peaks for $^{40}Ar^{+}$ within a hyperbolic QMF at different values of magnetic field (*Bz*) for a QMF of length *l*=100 mm. An increase in resolution is clearly observed up to a magnetic field of 0.035T. Transmission through the QMF decreases as magnetic field increases, which results in reduction of QMF resolution at higher values of magnetic field 0.045 - 0.06 T. A low-amplitude structure is present across the low mass and high mass sides of the mass peaks, due to minor changes in the acceptance of the QMF as the

position of the mass scan changes. This is because the initial phase space positions of a large number of ions are very close to the QMF acceptance boundary, resulting in small local variations of transmission as the mass scan traverses the mass peak. This observed structure on the peak is an artifact of the simulation and can be reduced by increasing the number of ions although at the expense of increased simulation time.

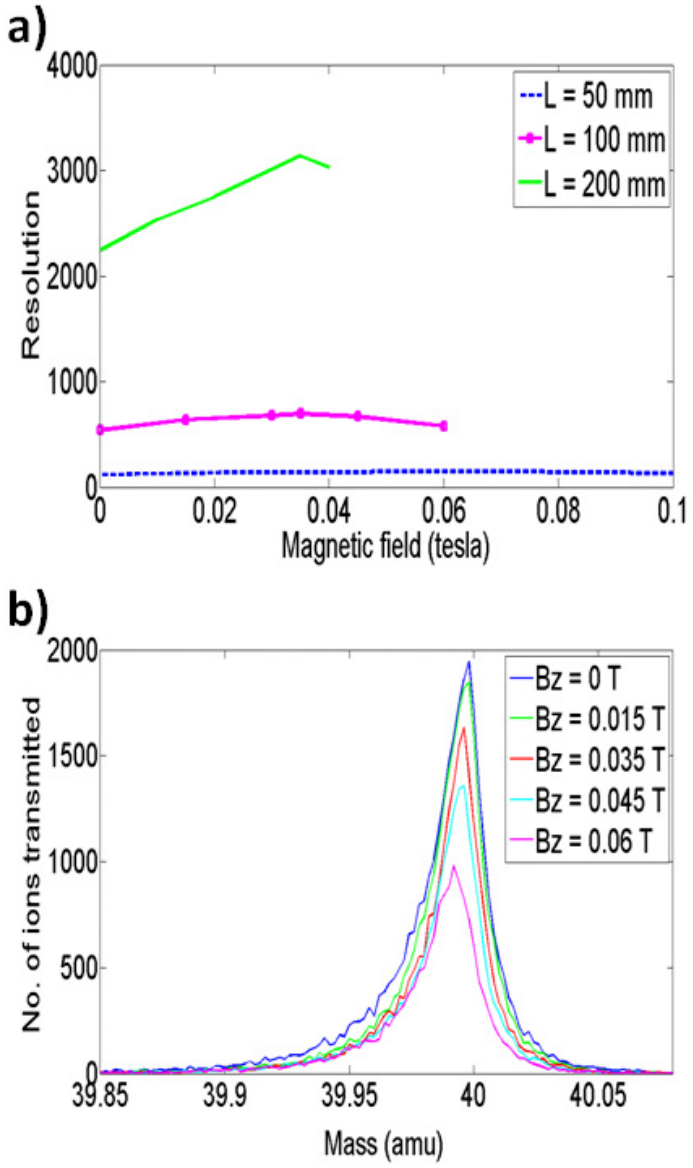


Figure 5.14: (a) The effect of magnetic field on resolution applied in z- direction (hyphenated *l*= 100mm, dotted *l*=50mm, solid line *l*=200) (b) Simulated mass peaks for $^{40}Ar^{+}$ with and without magnetic field for *l* = 100 mm.

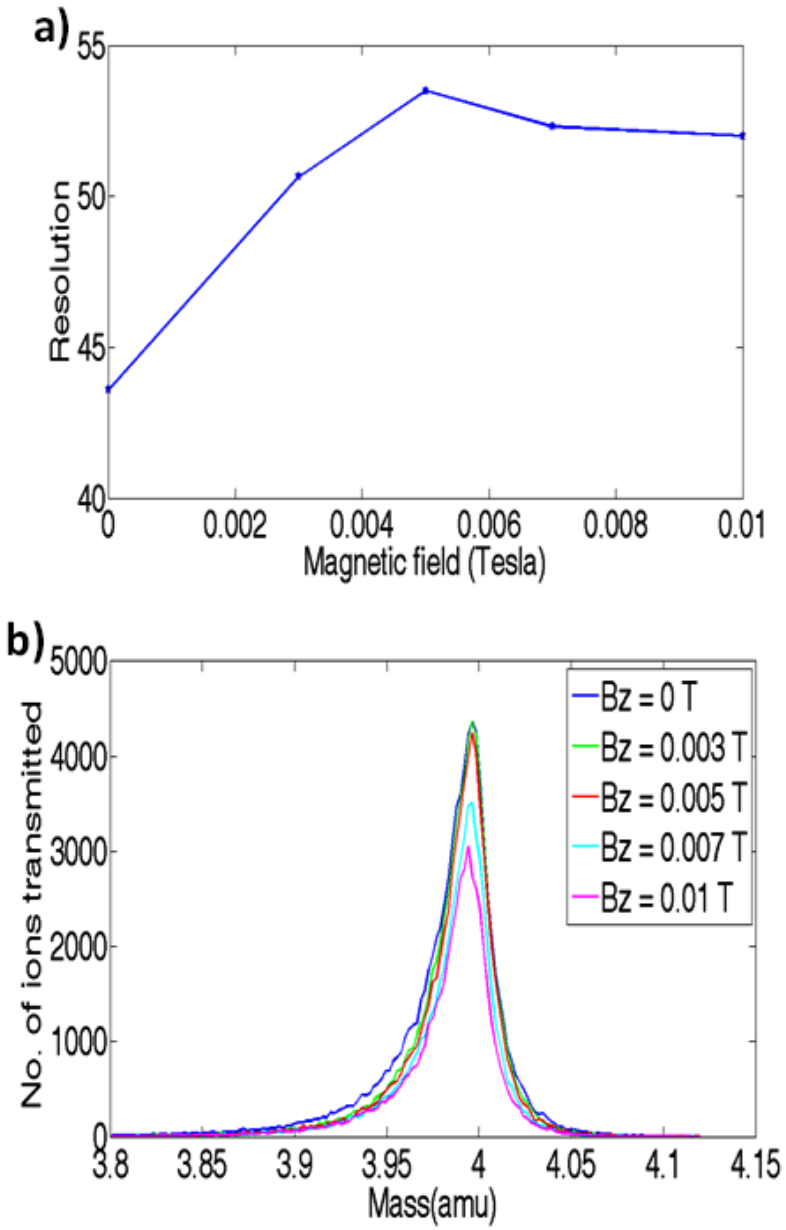


Figure 5.15: (a) The effect of magnetic field on resolution applied in z- direction for $^4He^+$ (b) Simulated mass peaks for $^4He^+$ with and without magnetic field.

Figure 5.15a shows the behavior of the resolution, measured at 10 % peak height as a function of axial magnetic field for $^4He^+$ ions. The length of the QMF was taken as 100mm. Resolution increases as *Bz* is varied between 0 - 0.005 T and then decreases as it is varied between 0.005 - 0.01 T, indicating that the QMF resolution will not increase indefinitely with

*Bz*. Figure 5.15b shows a set of peaks for $^{4}He^{+}$ within a hyperbolic QMF at different values of magnetic field (*Bz*). An increase in resolution is clearly observed up to a magnetic field of 0.005T. Transmission through the QMF decreases as magnetic field increases, which results in reduction of QMF resolution at higher values of magnetic field 0.005 - 0.01 T.

### *5.4.2.3 The performance of the QMS and the effect of ion energy on resolution in the presence of magnetic field in the z – direction*

Figure 5.16a shows the dependence of resolution on number of rf cycles with and without an applied magnetic field. The relationship between resolution and number (*N*) of rf cycles is well known and is given by $M/\Delta M = N^{n}/K$, where *n* is the slope and *K* is a constant [10]. For simulations without the magnetic field the value of *n* was found to be 2.05 and that of *K* to be about 27. For simulations with $B_z$ = 0.03 T, the value of *n* was found to be 2.18 and that of *K* to be about 40. These results clearly indicate that the predicted performance of the QMS increases in the presence of an axial magnetic field. Figure 5.16b shows the dependence of resolution on ion energy for $^{40}Ar^{+}$ with and without magnetic field applied. As can be seen from the Figure 5.16b, in both cases, resolution decreases with increase in ion energy. However, it can also be observed that percentage increase in resolution with magnetic field decreases as ion energy increases. An increase of approximately 24.5 % in resolution at 2 *eV* can be seen, whereas an increase of only 19.5 % at 10 *eV* is seen at the same value of magnetic field applied.

The effect can be best demonstrated with the help of ion trajectories in the presence of magnetic field at different ion energies. Figures 5.17 and 5.18 show trajectories of ions transmitted with and without magnetic field, at ion energies of 2 and 10 *eV* respectively. The

corresponding traces shown in the figures are for the same ion injected into the QMF at the same point in time (rf phase) and space and at the same point on the mass scale (m = 40.00 *amu*). In both figures the upper trace is for the case with no field applied and lower trace with *Bz* of 0.03 T. In Figure 5.17 the ion motion originates at $x = -2.03 \times 10^{-4}$ *m* and $y = -2.15 \times 10^{-4}$ *m* with initial velocity of $3.10 \times 10^{3}$ *m/s*. It can be seen from the figure that in the presence of magnetic field at lower ion energy (2 *eV*) ion motion in both the directions is affected. It is also seen that the amplitude of ion motion in the *x*- direction increases, whereas the amplitude in *y*- direction decreases.

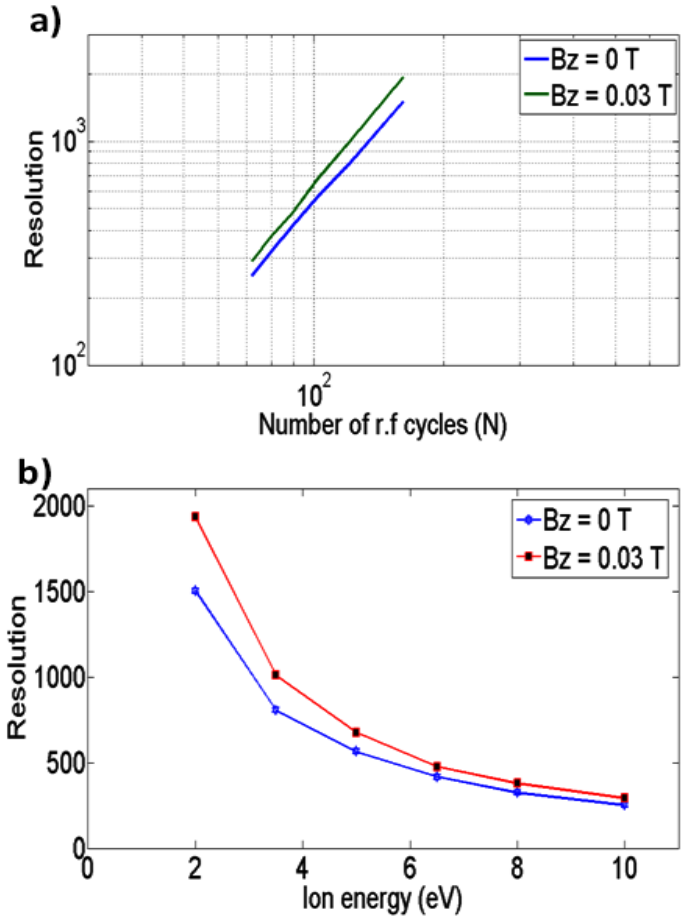


Figure 5.16: (a) The dependence of resolution on number of rf cycles with and without an applied magnetic field (b) The dependence of resolution on ion energy with and without an applied magnetic field.

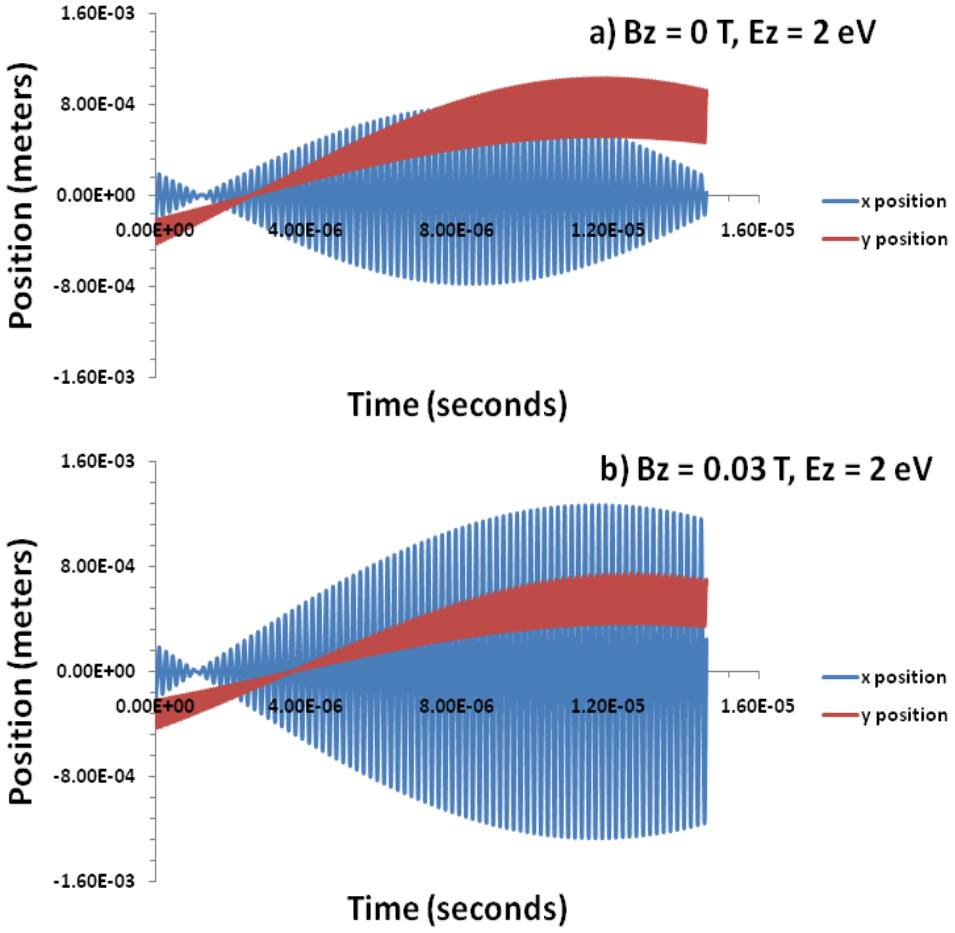


Figure 5.17: Numerical simulation of ion trajectories in x and y directions for $^{40}Ar^{+}$ with $E_z$ = 2 *eV* and with a) Bz = 0 T (upper trace) and b) Bz = 0.03 T (lower trace).

In Figure 5.18 the ion motion originates at $x = 2.94 \times 10^{-4}$ *m* and $y = -1.78 \times 10^{-4}$ *m* with initial velocity of $6.93 \times 10^{3}$ *m/s*. It can be observed from the figure that increase in ion energy has a major impact on behaviour of ion trajectories in the presence of magnetic field. It can be seen that ion motion in the *x*- direction remains unaffected, while ion motion in the *y*- direction is modified. It can be concluded that for a QMF with magnetic field applied in the *z*- direction, the effect of magnetic field on resolution is greater at lower ion energies. This is due to the increased length of time that the ion experiences the magnetic field.

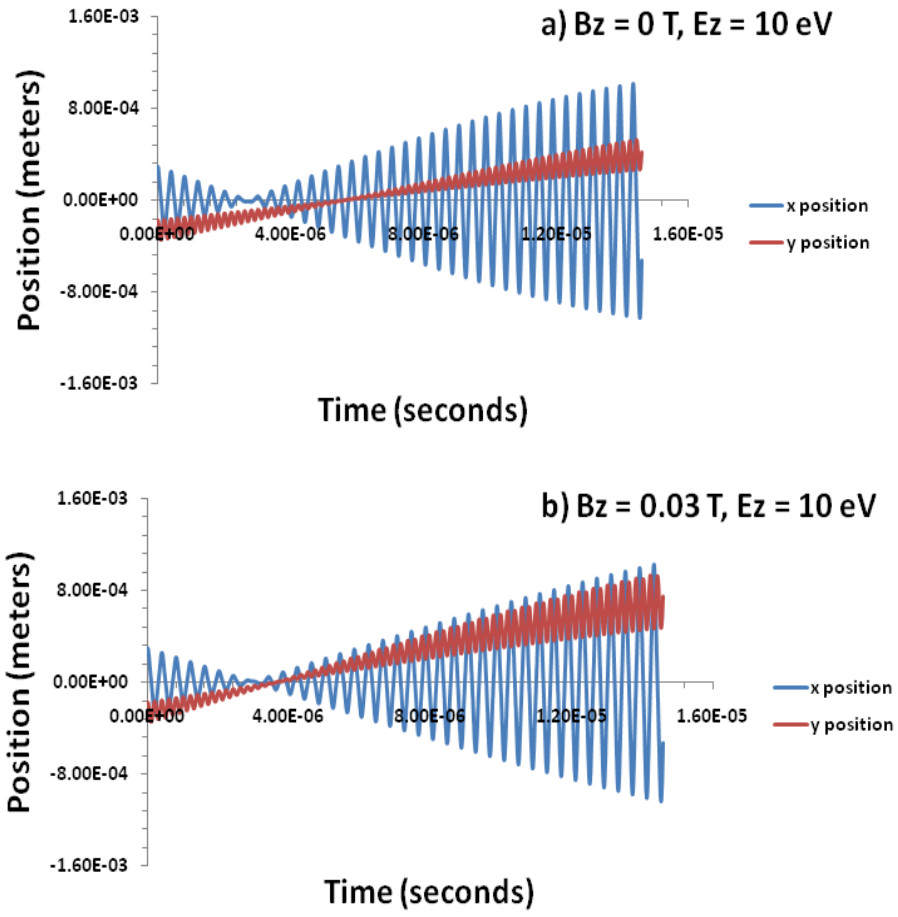


Figure 5.18: Numerical simulation of ion trajectories in x and y directions for $^{40}Ar^{+}$ *with* $E_z$ = 10 *eV* and with a) Bz = 0 T (upper trace) and b) Bz = 0.03 T (lower trace).

### *5.4.2.4 The effect of frequency on resolution in the presence of magnetic field in the z – direction*

Figure 5.19 shows the dependence of resolution on frequency for $^{40}Ar^{+}$ with and without magnetic field applied. As can be seen from the Figure 5.19, in both cases, resolution increases with increase in frequency. However, it can also be observed that percentage increase in resolution with magnetic field increases as frequency increases. An increase of

approximately 7.2 % in resolution at 2 MHz can be seen, whereas an increase of 20.3 % at 8 MHz is seen at the same value of magnetic field applied.

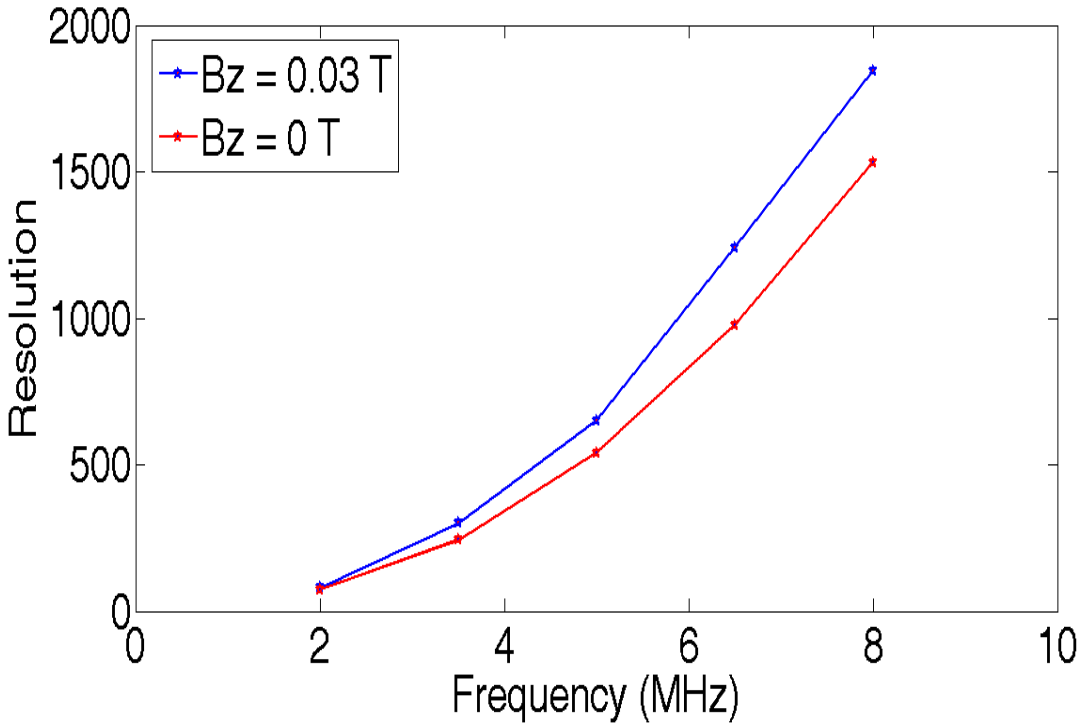


Figure 5.19: The dependence of resolution on frequency with and without an applied magnetic field.

The effect can be best demonstrated with the help of ion trajectories in the presence of magnetic field at different frequencies. Figures 5.20 and 5.21 show trajectories of ions transmitted with and without magnetic field, at frequencies of 2 and 8 MHz respectively. The corresponding traces shown in the figures are for the same ion injected into the QMF at the same point in time (rf phase) and space and at the same point on the mass scale (m = 39.99 *amu*). In both figures the upper trace is for the case with no field applied and lower trace with *Bz* of 0.03 T. In Figure 5.20 the ion motion originates at $x = -2.07 \times 10^{-4}$ *m* and $y = -3.65 \times$

$10^{-5}$ *m* with initial velocity of $4.90 \times 10^{3}$ *m/s*. It can be seen from the figure that in the presence of magnetic field at lower frequency (2 MHz) ion motion in both the directions is affected. It is also seen that the amplitude of ion motion in the *x*- direction gets slightly affected, whereas the amplitude in *y*- direction increases. However, the ion passes through the QMF.

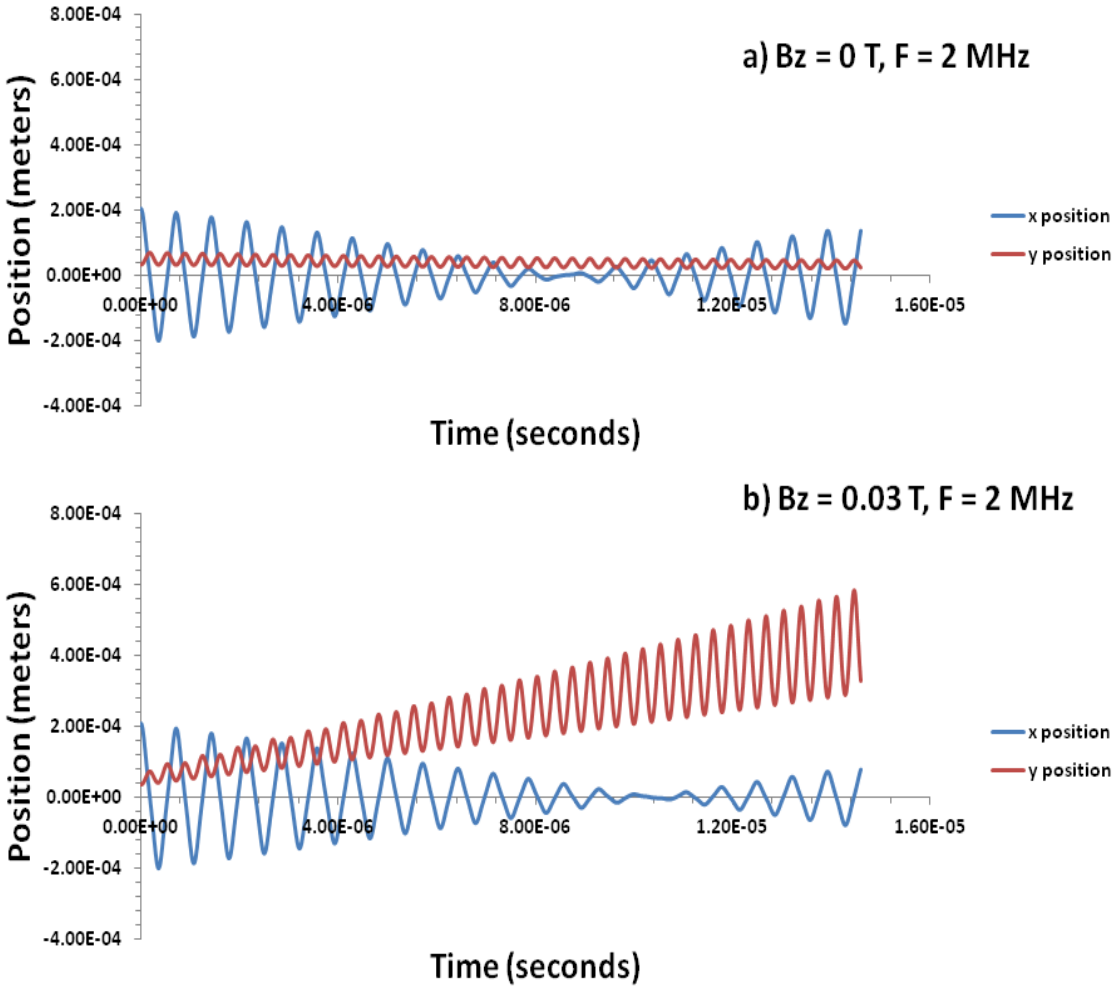


Figure 5.20: Numerical simulation of ion trajectories in x and y directions for $^{40}Ar^{+}$ with $f$ = 2 MHz and with a) Bz = 0 T (upper trace) and b) Bz = 0.03 T (lower trace).

In Figure 5.21 the ion motion originates at $x = -2.07 \times 10^{-4}$ *m* and $y = -3.64 \times 10^{-5}$ *m* with initial velocity of $4.90 \times 10^{3}$ *m/s*. It can be seen from the figure that in the presence of magnetic field at higher frequency (8 MHz) the amplitude of ion trajectory along *y*- direction increases and the amplitude of the trajectory oscillations in the *x*- direction remains nearly same. Nevertheless, the application of magnetic field therefore displaces the ion in the *y* direction so far that the ion is lost through impact with the electrodes ($r_0$ =1.5mm), thus contributing to a high percentage increase in resolution with higher frequencies.

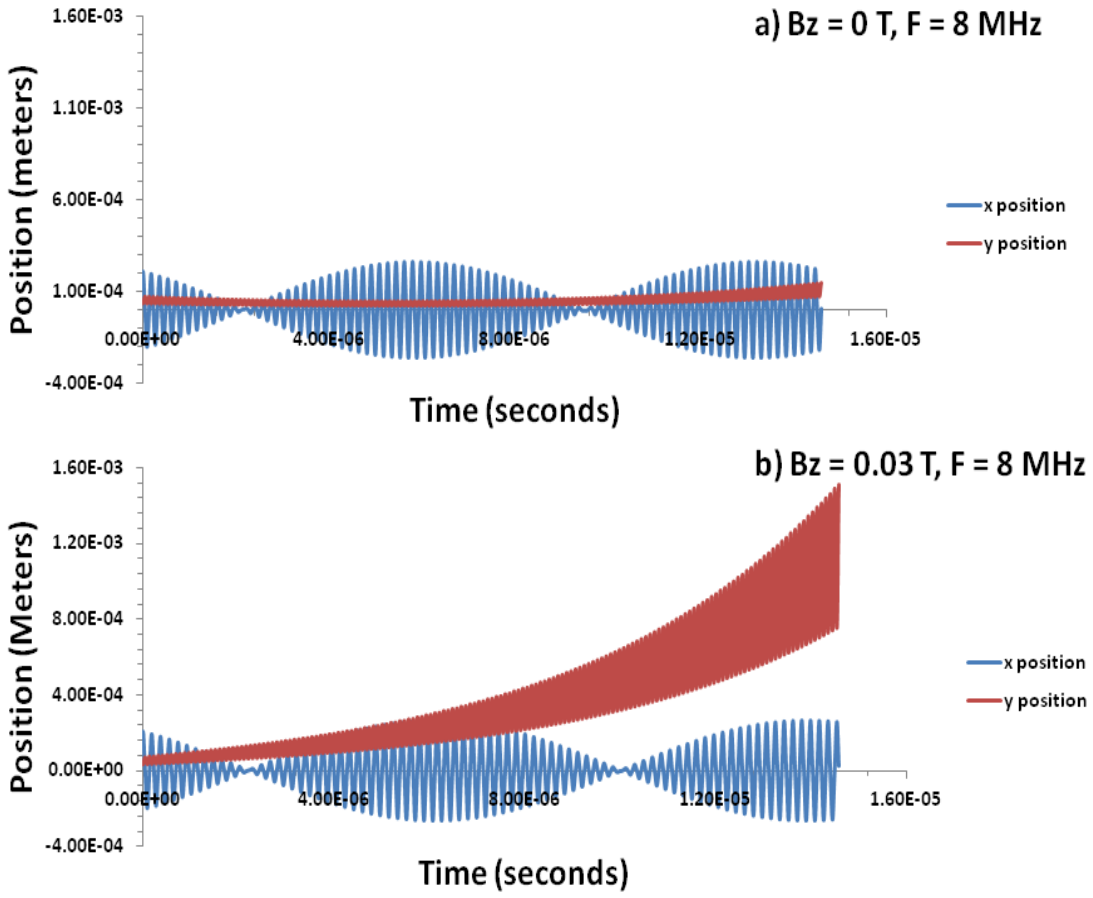


Figure 5.21: Numerical simulation of ion trajectories in x and y directions for $^{40}Ar^{+}$ with *f* = 10 MHz and with a) Bz = 0 T (upper trace) and b) Bz = 0.03 T (lower trace).

### *5.4.2.5 The dependence of mass on resolution increase in the presence of magnetic field in the z – direction*

Magnetic field required for approximately 24.5 % increase in resolution for $^{4}He^{+}$, $^{40}Ar^{+}$, and $^{132}Xe^{+}$ has been investigated. Figure 5.22 shows the dependence of axial magnetic field required for a given increase in resolution on mass of the ion. It is observed that a higher value of magnetic field is required for same percentage increase in resolution as the mass of the ion increases.

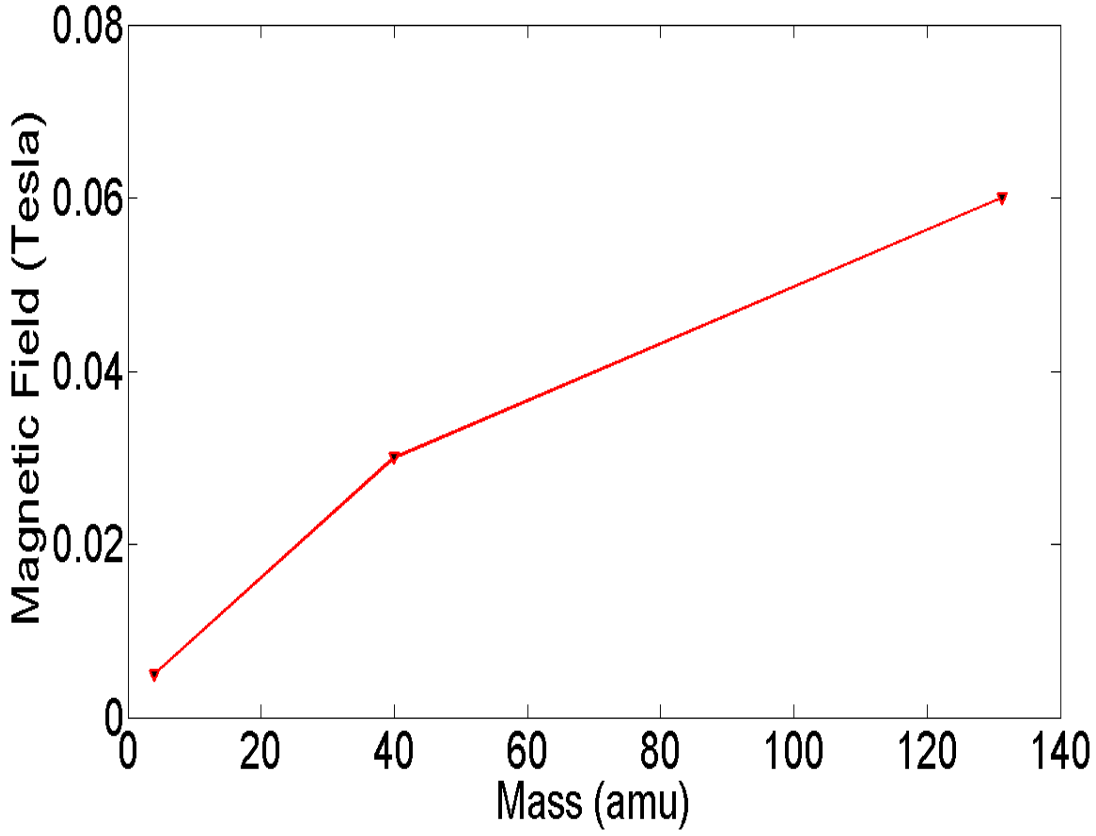


Figure 5.22: Magnetic field required for approximately 24.5 % increase in resolution for $^{4}He^{+}$, $^{40}Ar^{+}$, and $^{132}Xe^{+}$.

## 5.5 Effect of a transverse magnetic field on the performance of a Quadrupole Mass Spectrometer

Previously reported experimental works with QMF and the applied transverse magnetic field were carried out at low *U/V* ratio [1, 2]. Nowadays, since the commercially available QMS systems operate at a high *U/V* ratio; to take precise measurements with transverse magnetic field applied, a QMF with a tuneable electronics (*U/V* ratio), static electromagnets incorporated in *x* pair of electrodes along the length of the mass filter, and magnetic shielding to ion-source and detector are required. However since experimentation to optimise QMS performance can be time consuming and costly, QMS simulation using our numerical model offers many advantages.

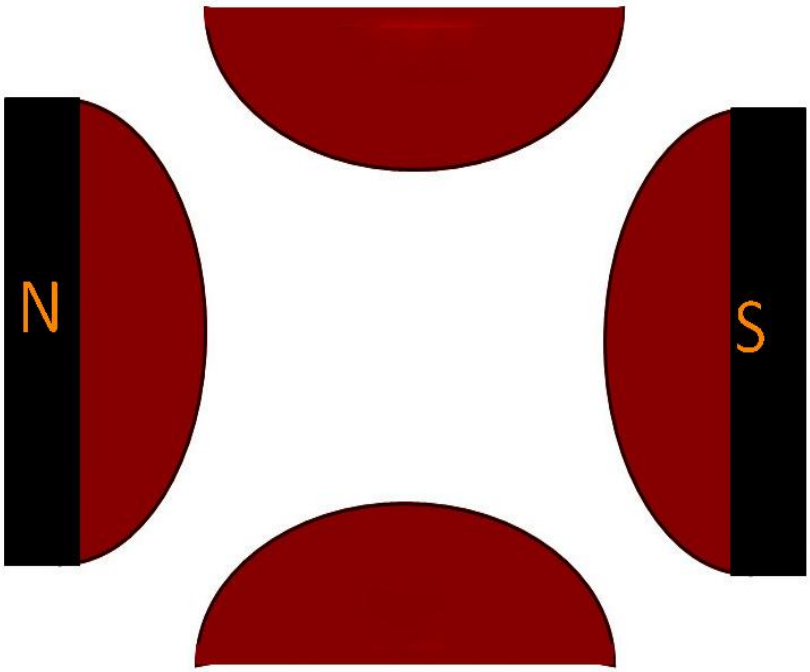


Figure 5.23: Schematic view of QMF electrodes with static magnets in transverse x-direction.

This section reports a study on a quadrupole mass spectrometer in which a static magnetic field is applied transversely to the body of the mass filter assembly. Previous experimental work showed this effect for Argon and the results were explained in terms of the additional Lorentz force on injected ions as a consequence of the magnetic field [1, 2]. Significant improvement in QMS performance was obtained under certain magnetic field conditions, and these have been explained in terms of our theoretical model. Our analysis also predicts for what values of operating parameters an enhancement of the quadrupole resolution is achieved when a transverse magnetic field is applied. Figure 5.23 shows a schematic diagram of QMF electrodes with static magnets in transverse *x*-direction.

### *5.5.1The effect of U/V ratio on the performance of QMF with applied magnetic field in the x- direction*

Reported in Figure 5.24 are the simulated mass peaks for $^{40}Ar^{+}$ ions generated using the computer software. All the simulations used 150 steps across the mass range, with $2.5 \times 10^5$ ion trajectories run at each point on the peak. Mass peaks for $^{40}Ar^{+}$ are generated for a hyperbolic quadrupole mass filter with length ($l$) of 100 mm. The inscribed radius of the QMF was taken to be 2.6 mm. The frequency of the rf voltage used in the simulation was 4 MHz and the ion energy was chosen as 5 *eV*. The ion source radius ($r_{ie}$ ) was selected as 0.5 mm and the exit radius was chosen as 5.2 mm.

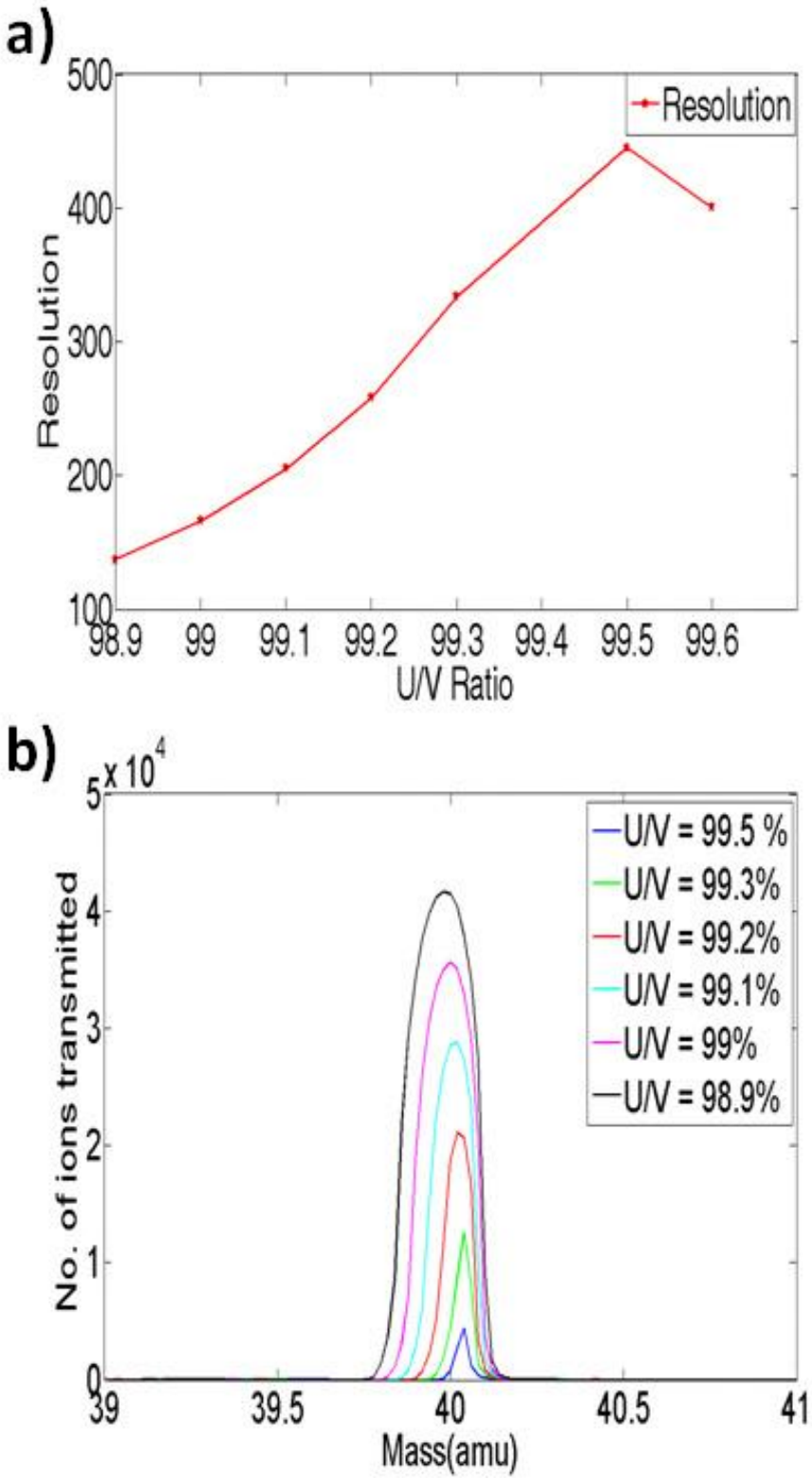


Figure 5.24: a) shows the dependency of resolution on *U/V* ratio in the presence of transverse magnetic field in the *x* direction (*Bx* = 0.02 T), b) shows set of peaks for $^{40}Ar^{+}$ within a hyperbolic QMF at different values of *U/V* ratio with magnetic field applied in the *x*-direction

Figure 5.24a shows the dependency of resolution on *U/V* ratio in the presence of transverse magnetic field in the *x* direction (*Bx* = 0.02 T), the resolution increases as *U/V* ratio is varied between 98.9 – 99.5%, however the QMF resolution will not increase indefinitely with *U/V* ratio. This is because as *U/V* ratio increases, the peak shape eventually degrades. In the case of *U/V* ratio = 99.5%, the predicted value of resolution in the presence of magnetic field is in excess of 480, if achieved in practice, is 50% higher than the resolution (320) obtained for a QMF operating without magnetic field with the same number of rf cycles at *U/V* ratios near to the peak of Matheiu Stability diagram for zone 1. This results show that at certain value of *U/V* ratios there is a resolution enhancement upon application of transverse magnetic field. Figure 5.24b shows set of peaks for $^{40}Ar^{+}$ within a hyperbolic QMF at different values of *U/V* ratio with magnetic field applied in the *x*-direction. An increase in resolution is clearly observed at the expense of reduction in number of ions transmitted.

### *5.5.2 The effect of magnetic field in the x direction on the resolution of QMF*

Figure 5.25a shows the behaviour of the resolution as a function of transverse magnetic field for *U/V* ratio 99.5%. The resolution increases as *Bx* is varied between 0 - 0.002 T, however the QMF resolution will not increase indefinitely with *Bx*. This is because as *Bx* increases, the peak shape eventually degrades. This results show that at any fixed value of *U/V* ratio (The limit of which depends upon operating conditions) there is a resolution enhancement by simply applying transverse magnetic field to the body of the mass filter.

Figure 5.25b shows a set of peaks for $^{40}Ar^{+}$ within a hyperbolic QMF at different values of magnetic field applied in the *x*-direction. An increase in resolution is clearly observed up to a magnetic field of 0.02T at the expense of reduction in number of ions

transmitted. There is also a reduction in the low mass tail of the mass spectra with a magnetic field.

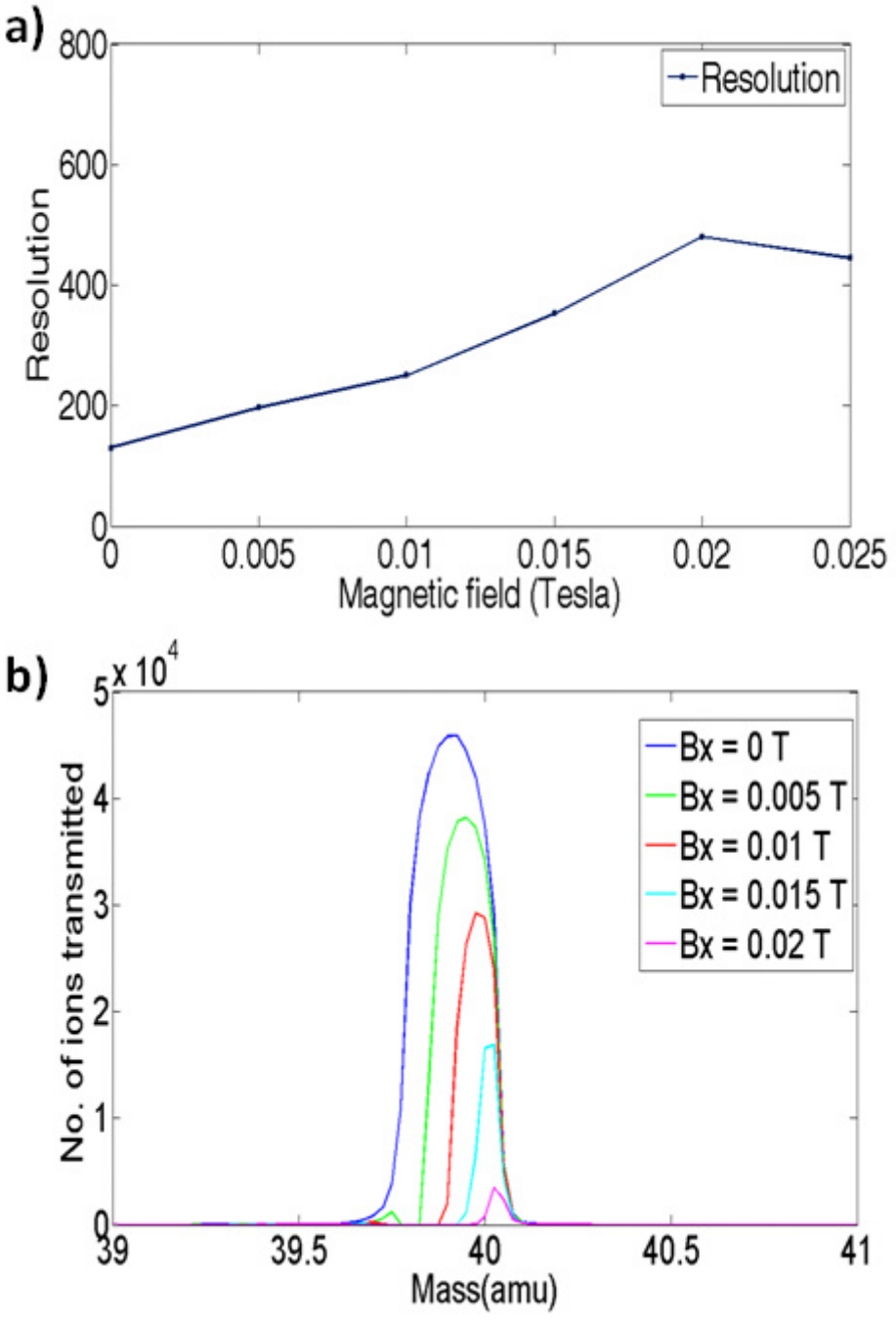


Figure 5.25: (a) The effect of magnetic field on resolution of $^{40}Ar^{+}$ applied in *x*- direction for *U/V* 99.5%, (b) Simulated mass peaks for $^{40}Ar^{+}$ with and without magnetic field for *U/V* 99.5%.

Figure 5.26 shows set of peaks for $^{40}Ar^{+}$ at different values of magnetic field for *U/V* ratio 99.99%. As seen from Figure 5.26, upon application of very small magnetic fields the mass spectrum suffers from post cursor peak, degradation in the peak and loss of sensitivity. The ideal operating point is different in the presence of magnetic field in the *x* direction because the tip of the stability diagram is different as stability parameters *a* and *q* have dependence on **B**. Moreover, it also depends upon the operating parameters of the QMF which will be explained in the following sections.

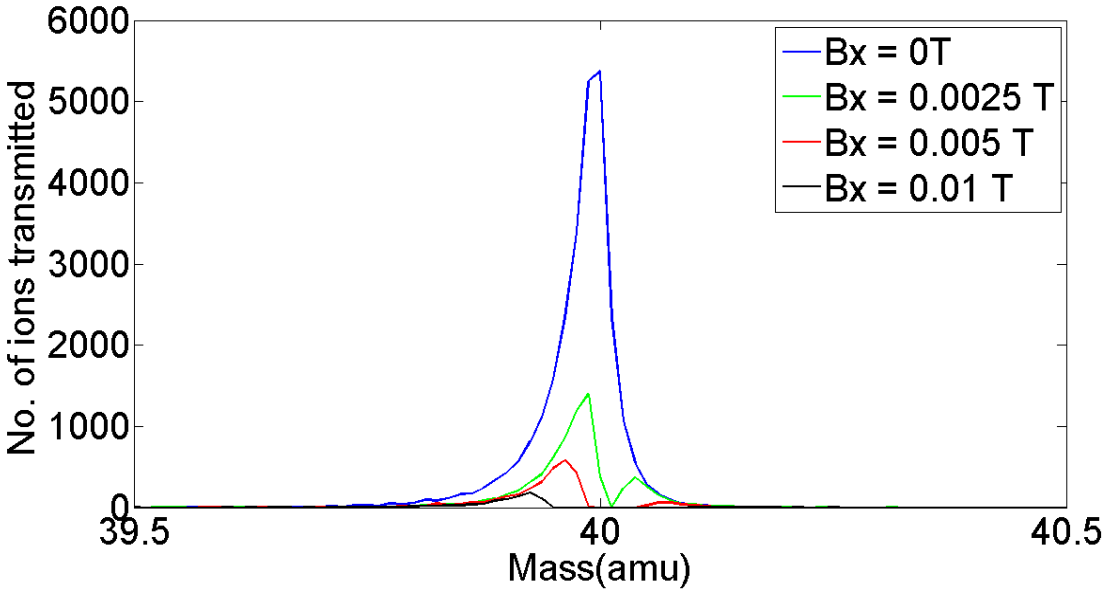


Figure 5.26: Simulated mass peaks for $^{40}Ar^{+}$ with and without magnetic field for *U/V* 99.99%.

### *5.5.3 The effect of magnetic field in the x direction on ion trajectories*

Figure 5.27 shows typical behaviour of the ion trajectories calculated using the theoretical model for ions transmitted with and without the transverse magnetic field applied. The corresponding traces shown in the figure are for the same ion injected into the mass filter at

the same point in time (rf phase) and space and at the same point on the mass scale (m = 39.91 *amu*). The upper trace of the figure is for the case with no field applied and lower trace with $B_x$ of 0.02 T.

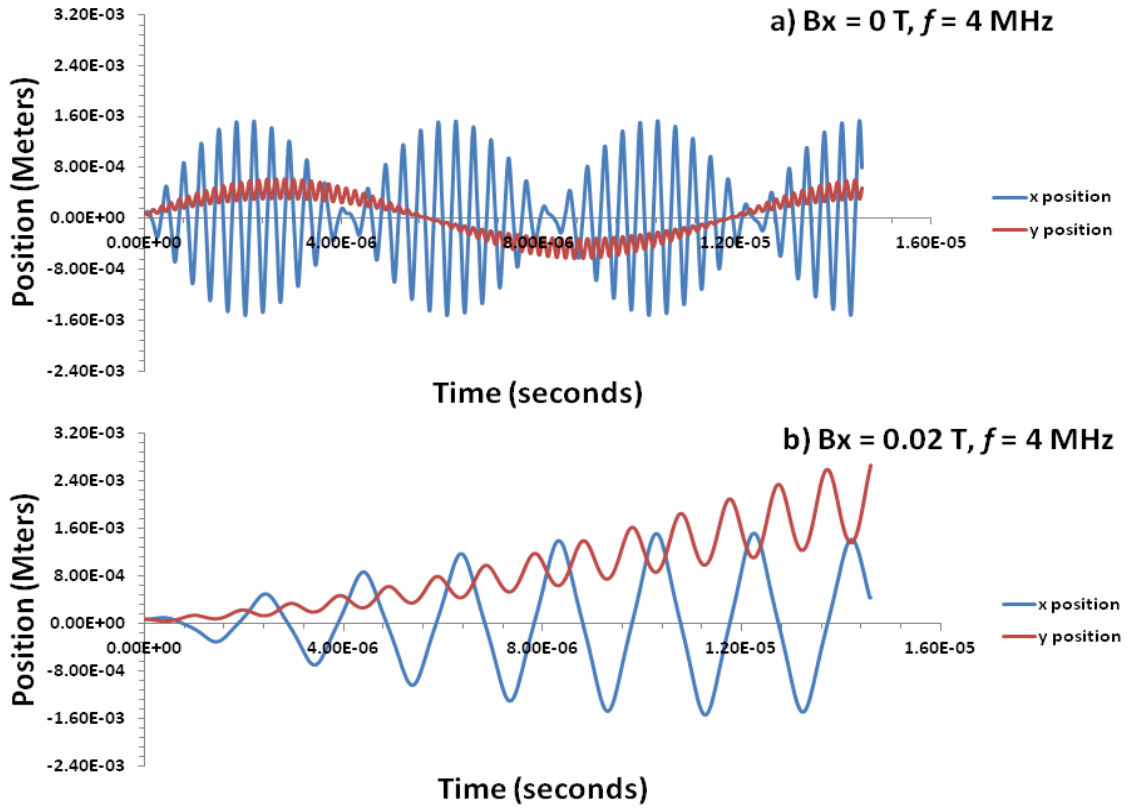


Figure 5.27: Numerical simulation of ion trajectories in x and y directions for $^{40}Ar^{+}$ with a) $B_x$ = 0 T (upper trace) and b) $B_x$ = 0.02 T (lower trace).

Ion motion in Figure 5.27 originates at $x = 7.77 \times 10^{-5}$ *m* and $y = 8.7 \times 10^{-5}$ *m* with an initial velocity of $4.90 \times 10^{3}$ *m/s*. In the lower trace, due to the Lorentz force provided by $B_x$, the amplitude of ion trajectory in *y*- direction increases; however ion trajectory in the *x*-direction remains unaffected. The application of magnetic field therefore displaces the ion in the *y* direction so that the ion is lost through impact with the electrodes. It should be noted that ion motion in *x* direction (parallel to field) is unaffected; it is ion motion in the *y*

direction (perpendicular to the field) which is modified, and this is to be expected since the ion motion is subjected to Lorentz force $F = q\ (E + v \times B)$ where $v$ is the instantaneous velocity.

### *5.5.4 The effect of frequency on resolution of QMF in the presence of magnetic field in the x direction*

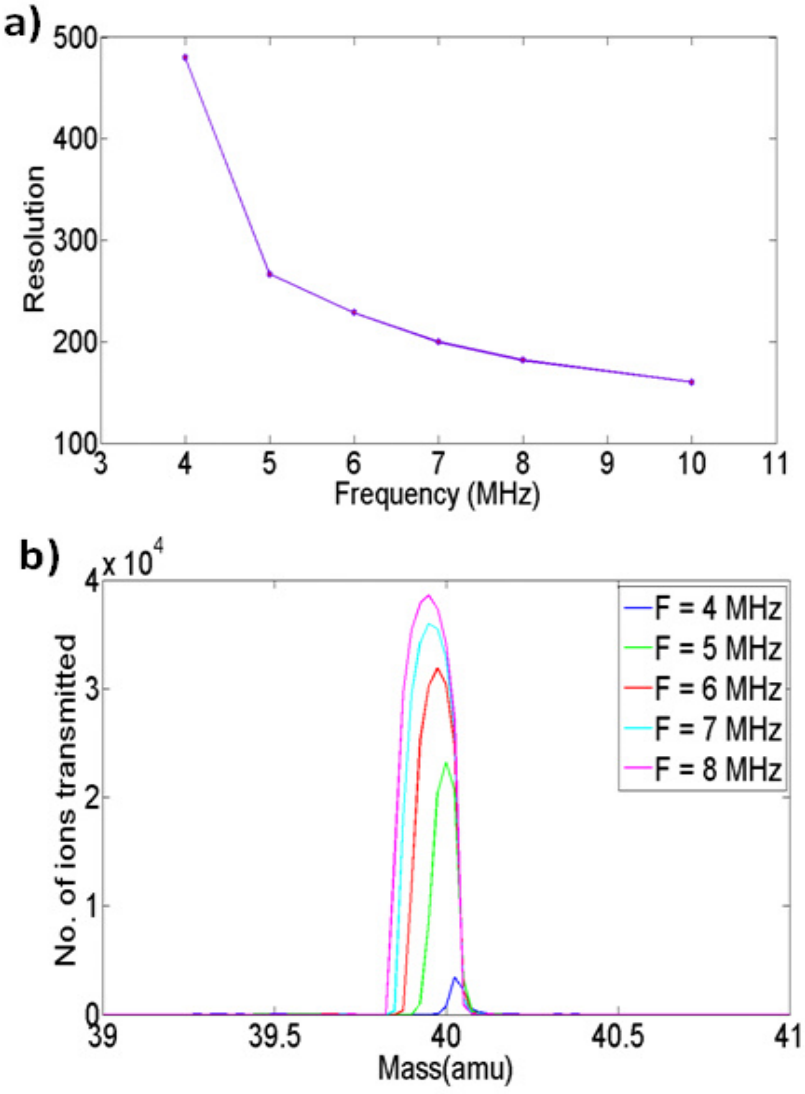


Figure 5.28: a) the dependence of resolution on frequency with an applied magnetic field; b) mass peaks for $^{40}Ar^{+}$ at different frequencies with applied magnetic field of $Bx$ = 0.02 T.

Figure 5.28 shows the effect of frequency on resolution in the presence of a magnetic field. With a transverse magnetic field applied, the effect of frequency of the rf signal on resolution is very different to that normally observed in a conventional QMF. The resolution ***decreases*** with increase in frequency and transmission increases. This effect is due to the Lorentz force provided in the transverse direction by the magnetic field. Figure 5.28a shows the dependence of resolution on frequency with an applied magnetic field; whereas, Figure 5.28b shows mass peaks for $^{40}Ar^{+}$ at different frequencies with applied magnetic field of $Bx$ = 0.02 T.

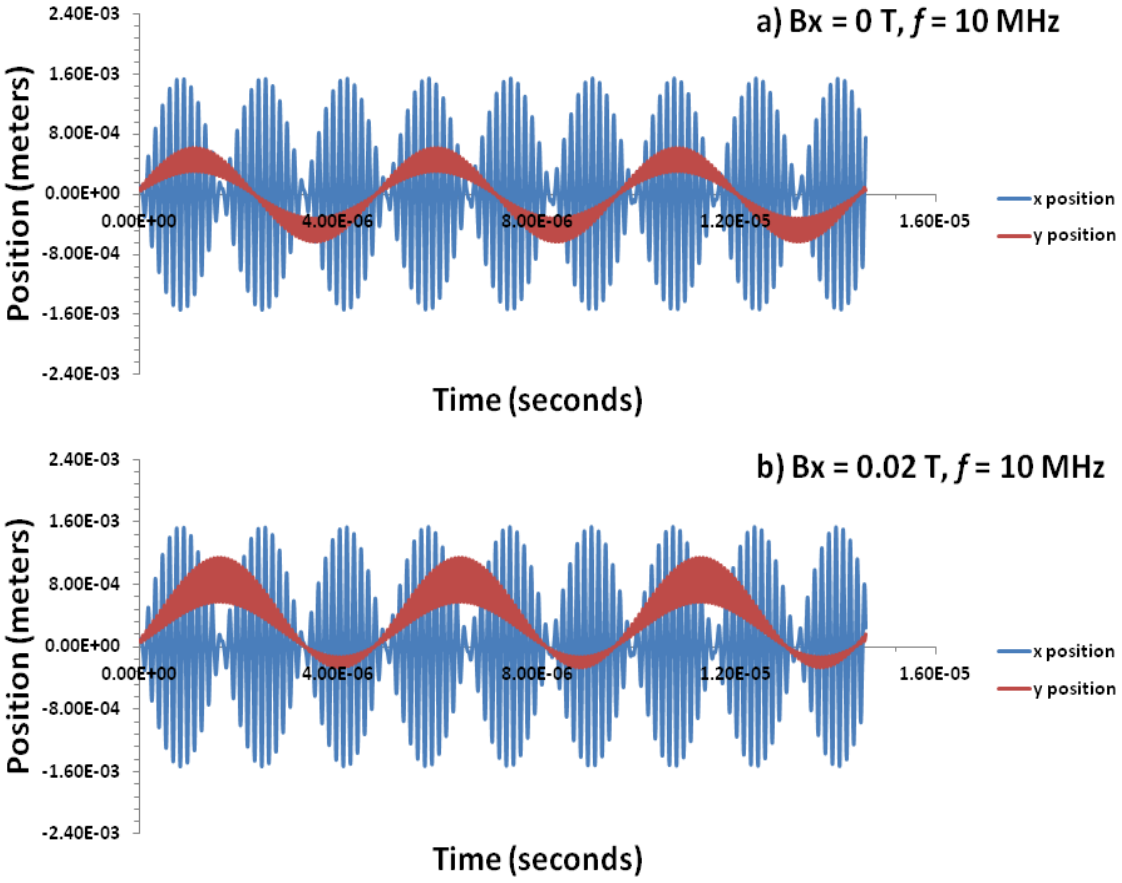


Figure 5.29: Numerical simulation of ion trajectories in x and y directions for $^{40}Ar^{+}$ with $f$ = 10 MHz and with a) $B_x$ = 0 T (upper trace) and b) $B_x$ = 0.02 T (lower trace).

The effect can be best demonstrated with the help of ion trajectories in the presence of a transverse magnetic field at different frequencies. Figures 5.27 and 5.29 show trajectories of ions transmitted with and without magnetic field, at frequencies of 4 and 10 MHz respectively. The corresponding traces shown in the figures are for the same ion injected into the QMF at the same point in time (rf phase) and space and at the same point on the mass scale (m = 39.91 *amu*). In both figures the upper trace is for the case with no field applied and lower trace with $B_x$ of 0.02 T. In Figure 5.27 the ion was lost through impact with the electrodes.

In Figure 5.29 the ion motion also originates at $x = 7.77 \times 10^{-5}$ *m* and $y = 8.70 \times 10^{-5}$ *m* with the same initial velocity of $4.90 \times 10^{3}$ *m/s*. It can be observed from the figure that increase in frequency has a major impact on behaviour of ion trajectories in the presence of magnetic field. It can be seen that ion motion in the *x*- direction remains unaffected and the amplitude of ion motion along *y*- axis only slightly increases. Therefore, the ion was successfully transmitted in the presence of the magnetic field at the higher frequency of 10 MHz. In this case although the magnetic field is same as Figure 5.27 ($B_x$ = 0.02 T) the ion mean velocity in the *y* direction is greater since the frequency is greater, and the component of Lorentz force correspondingly greater in axial direction $F_z = -qv_yB_x$. Thus reducing the total Lorentz force provided by the magnetic field in the *x*- direction on the ion at higher frequencies, since $F = qB_x(v_z - v_y)$. It can be concluded that for a QMF with magnetic field applied in the *x*- direction, the effect of magnetic field on resolution enhancement is greater at lower frequencies.

### *5.5.5 The effect of ion energy on resolution of QMS in the presence of magnetic field in the x direction*

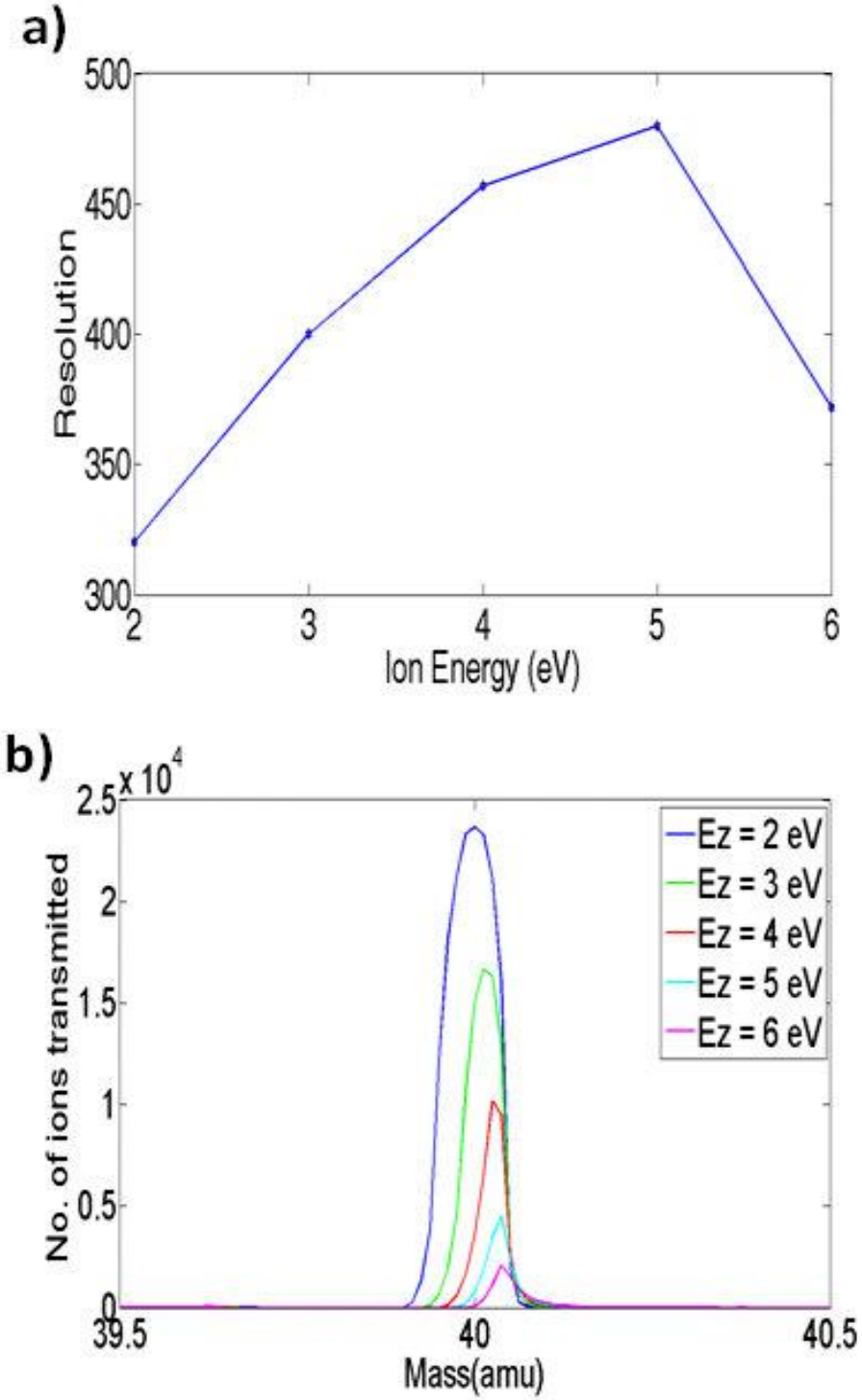


Figure 5.30: a) the dependence of resolution on ion energy with an applied magnetic field; b) mass peaks for $^{40}Ar^{+}$ at different ion energies with applied magnetic field of $Bx$ = 0.02 T.

Figure 5.30 shows the effect of ion energy on resolution in the presence of a magnetic field. With a transverse magnetic field applied, the effect of ion energy on resolution is ***different*** to that normally observed in a conventional QMS. The resolution increases with increase in ion energy from 2-5 eV and then decreases. This effect is attributed to the Lorentz force provided in the transverse direction by the magnetic field. Figure 5.30a shows the dependence of resolution on ion energy with an applied magnetic field; whereas, Figure 5.30b shows mass peaks for $^{40}Ar^{+}$ at different ion energies with applied magnetic field of $Bx$ = 0.02 T.

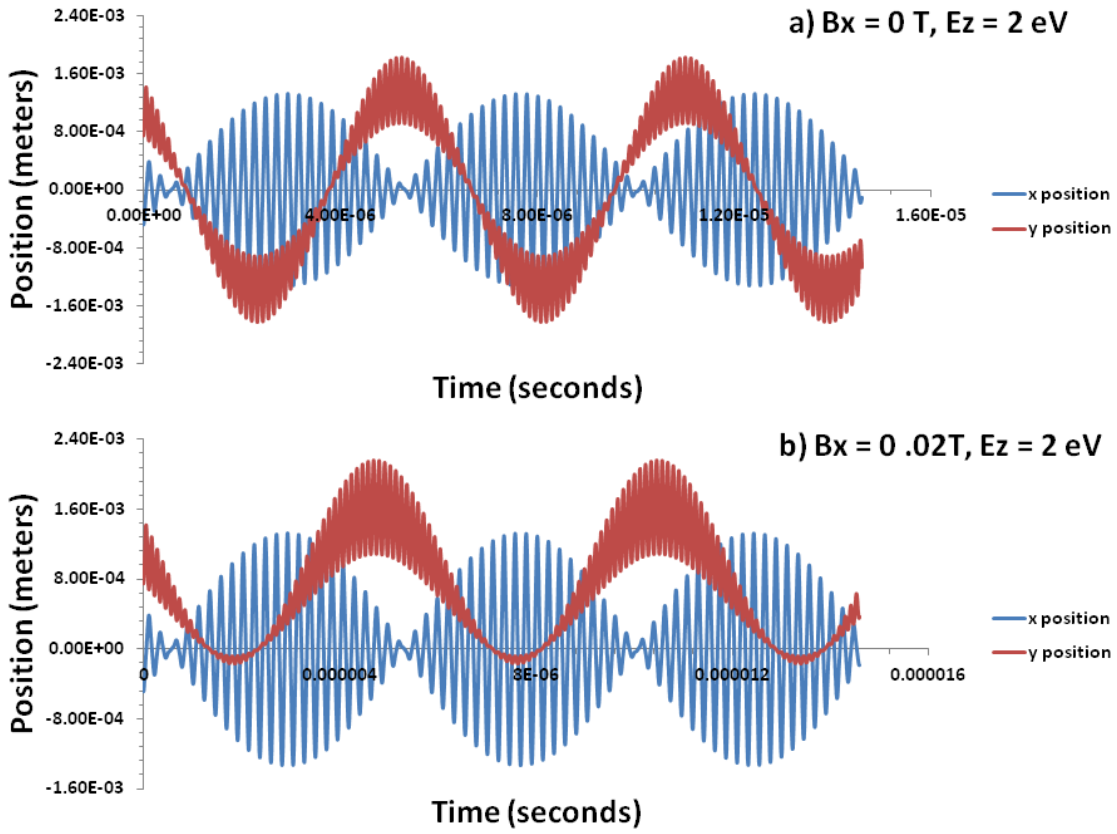


Figure 5.31: Numerical simulation of ion trajectories in x and y directions for $^{40}Ar^{+}$ with $Ez$ = 2 eV and with a) $B_x$ = 0 T (upper trace) and b) $B_x$ = 0.02 T (lower trace).

The effect can be best demonstrated with the help of ion trajectories in the presence of a transverse magnetic field at different ion energies. Figures 5.31 and 5.32 show trajectories of ions transmitted with and without magnetic field, at ion energies of 2 and 5 eV respectively. The corresponding traces shown in the figures are for the same ion injected into the QMF at the same point in time (rf phase) and space and at the same point on the mass scale ($m$ = 40.00 *amu*). In both figures the upper trace is for the case with no field applied and lower trace with $B_x$ of 0.02 T.

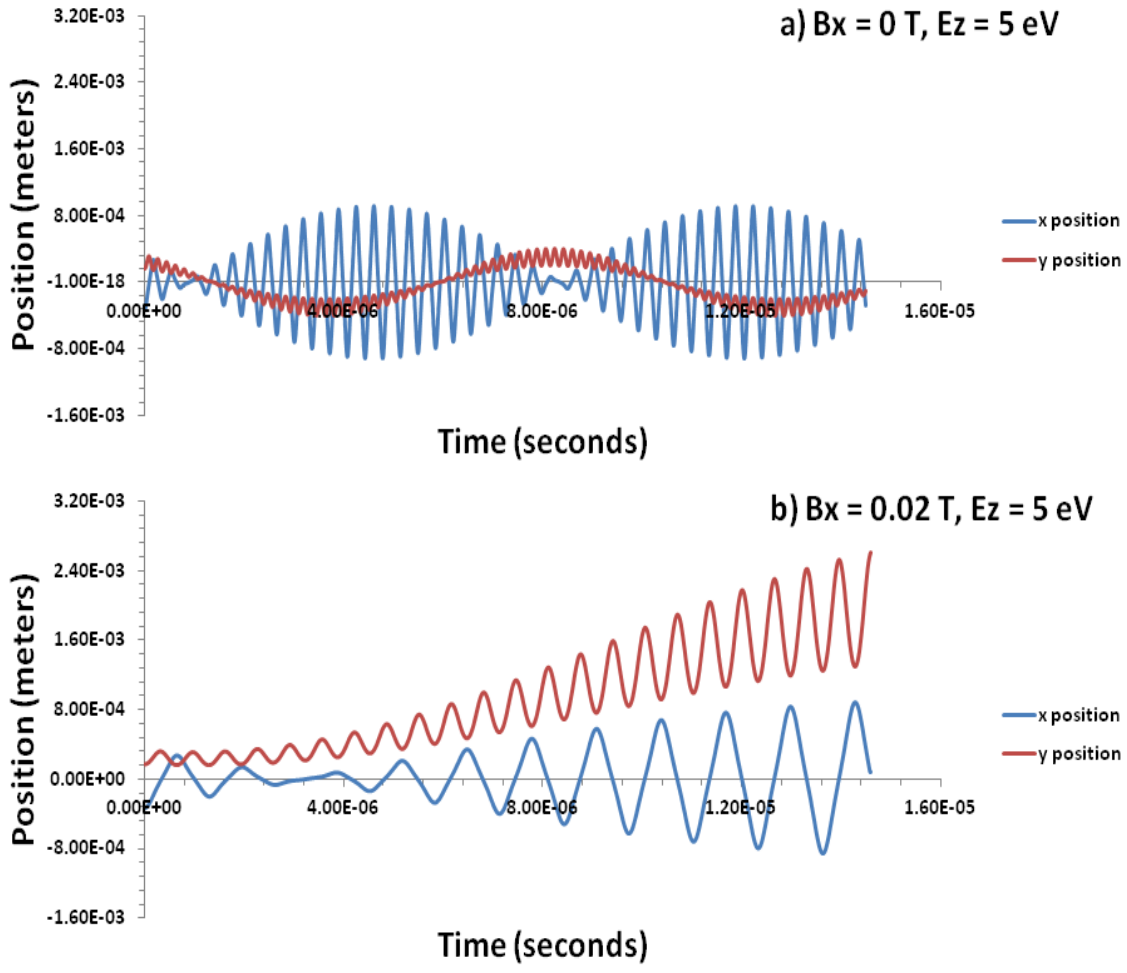


Figure 5.32: Numerical simulation of ion trajectories in x and y directions for $^{40}Ar^{+}$ with $E_z$ = 5 *eV* and with a) *Bx* = 0 (upper trace) and b) *Bx* = 0.02 T (lower trace).

Ion motion in Figure 5.31 originates at $x = -4.84 \times 10^{-4}$ *m* and $y = 7.45 \times 10^{-4}$ *m* with initial velocity of $3.10 \times 10^{3}$ *m/s*.It can be seen from the figure that in the presence of magnetic field at lower ion energy (2 *eV*) ion motion in *y* direction is affected; however, the increase in amplitude of ion trajectory in *y* direction is not sufficient for the ion to be rejected by colliding with the electrodes. In Figure 5.32 the ion motion also originates at $x = -3.35 \times 10^{-4}$ *m* and $y = 1.64 \times 10^{-4}$ *m* with the same initial velocity of $4.90 \times 10^{3}$ *m/s*. It can be observed from the figure that increase in ion energy (5 *eV*) has a major impact on behaviour of ion trajectories in the presence of magnetic field. The amplitude of ion trajectory in *y* direction increases so far that the ion is lost by upon collision with electrodes. It can be concluded that for a QMF with magnetic field applied in the *x* direction, the effect of magnetic field on resolution enhancement is greater at higher ion energies because of increased Lorentz force due to the velocity component.

### *5.5.6 The effect of length on mass spectra in the presence of magnetic field in the x direction*

The length of the QMF also plays an important role in the presence of transverse magnetic field. As the *U/V* ratio increases the length should be sufficiently long enough to produce mass spectrum without pre or postcursors. Figure 5.33 shows mass spectra for a magnetic field of $Bx = 0.02$ and *U/V* ratio of 99.5%. As seen from figure at lengths 50 mm and 75 mm, a precursor occurs and this effect can be attributed to the less time ions spend inside the field to reduce the low mass tail appropriately. As the length increases the peak shape starts to get better and the precursor vanishes. Also it should be noted again that that in the presence of magnetic field, **B** has further dependence on all QMF operating and geometrical parameters depending upon the orientation of the field.

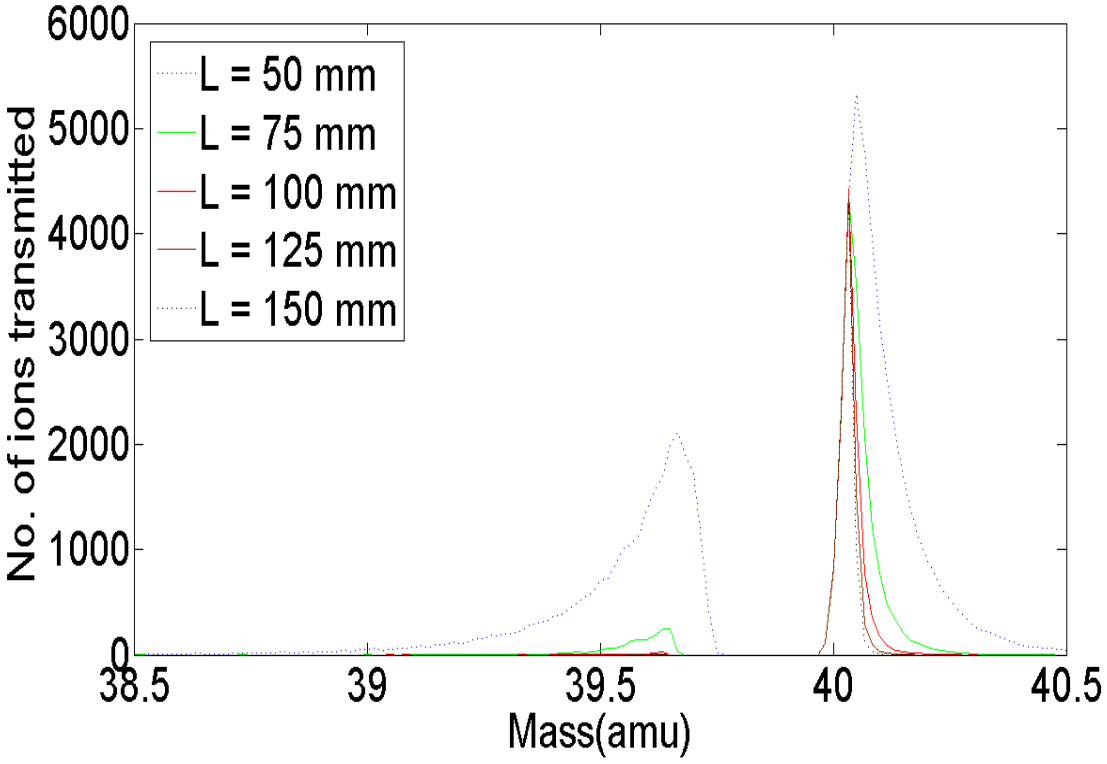


Figure 5.33: Mass peaks for $^{40}Ar^{+}$ at different ion energies with applied field of $Bx$ = 0.02 T.

## 5.6 Conclusions

Experimental results for a low resolution QMS instrument show an increase in resolution when a static, ***axial*** magnetic field is applied along the mass filter in the *z*- direction. This enhanced resolution observed experimentally has been simulated theoretically using our numerical model, which solves the equation of motion for individual ions injected into the QMF with a magnetic field applied. By determining the ion trajectories for a large number of ions (>$10^5$), individual mass spectra may be simulated. Also, simulation results for a QMS have been presented showing the effect of ***transverse*** magnetic field in the *x* direction, applied along the whole length of the mass filter. The effects of different input parameters such as variation of ion energy, drive frequency and electrode length under the influence of

transverse magnetic field have been examined and remain the subject of ongoing investigation.

The experimental results in both cases (axial and transverse magnetic field) may be explained by considering the additional Lorentz force produced by ion motion in the magnetic field. All ions oscillating transversely to the applied magnetic field will experience a Lorentz force in addition to the time varying electrostatic force due to alternating quadrupole field. The resulting complex trajectories result in rejection of ions in the low mass tail in addition to the high mass tail depending of the orientation of the magnetic field. This gives increased resolution for a given set of operating parameters. High resolutions (R > 3000) are predicted for a single filter QMF of length 200 mm with an applied magnetic field in axial *z* - direction of *Bz* = 0.03 T. This increase in performance allows wider instrument application.

**References**


1. Tunstall, J.J.; Taylor, S.; Vourdas, A.; Leck, J.H.; Batey, J. Application of static magnetic field to the mass filter of a quadrupole mass spectrometer. *Vacuum*, 1999, *53*, 211-213.
2. Srigengan, B.; Gibson, J.R.; Taylor, S. Ion trajectories in quadrupole mass spectrometer with a static transverse magnetic field applied to mass filter. *IEE Proc-Sci. Meas. Technol*. 2000, 147 (6), 2000, 274-278.
3. Poritsky, H.; Gerrard, J.P. An integrable case of electron motion in electric and magnetic field. *J. A_pul.. Ph.v s.* 1952, *23, (8*), 928-930.

4. Pavlenko, Y.G.; Toporoba, A.N. New mass spectrometer quadrupole in a magnetic field. *Rudiotekh. Electron.* 1996, *41*, 508-512.
5. Gooden J.K.; Rempel D.L.; Gross, M.L. Evaluation of Different Combinations of Gated Trapping, RF-Only Mode and Trap Compensation for In-Field MALDI Fourier Transform Mass Spectrometry. *Journal of the American Society for Mass Spectrometry*. 2004, *15*, 1109-1115.
6. Purcell, E.M. *Electricity and magnetism*. Berkeley Physics Course, 2, US, 1985.
7. Jiles, D. *Introduction to magnetism and magnetic materials*. Chapman & Hall, US, 1998.
8. Grant, I.S.; Phillips, W. R. *Electro-magnetism*. Wiley, Manchester (UK), 1997.
9. John D. Kraus, *Electromagnetics*, McGraw-Hill, New York, 1991.
10. Dawson, P.H. *Quadrupole mass spectrometry and its applications*, Elsevier: Amsterdam 1976.

# Chapter 6

# Quadrupole Mass Spectrometer in the Third Stability Zone with Magnetic Field Applied

## 6.1 Introduction

Most commercial quadrupole mass spectrometers operate in stability zone 1 (*a = 0.237, q = 0.706*) [1]. However, there are certain advantages such as mass spectral peak shape, reduction of low mass tails and increase resolution to be obtained if the QMS is operated in the third stability zone. Stability zone 3 requires higher operating voltages, which have previously been seen as a disadvantage. Nevertheless, with the introduction of miniature QMFs, the increased voltage budget currently may not be an obstacle anymore [2]. There are number of applications that require high resolution, for example the quantitative measurement of hydrogen isotopes in the presence of helium isotopes. This usually requires a minimum resolution of 930 depending upon which isotopes are to be distinguished [3-5]. These resolutions especially at the lower end of the mass range (1-6 *amu*) are not readily achievable with commercially available QMS instruments.

Stability zone 3 is a sloping rectangular area providing two tips, one at the upper left (*a = 3.16, q = 3.23*), and second at lower right (*a= 2.52, q = 2.82*) corners that enable high resolution mass scanning to be achieved [6]. With stability zone 3 the ions require a lower exposure to number of rf cycles to achieve the same resolution as compared with zone 1 [7].

Du *et al* investigated the use of the third stability region for inductively coupled plasma mass spectrometry ICP-MS. Resolution of up to 4000 was obtained for *m/z* 59 *amu* with operation at the upper tip. This resolution is not generally high enough to separate atomic ions from molecular ion interferences. However, operation at a moderate resolution (e.g. 500-1000) measured at 50% peak height was found to give very high abundance sensitivity and it was concluded that operation of QMF in zone 3 may be advantageous for specialized applications in ICP-MS [8].

Later research showed elemental analysis with quadrupole mass filters operated in higher stability regions, and it was concluded that there is an increase in resolution when QMF is operated in higher stability regions [7]. Hogan and Taylor performed computer simulation with a large number of ions ($10^8$) to investigate the operation of QMS in first and third stability zones, and it was concluded that QMS operation in zone 3 provides an improved immunity from the effects of the variation in the value of electrode radius $r$ to field radius $r_0$ which is referred as $(r / r_0)$ compared to zone 1 [2]. More recently, Sreekumar *et al* performed simulations for a QMS operated in zone 3 with large number of ions ($>10^7$) to achieve a required resolution for the qualitative and quantitative identification of low mass isotopes in the mass range 1-6 *amu* [9].

In this chapter the application of magnetic field to the mass filter will be considered in addition to the conventional electric fields when operating in stability zone 3. It will be assumed in the model that the QMS contains hyperbolic rods as electrodes and the magnetic field is applied along the full length of the mass filter assembly.

## 6.2 The Third Stability Zone

The third stability region is shown in Figure 6.1. It has a rectangular shape and is near $a$=3, $q$=3. The upper and lower tips of the zone 3 are shown in Figure 6.1a and b respectively. Values of $\beta_x$ vary from 1 to 2 and $\beta_y$ from 0 to 1. A scan line that passes through the centre of the stability zone 3 gives a resolution of about 22 [6]. Mass analysis is possible with scan lines that pass through the upper tip ($a$, $q$) = (3.16, 3.23) or through the lower tip ($a$, $q$) = (2.52, 2.82). Scan lines that pass through these tips do not pass through the stability zone 1. So a mass filter operated in the third region does not require any additional device to reject higher mass ions.

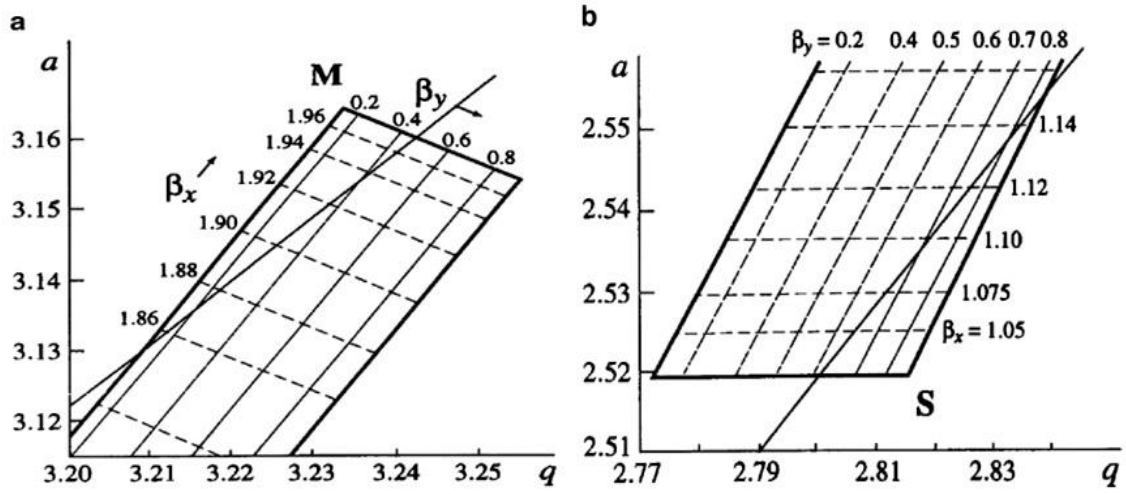


Figure 6.1: The third stability regions showing (a) the upper tip and (b) the lower tip, diagram taken from [6].

Coordinates of the tips of zone 1 and zone 3 regions are shown in Table 6.1. Moreover, as described previously, the amplitudes of $U$ and $V$ are determined by the stability zone, the frequency, the ion mass and the $r_0$ of the QMF.

Table 6.1: Mathieu coefficient values for zone 1 and zone 3

| **Zone** | $a_{tip}$ | $q_{tip}$ |
|---|---|---|
| 1 | 0.237 | 0.706 |
| 3 (upper) | 3.16 | 3.23 |
| 3 (lower) | 2.52 | 2.82 |

## 6.3 Effect of axial magnetic field on the performance of QMS operating under stability zone 3

This section considers the case of a quadrupole mass spectrometer in which a static magnetic field is applied axially in the *z*- direction along the length of the mass filter operating under stability zone 3. The analysis also predicts for which values of operating parameters an enhancement of the instrument resolution is achieved when an axial magnetic field is applied. The model predicts instrument resolution R > 3000 for Argon for a QMS with a 100mm long mass filter via application of an axial magnetic field.

### *6.3.1 The effect of magnetic field in z- direction on the resolution of QMF*

The simulated mass peaks for $^{40}Ar^{+}$ ions using the computer software are shown in Figure 6.2b. All the simulations used 150 steps across the mass range, with $9 \times 10^5$ ion trajectories run at each point on the peak. Mass peaks for $^{40}Ar^{+}$ are generated for a hyperbolic quadrupole mass filter with length ($l$) of 100 mm. The inscribed radius of the QMF was taken to be 1.5 mm. The frequency of the rf voltage used in the simulation was 5 MHz and the ion energy was chosen as 5 *eV*. The ion source radius ($r_{ie}$ ) was selected as 0.5 mm and the exit radius

was chosen as 3 mm. For zone 3, a *U/V* ratio of 100% corresponds to $q$ = 3.0 and $a$ = 2.8 which is near the centre of the stability zone 3. The operating point (*U/V* ratio) was selected as 104.82%.With increasing *U/V* ratio the scan line approaches the upper left tip of stability zone 3, so a *U/V* ratio of 104.82 % corresponds to the scan line operating very close to the tip of the stability region. Figure 6.2a shows the behaviour of the resolution, measured at 10 % peak height as a function of axial magnetic field, the resolution increases as *Bz* is varied between 0 - 0.002 T and then decreases as it is varied between 0.002 - 0.0075 T, the results indicates that the QMS resolution will not increase indefinitely with *Bz*. This is because as *Bz* increases, the peak shape eventually degrades. For a QMF of length *l*=100 mm the predicted value of resolution is in excess of 3000 which if achieved in practice would allow specialist high resolution RGA applications.

Figure 6.2b shows a set of peaks for $^{40}Ar^{+}$ within a hyperbolic QMF at different values of magnetic field (*Bz*). An increase in resolution is clearly observed up to a magnetic field of 0.002T. Transmission through the QMF decreases as magnetic field increases, which results in reduction of QMF resolution at higher values of magnetic field 0.003 - 0.0075 T. A shift in mass peak is observed at higher values of magnetic field. Even with B=0 this is a common feature of QMF operating in stability zone 3, if the position of scan line (*U/V* ratio) is changed. In this case the U/*V* ratio is maintained constant at 104.82%; nevertheless, a shift in mass speak is observed due to the dependence of magnetic field B on stability parameters $a$ and $q$ of the Mathieu stability diagram.

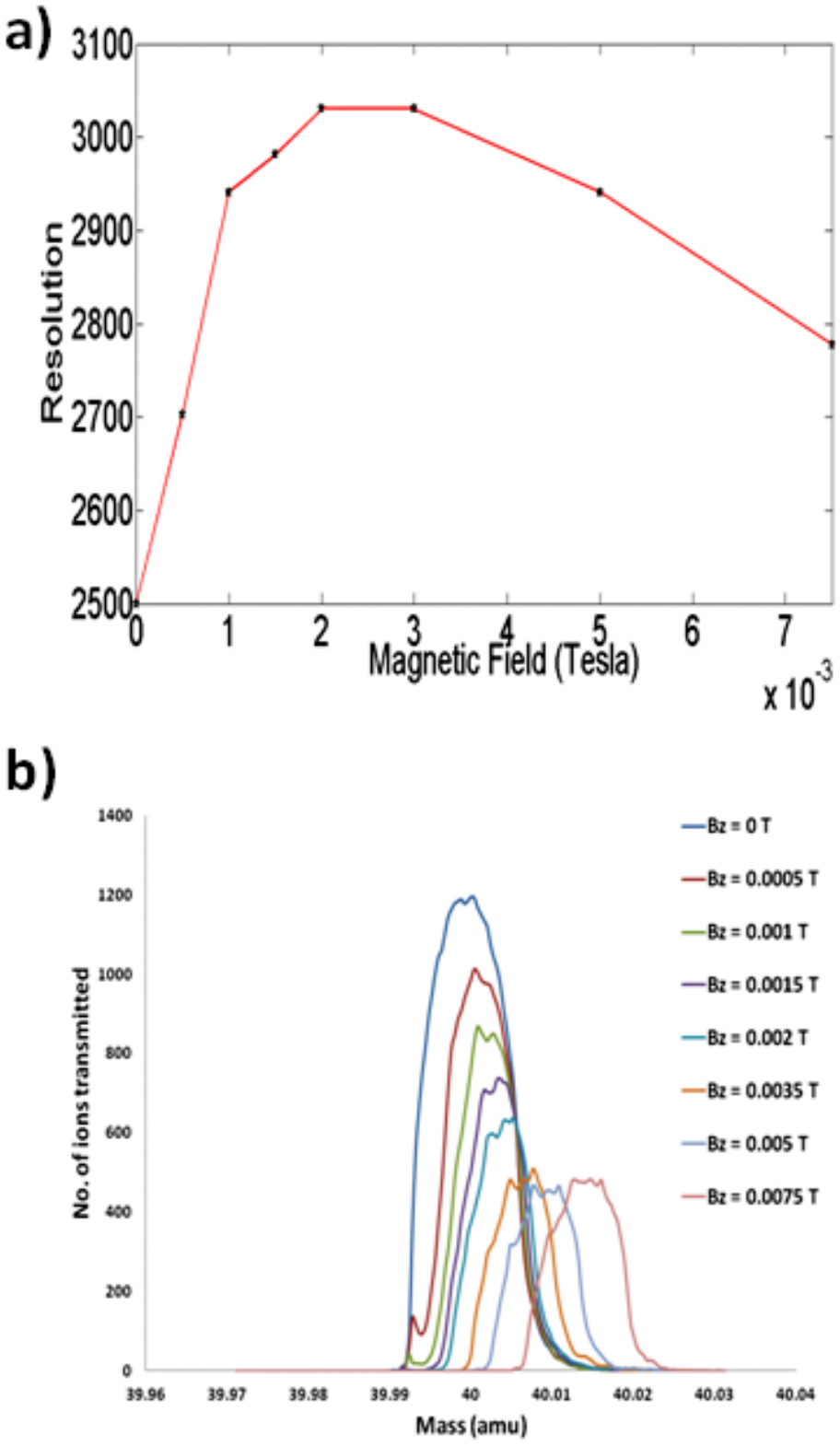


Figure 6.2: (a) The effect of magnetic field on resolution applied in z- direction (b) Simulated mass peaks for $^{40}Ar^{+}$ with and without magnetic field.

### *6.3.2 The effect of magnetic field in the z- direction on ion trajectories*

Figure 6.3 shows typical behaviour of the ion trajectories calculated using the theoretical model for ions transmitted with and without the axial magnetic field applied. All the simulations were carried out in stability zone 3. The corresponding traces shown in the figure are for the same ion injected into the mass filter at the same point in time (rf phase) and space and at the same point on the mass scale (m = 40.00 *amu*). The upper trace of the figure is for the case with no field applied and lower trace with $B_z$ of 0.0015 T.

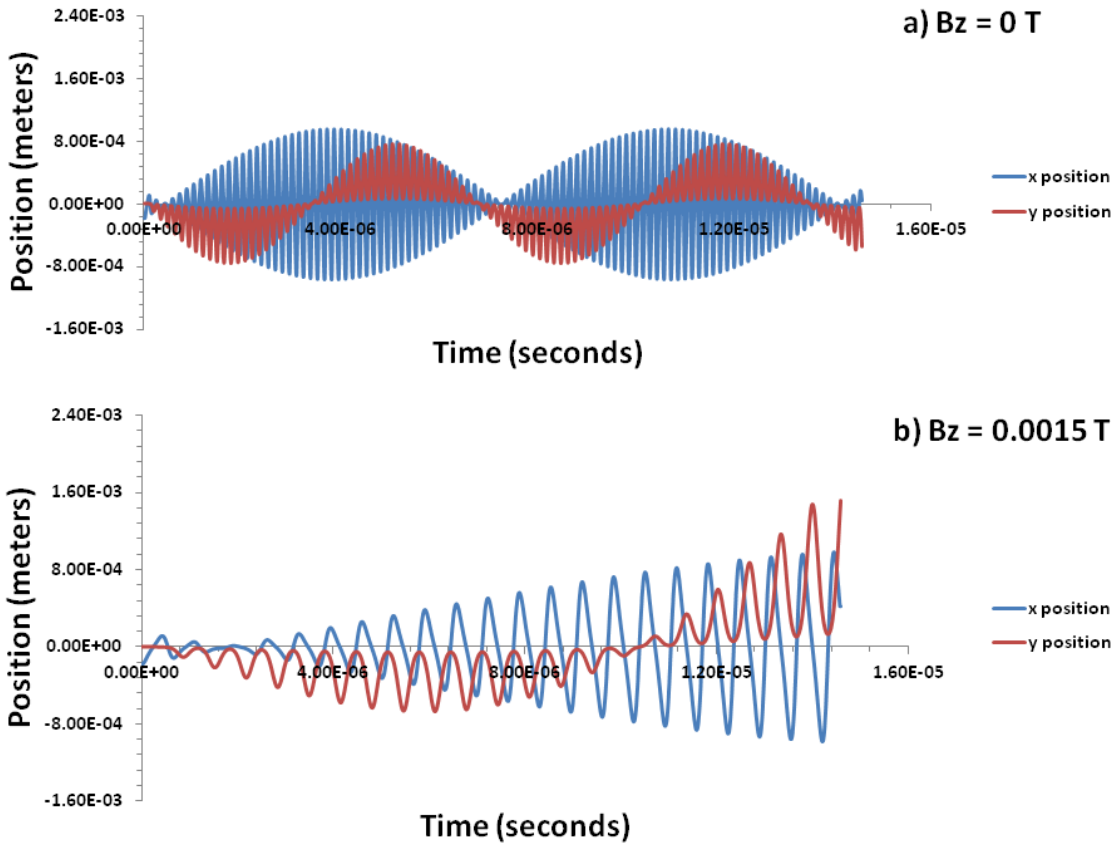


Figure 6.3: Numerical simulation of ion trajectories in x and y directions for $^{40}Ar^{+}$ with a) Bz = 0 (upper trace) and b) Bz = 0.0015 T (lower trace).

Ion motion in Figure 6.3 originates at $x = -1.78 \times 10^{-4}$ *m* and $y = 1.64 \times 10^{-6}$ *m* with initial velocity of $4.90 \times 10^{3}$ *m/s*. In the lower trace, due to the Lorentz force provided by $B_z$, the amplitude of ion trajectory along *y*- direction increases. The application of magnetic field therefore displaces the ion in the *y* direction so that the ion is lost through impact with the electrodes ($r_0$=1.5mm).

### *6.3.3 The effect of ion energy on resolution in the presence of magnetic field in the z – direction*

Figure 6.4 shows the dependence of resolution on ion energy for $^{40}Ar^{+}$ with and without magnetic field applied. As can be seen from the Figure 6.4, in both cases, resolution decreases with increase in ion energy. However, it can also be observed that percentage increase in resolution with magnetic field decreases as ion energy increases.

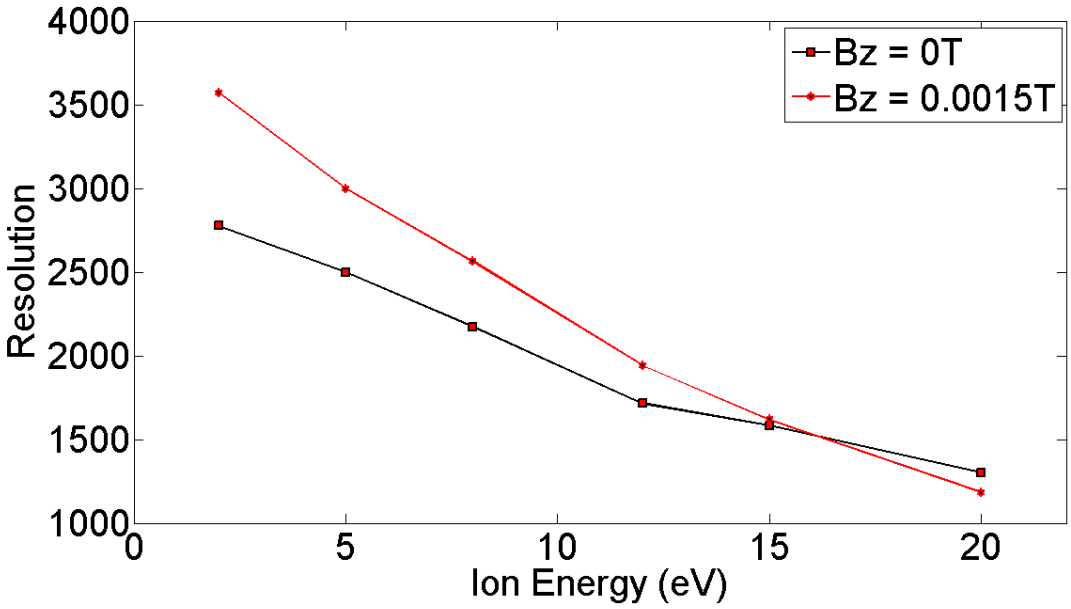


Figure 6.4: The dependence of resolution on ion energy with and without an applied magnetic field.

It should also be noted that in the presence of magnetic field of same strength the resolution becomes worse at *Ez = 20 eV*. This affect is attributed to the fact that in the presence of axial magnetic field the percentage increase in resolution is higher at higher number of rf cycles (as explained previously in chapter 4). Moreover, the behaviour of the peak shapes for stability zone 3 contributes to this effect. Figure 6.5a shows mass peaks for $^{40}Ar^{+}$ with and without an axial magnetic field applied of *Bz* = 0.0015 T for Ez = 2 *eV*. Whereas, Figure 6.5b shows mass peaks for $^{40}Ar^{+}$ with and without an axial magnetic field applied of *Bz* = 0.0015 T for *Ez* = 20 *eV*.

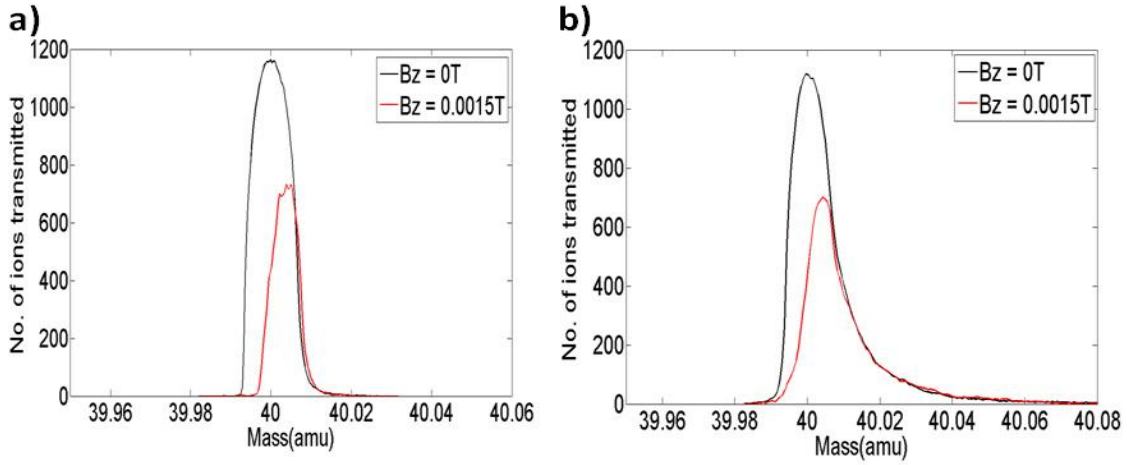


Figure 6.5: Mass peaks for $^{40}Ar^{+}$ with and without an axial magnetic field applied a) for Ez = 2 *eV*. b) for Ez = 20 *eV*.

As seen from Figure 6.5a at low values of ion energy (i.e. large number of rf cycles) the shape of the mass peaks are excellent with very low amplitude of high mass tail, which is a common feature of mass peak obtained if a QMF is operated in zone 3. Excellent peak shapes (low tailing of the peak) contribute to a high percentage increase in resolution with the magnetic field applied, as it is measured at 10% peak height. Figure 6.5b shows mass peaks at a high value of ion energy (i.e. low number of rf cycles); the shape of the mass speak is

poor as the amplitude of high mass tail is very high. This contributes to an increase of low percentage or a decrease in resolution depending on the value of magnetic field. This is due to the peak degradation as sensitivity decreases and also due to the presence of a high mass tail on the peak.

### *6.3.4 The effect of frequency on resolution in the presence of magnetic field in the z – direction*

Figure 6.6 shows the dependence of resolution on frequency for $^{40}Ar^{+}$ with and without magnetic field applied. As can be seen from the Figure 6.6, in both cases, resolution increases with increase in frequency. However, it can also be observed that percentage increase in resolution with magnetic field increases as frequency increases. This affect is attributed to the fact that in the presence of axial magnetic field the percentage increase in resolution is higher at higher frequencies (i.e. at large number of rf cycles) as explained previously.

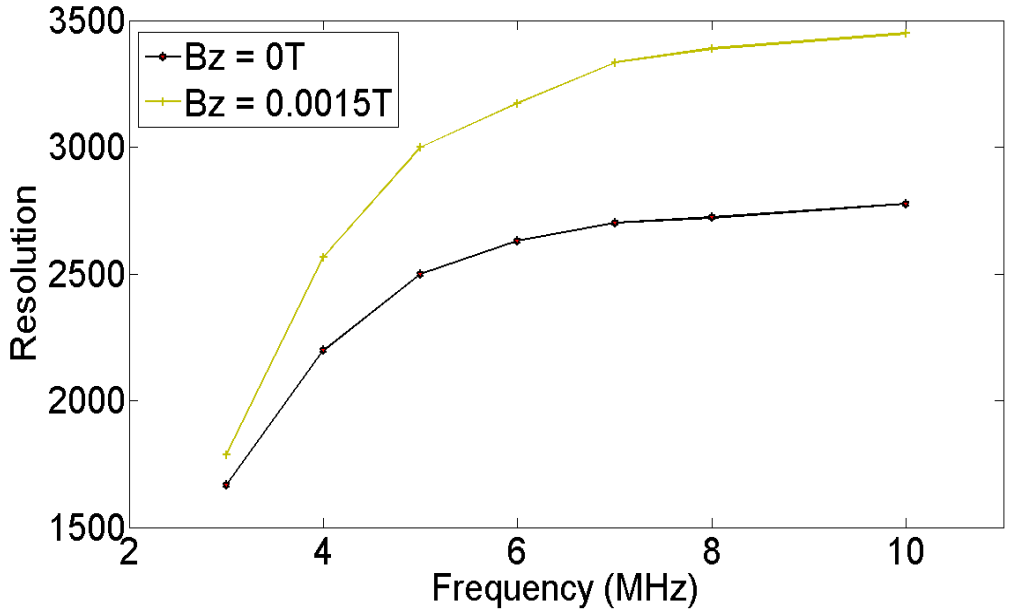


Figure 6.6: The dependence of resolution on frequency with and without an applied magnetic field.

Moreover, as discussed in the previous subsection the behaviour of the peak shapes for stability zone 3 contributes a lot to this effect. Figure 6.7a shows mass peaks for $^{40}Ar^{+}$ with and without an axial magnetic field applied of $Bz$ = 0.0015 T for $f$ = 4 MHz. Whereas, Figure 6.7b shows mass peaks for $^{40}Ar^{+}$ with and without an axial magnetic field applied of $Bz$ = 0.0015 T for $f$ = 8 MHz.

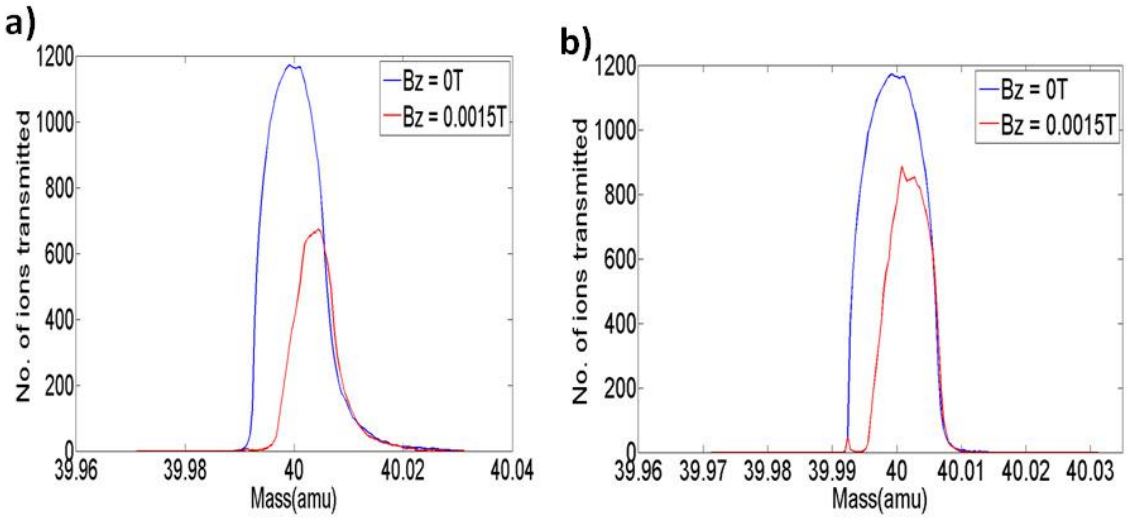


Figure 6.7: Mass peaks for $^{40}Ar^{+}$ with and without an axial magnetic field applied a) for $f$ = 4 MHz; b) for $f$ = 8 MHz.

As seen from Figure 6.7a at low values of frequency (i.e. low number of rf cycles) the shape of the mass speak is poor as the amplitude of high mass tail is very high. This contributes to an increase of low percentage or a decrease in resolution depending on the value of magnetic field, due to the peak degradation as sensitivity decreases and also due to the presence of high mass tail. Figure 6.7b shows mass peaks at a high value of frequency (i.e. large number of rf cycles); excellent peak shapes (low tailing of the peak) gives an increase in resolution with the magnetic field applied. Resolution measured at 10% peak height.

## 6.4 Isotopes

The existence of isotopes was first established by the chemist: Soddy [10]. Isotopes are variants of atoms of the same element which have the same atomic number (i.e., the same number of protons) but different mass number. The word 'isotope' is derived from two Greek words *isos topes* meaning 'the same place' and referring to their identical position in the periodic table of the chemical elements. The development of Aston's mass spectrograph in 1919 [11], showed that many of the natural elements are composed of atoms with different masses. Isotopes of an element have similar chemical properties. In addition to the natural isotopes, others can be made artificially. These are the radioactive isotopes or radioisotopes.

### 6.4.1 Low mass Isotopes

An atom is composed of three types of stable particles: protons (+), neutrons (0), and electrons (-); the electrons are bound to the nucleus by the force due to the positively charged protons [12]. In the periodic table, elements with lowest mass are hydrogen with an atomic weight of 1.00794 *amu* and helium 4 with an atomic weight of 4.002602 *amu*.

### 6.4.2 Hydrogen Isotopes

The isotopes of the element hydrogen are protium, deuterium, and tritium. They are distinguished by the difference in the number of neutrons. The isotopes of hydrogen are shown in Figure 6.8. Protium, with an atomic weight of 1.007825 *amu* has no neutron, deuterium with an atomic weight of 2.014101779 *amu* has one neutron, and tritium with an

atomic weight of 3.01604927 *amu* has two neutrons. Table 6.1 shows some isotopes of low mass gases taken from Sreekumar *et al* [9].

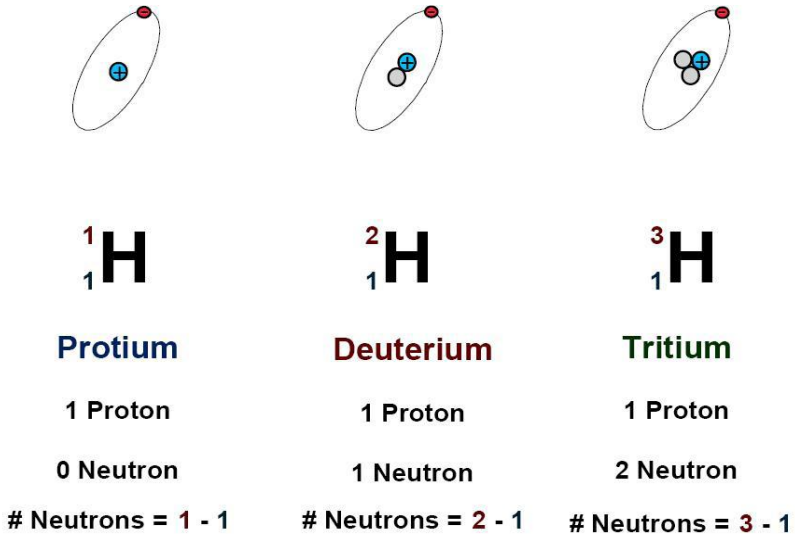


Figure 6.8: Hydrogen Isotopes.

Table 6.1: Low Mass Isotopes

| Species | Mass (*amu*) |
|---|---|
| $H_2^+$ | 2.10565 |
| $^3He^+$ | 3.016029319 |
| $HD^+$ | 3.021926779 |
| $^4He^+$ | 4.002602 |
| $HT^+$ | 4.02387427 |
| $D_2^+$ | 4.028203558 |
| $T_2^+$ | 6.03209854 |

### 6.4.3 Helium Isotopes

Figure 6.9 shows the helium atom consists of a nucleus comprising of two positively charged protons and two uncharged neutrons, orbited by a two negatively charged electrons. Helium is the second lightest element after hydrogen and is less dense than air by about one seventh.

Natural helium has two stable isotopes helium-3 (3He) and helium-4 (4He). The isotopes 5 through 10 are exotic isotopes that are radioactively unstable and they are extremely short lived. The stable isotopes of helium: 3He has two protons and one neutron and 4He has two protons and two neutrons. Figure 6.10 shows the natural helium isotopes (helium-3 and helium-4).

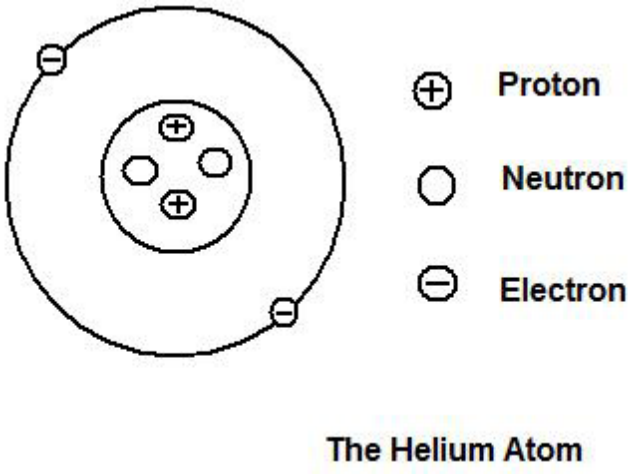


Figure 6.9: Helium Atom.

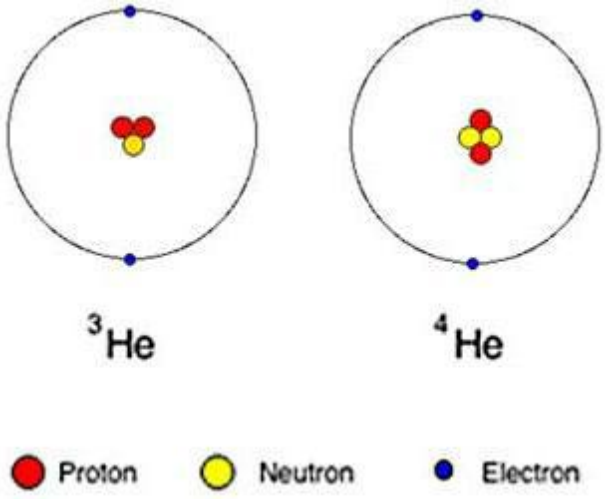


Figure 6.10: Natural Helium Isotopes.

### *6.5 Ultra high resolution QMF for identification of low mass isotopes and the effect of transverse magnetic field on the resolution of QMF*

In this section a study using a quadrupole mass spectrometer (QMS) is reported in which a static magnetic field is applied transversely to the body of the mass filter operating under stability zone 3. Significant improvement in QMS performance was obtained under certain magnetic field conditions, and these have been explained in terms of the theoretical model. The analysis also predicts for what values of operating parameters an enhancement of the quadrupole resolution is achieved when a transverse magnetic field is applied.

#### *6.5.1 The effect of magnetic field in the x direction on the resolution of QMF*

*Mass spectral studies of $HT^+$ and $D_2^+$ mixture*

All the simulations are carried out in zone 3 and use 150 steps across the mass range, with 9 $\times 10^5$ ion trajectories run at each point on the peak. Mass peaks for $HT^+$ and $D_2^+$ mixture are generated for a hyperbolic quadrupole mass filter with length ($l$) of 200 mm. The inscribed radius of the QMF was taken to be 2 mm and the ion energy was chosen as 5 *eV*. The ion source radius ($r_{ie}$ ) was selected as 0.5 mm and the exit radius was chosen as 4 mm. The operating point (*U/V* ratio) was selected as 104.82%, where 100% corresponds to the *U/V* ratio at $q$ = 3.0 and $a$ = 2.8 which is near the centre of the stability zone 3. The difference in mass between the two species is 0.0043293 *amu*, requiring a minimum resolution of 930 for mass separation [9].

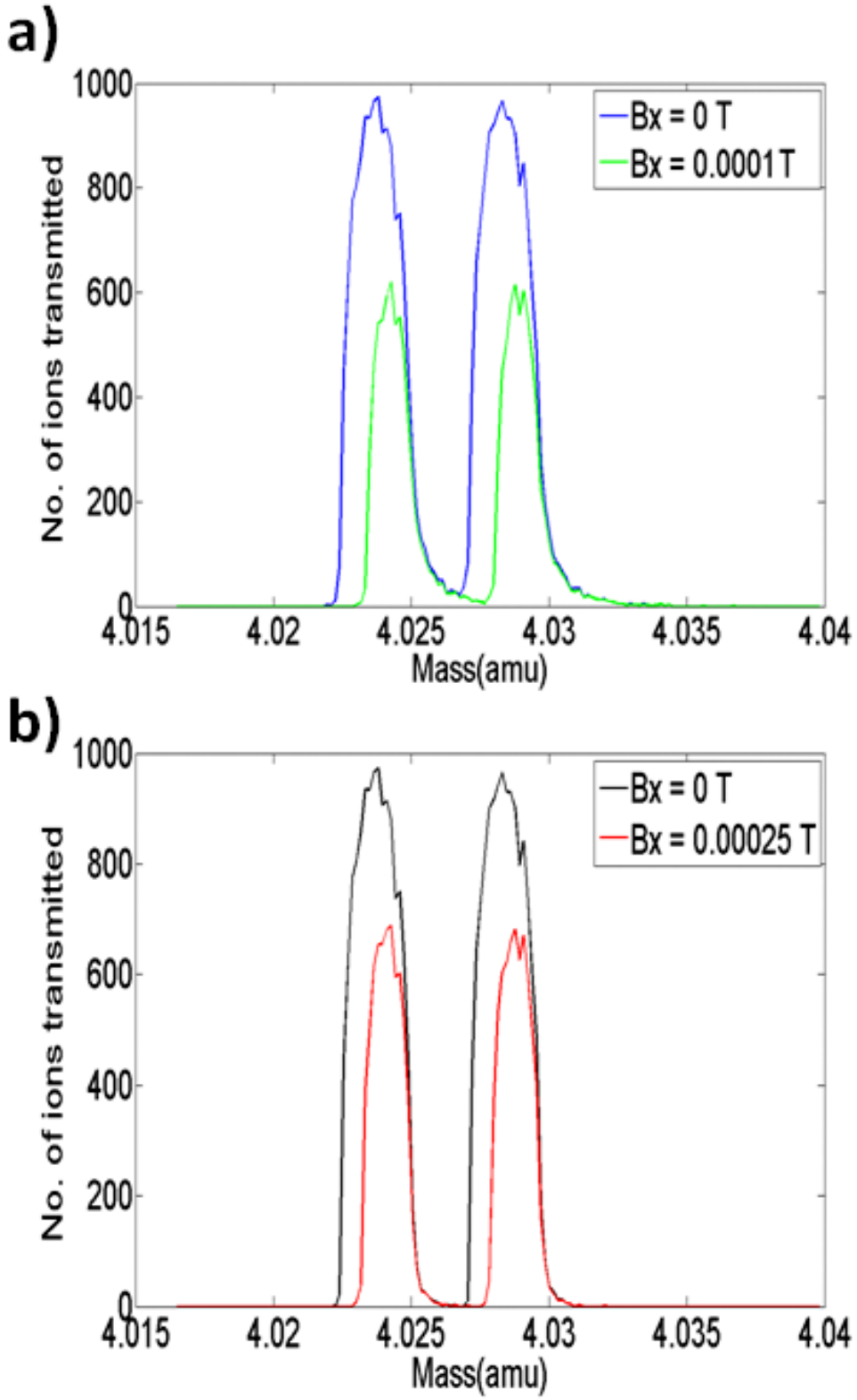


Figure 6.11: (a) Simulated mass peaks for $HT^+$ and $D_2^+$ mixture with and without magnetic field applied ($B_x$ = 0.0001 T), frequency 5 MHz (b) Simulated mass peaks for $HT^+$ and $D_2^+$ with and without magnetic field applied ($B_x$ = 0.00025 T), frequency 8 MHz.

Figure 6.11a shows a set of peaks obtained without and with an applied transverse magnetic field ($B_x$) for $HT^+$ and $D_2^+$ mixture within a hyperbolic QMF at a frequency of 5 MHz. An increase in resolution is clearly observed with an applied magnetic field of 0.0001 T; howbeit at the expense of sensitivity. Figure 6.11b shows a set of peaks obtained without and with an applied magnetic field of 0.00025 T for $HT^+$ and $D_2^+$ mixture at a frequency of 8MHz. From Figure 6.11a it can be seen that there is a clear improvement in resolution at 10% peak height with magnetic field applied, from approximately R = 1829 to R = 2163 for the case with $HT^+$ and from R = 1832 to R = 2166 for the case with $D_2^+$. Whereas, from Figure 6.11b it can be seen that upon application of magnetic field the resolution increases approximately from, R = 2438 to R = 3860 for the case with $HT^+$ and from R = 2517 to R = 3717 for the case with $D_2^+$. However, it should be noted that a higher value of magnetic field was required at higher frequency to increase the resolution by a sufficient value; this effect will be explained later in the section. The obtained resolutions are far higher than the minimum resolution required to separate the two species; this simulation result clearly illustrates the resolution enhancement provided by a transverse magnetic field.

*Mass spectral studies of $^{40}Ar^+$*

The simulated mass peaks for $^{40}Ar^+$ ions using the computer software are shown in Figure 6.12. All the simulations used 150 steps across the mass range, with $5 \times 10^5$ ion trajectories run at each point on the peak. Mass peaks for $^{40}Ar^+$ are generated for a hyperbolic quadrupole mass filter with length ($l$) of 100 mm. The inscribed radius of the QMF was taken to be 1.5 mm. The frequency of the rf voltage used in the simulation was 4 MHz and the ion energy was chosen as 5 *eV*. The ion source radius ($r_{ie}$ ) was selected as 0.5 mm and the exit radius was chosen as 3 mm. Figure 6.12 a shows the behaviour of the resolution, measured at 10 %

peak height as a function of transverse magnetic field for two different values of *U/V* ratios, 104.81 % (solid line) and 104.82 % (dotted line).

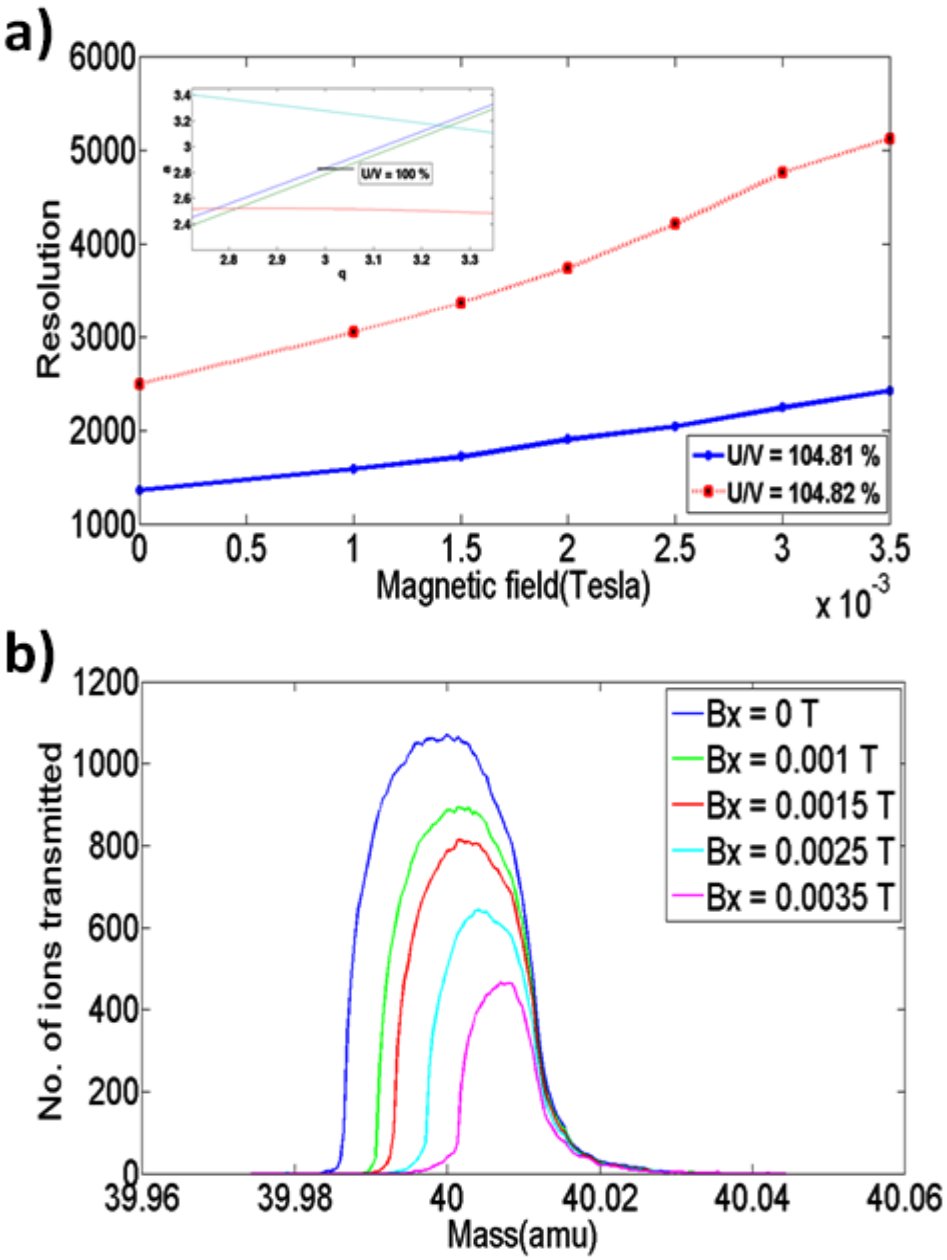


Figure 6.12: (a) The effect of magnetic field on resolution of $^{40}Ar^{+}$ applied in *x*- direction (solid line (*U/V* = 108.81) and dotted line (*U/V* = 104.82 %), the zone 3 detail of the Mathieu stability diagram is shown in the inset (b) Simulated mass peaks for $^{40}Ar^{+}$ with and without magnetic field.

The zone 3 detail of the Mathieu stability diagram is shown in the inset, where a *U/V* ratio of 100 % corresponds to $q$ = 3.0 and $a$ = 2.8 which is near the centre of the stability zone 3. With increasing *U/V* ratio the scan line approaches the upper left tip of stability zone 3, so a *U/V* ratio of 104.82 % corresponds to the scan line operating very close to the tip of the stability region. The resolution increases as *Bx* is varied between 0 - 0.0035 T, however the QMF resolution will not increase indefinitely with *Bx*. This is because as *Bx* increases, the peak shape eventually degrades. In the case of *U/V* ratio = 104.82 %, the predicted value of resolution is in excess of 5000, if achieved in practice, thus will allow specialist high-resolution QMS applications. This result shows that at any fixed value of *U/V* ratio there is a resolution enhancement by simply applying transverse magnetic field to the body of the mass filter.

Figure 6.12b shows a set of peaks for $^{40}Ar^{+}$ within a hyperbolic QMF at different values of magnetic field applied in the *x*-direction. An increase in resolution is clearly observed up to a magnetic field of 0.0035T at the expense of reduction in number of ions transmitted. There is also a reduction in the low mass tail of the mass spectra with a magnetic field.

### *6.5.2 The effect of magnetic field in the x direction on ion trajectories*

The simulation program is incorporated with a trace facility and this allows the details of individual ions to be recorded. Figure 6.13 shows typical behaviour of the ion trajectories calculated using the theoretical model for ions transmitted with and without the transverse magnetic field applied. All the simulations were carried out in stability zone 3. The corresponding traces shown in the figure are for the same ion injected into the mass filter at

the same point in time (rf phase) and space and at the same point on the mass scale (m = 40 *amu*). The upper trace of the figure is for the case with no field applied and lower trace with $B_x$ of 0.002 T.

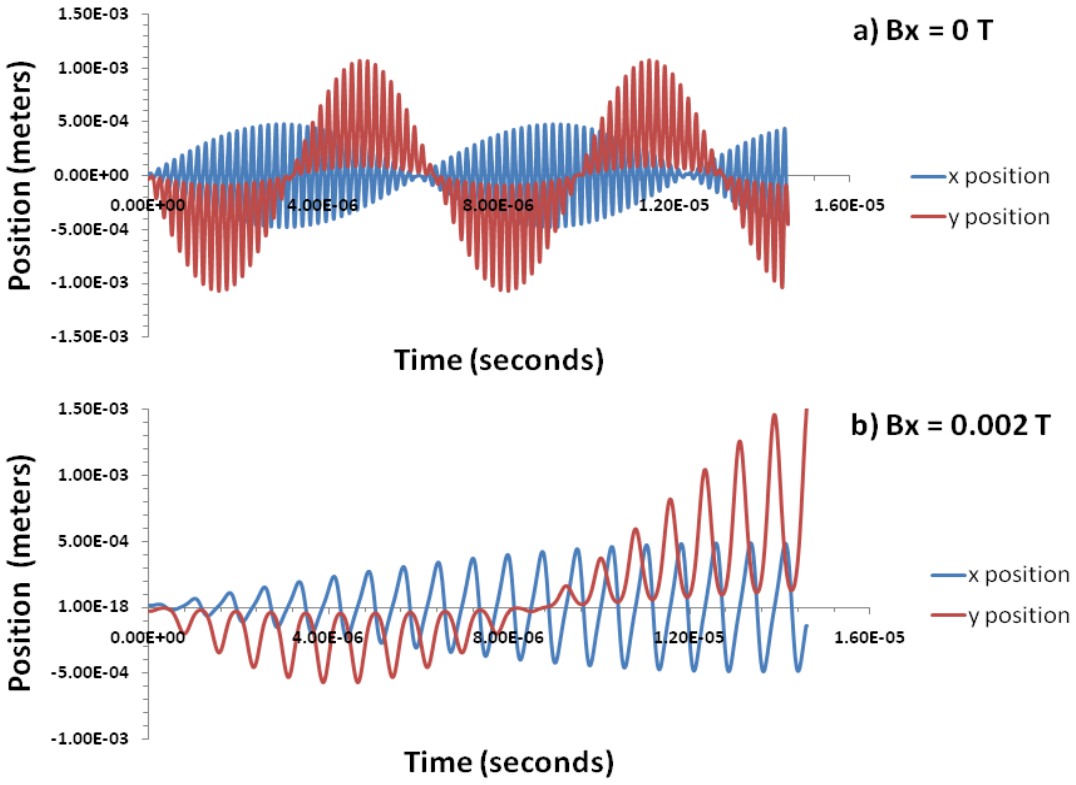


Figure 6.13: Numerical simulation of ion trajectories in x and y directions for $^{40}Ar^{+}$ with a) $B_x$= 0 T (upper trace) and b) $B_x$ = 0.002 T (lower trace).

Ion motion in Figure 6.13 originates at $x = 1.38 \times 10^{-5}$ *m* and $y = -3.11 \times 10^{-5}$ *m* with an initial velocity of $4.90 \times 10^{3}$ *m/s*. In the lower trace, due to the Lorentz force provided by $B_x$, the amplitude of ion trajectory in *y*- direction increases; however ion trajectory in the *x*-direction remains unaffected. The application of magnetic field therefore displaces the ion in the *y* direction so that the ion is lost through impact with the electrodes ($r_0$=1.5mm). It should be noted that ion motion in *x* direction (parallel to field) is unaffected; it is ion motion in the *y* direction (perpendicular to the field) which is modified, and this is to be expected since the

ion motion is subjected to Lorentz force $F = q\ (E + v \times B)$ where $v$ is the instantaneous velocity.

### *6.5.3 The effect of ion energy and frequency on resolution of QMF in the presence of magnetic field in the x direction*

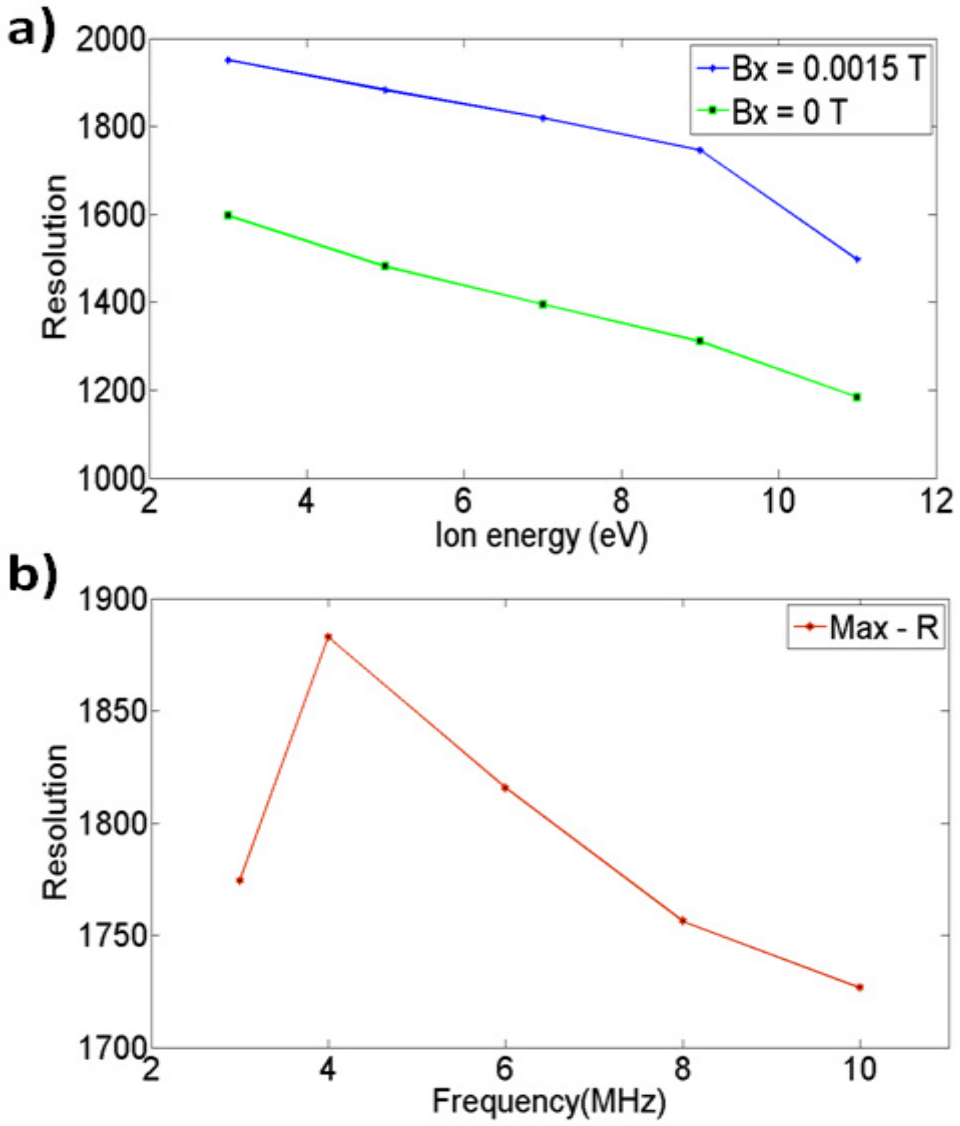


Figure 6.14: (a) The dependence of resolution on ion energy with and without an applied magnetic field (b) The dependence of resolution on frequency with and without an applied magnetic field.

Figure 6.14a shows the dependence of resolution on ion energy for $^{40}Ar^{+}$ with and without magnetic field applied. As can be seen from the Figure 6.14a, in both the cases, resolution decreases with increase in ion energy. This feature is commonly observed for QMS systems and is due to the reduced number of rf cycles experienced by the ion as the ion energy increases. However, these results clearly indicate that the predicted performance of the QMF increases in the presence of transverse magnetic field. Figure 6.14b shows the effect of frequency on resolution in the presence of a magnetic field. With a transverse magnetic field applied, the effect of frequency of the rf signal on resolution is ***different*** to that normally observed in a conventional QMF. The resolution first increases by a small amount as observed from frequency 3 to 4 MHz and then decreases with increase in frequency. This effect is attributed to the Lorentz force provided in the transverse direction by the magnetic field.

The effect can be best demonstrated with the help of ion trajectories in the presence of a transverse magnetic field at different frequencies. Figures 6.15 and 6.16 show trajectories of ions transmitted with and without magnetic field, at frequencies of 6 and 10 MHz respectively. The corresponding traces shown in the figures are for the same ion injected into the QMF at the same point in time (rf phase) and space and at the same point on the mass scale (m = 40.00 *amu*). In both figures the upper trace is for the case with no field applied and lower trace with $B_x$ of 0.002 T. Ion motion in Figure 6.15 originates at $x = 3.45 \times 10^{-5}$ *m* and $y = 3.88 \times 10^{-5}$ *m* with initial velocity of $4.90 \times 10^{3}$ *m/s*. It can be seen from the figure that in the presence of magnetic field at lower frequency (6 MHz) ion motion in both the directions is affected. It is also seen that the amplitude of ion motion in the *x*- direction decreases, whereas the amplitude in *y*- direction increases, resulting in loss of ions through impact with electrodes, and correspondingly higher resolution.

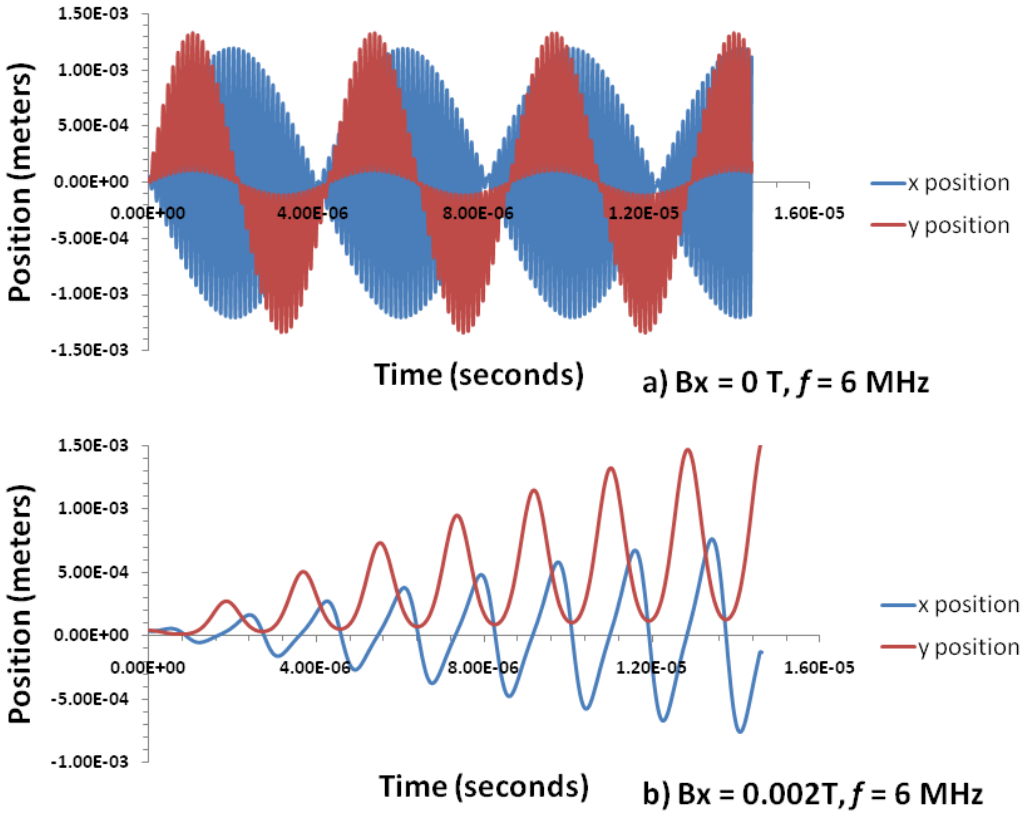


Figure 6.15: Numerical simulation of ion trajectories in x and y directions for $^{40}Ar^{+}$ with $f$ = 6 MHz and with a) $B_x$ = 0 T (upper trace) and b) $B_x$ = 0.002 T (lower trace).

In Figure 6.16 the ion motion also originates at $x = 3.45 \times 10^{-5}$ *m* and $y = 3.88 \times 10^{-5}$ *m* with the same initial velocity of $4.90 \times 10^{3}$ *m/s*. It can be observed from the figure that increase in frequency has a major impact on behaviour of ion trajectories in the presence of magnetic field. It can be seen that ion motion in the *x*- direction remains unaffected and the amplitude of ion motion along *y*- axis only slightly increases. Therefore, the ion was successfully transmitted in the presence of the magnetic field at the higher frequency of 10 MHz. In this case although the magnetic field is same as Figure 6.15 ($B_x$ = 0.002 T) the ion velocity is greater since the frequency is greater, and the component of Lorentz force correspondingly greater. It can be concluded that for a QMF with magnetic field applied in

the *x*- direction, the effect of magnetic field on resolution enhancement is greater at lower frequencies.

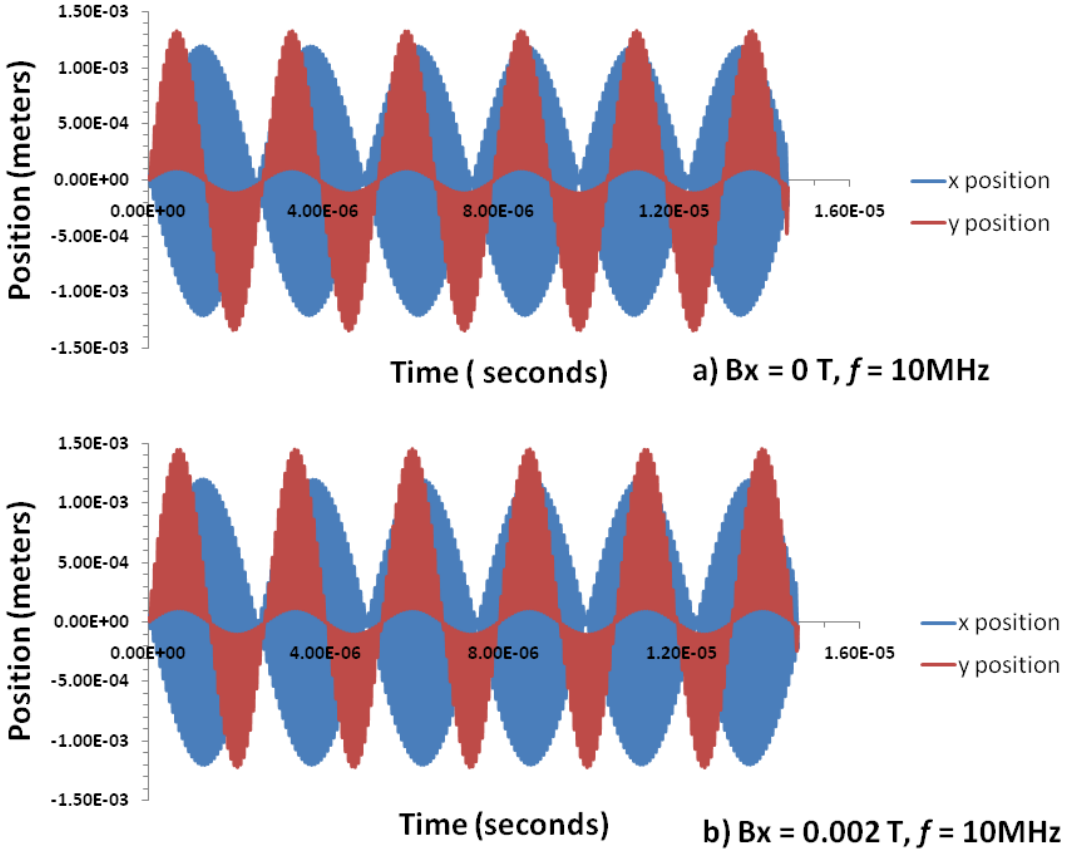


Figure 6.16: Numerical simulation of ion trajectories in x and y directions for $^{40}Ar^{+}$ with $f$ = 10 MHz and with a) $B_x$ = 0 T (upper trace) and b) $B_x$ = 0.002 T (lower trace).

## 6.6 Conclusions

Simulation results for a QMS operating in the stability zone 3 have been presented showing the effect of axial and transverse magnetic field, applied along the whole length of the mass filter. The effects of different input parameters such as variation of ion energy and drive frequency have been examined. The effects may be explained in each case by considering the additional Lorentz force produced by ion motion in the magnetic field. All ions entering the

mass filter with trajectories not parallel to the direction of magnetic field will experience Lorentz force, which modifies their motion. The increase in resolution is ascribed to the modification of the ion motion in the mass filter by the magnetic field. This results in rejection of ions in the low mass tail, giving increased resolution for a set of operating parameters. In certain cases however high values of Lorentz force do not produce resolution enhancement (see Figure 6.15 and Figure 6.16). There remains an optimum value of applied magnetic field for a given QMF. High resolutions (R > 3500) are predicted for low mass isotopes (1-6 *amu*) with a QMF of length 200 mm and (R > 5000) for Argon with a QMF of length 100 mm as a result of the applied transverse magnetic field. These features suggest wider application than hitherto for such QMS instruments e.g. applications in which extremely high QMS resolution and/or high abundance sensitivity is required. These include identification of low mass isotopes in the mass range (1-6 *amu*), as this issue is of some importance in the nuclear industry for protecting of personnel involved in the handling of radioactive material.

**References**


1. Dawson, P.H. *Quadrupole mass spectrometry and its applications*, Elsevier: Amsterdam 1976.
2. Hogan, T.J.; Taylor, S. Performance Simulation of a Quadrupole Mass Filter Operating in the First and Third Stability Zones. *IEEE*. 2008, *57 (3)*, 498-508.
3. Hiroki, S.; Abe, T.; Murakami, Y. Separation of Helium and Deuterium Peaks with a Quadrupole Mass Spectrometer by Using the Second Stability Zone in the Mathieu Diagram. *Rev. Sci. Instrum.* 1992, *63*(8), 83874–3876.

4. Hiroki, S.; Abe, T.; Murakami, Y. Detection of a $10^{-4}$ Helium Peak in a Deuterium Atmosphere Using a Modified High-Resolution Quadrupole Mass Spectrometer. *Rev. Sci. Instrum.* 1994, *65*(6), 1912–1917.
5. Frattolillo, A.; De Ninno, A. A Powerful Tool to Quantitatively Detect Tiny Amounts of $^{4}$He in a Deuterium Rich Background for Fusion Research. *Proceedings of the 22nd IEEE Symposium on Fusion Engineering*; Albuquerque, NM, June, 2007.
6. Douglas, D.J. Linear quadrupoles in mass spectrometry. *Mass Spectrometry Reviews*. 2009, *28*, 937-960.
7. Du, Z.; Douglas, D. J.; Konenkov N. Elemental Analysis with Quadrupole Mass Filters Operated in Higher Stability Regions. *J. Anal. At. Spectrom.* 1999, *14*(8), 1111–1119
8. Du, J.; Olney, T.N.; Douglas, D. J. Inductively Coupled Plasma Mass Spectrometry with a Quadrupole Mass Filter Operated in the Third Stability Region. *J. Am. Soc. Mass Spectrom.* 1997, *8*, 1230-1236.
9. Sreekumar, J.; Hogan, T.J.; Taylor, S.; Turner, P.; Knott, C. A Quadrupole Mass Spectrometer for Resolution of Low Mass Isotopes. *J. Am. Soc. Mass Spectrom.* 2010, *21*, 1364–1370.
10. Soddy, F. The origins of the conceptions of isotopes. *Nobel lecture*, 1922.
11. Aston, F.W.: Isotopes. Arnold, London.1922.
12. Meldrum, A.N.: The development of the atomic theory. H. Milford, Oxford university press. 1920.

# Chapter 7

# Factors influencing the QMF resolution for operation in stability zones 1 and 3

## 7.1 Introduction

It is well known that the resolution of a QMF can be increased by operating closer to the tip of the stability region [1, 2]. However, it was also reported that, in practice the resolution is limited by the residence time of ions in the quadrupole field and by field imperfections in the QMF. When the resolution is limited by ion residence time in the QMF, the resolution (R) is known to be dependent on number (N) of radio frequency (rf) cycles experienced by the ions in the mass filter [1], according to $\mathbf{R} = \boldsymbol{N^n/K}$, where *n* is either exactly or closely equal to 2 and *K* is a constant. For operation in the stability zone 1, Paul *et al* calculated *K* as 12.25 [3]. In Dawson (1976) the design and performance of the QMF is described in detail and it was reported that the constant *K* may be assumed to be 20 for all practical purposes [1, chapter 6].

When operated in stability zone 1 low energy ions exhibit high mass resolutions because of increased ion residence time in the QMF. High ion energy gives poor resolution with tails on the peak especially on the low mass side. An alternative way to increase ion residence time is to use a longer QMF. In 1962 Von Zahn a member of the Paul group, constructed a QMF of 5.82 m in length and reported a resolution of the order of 16000, for

high-precision mass measurements [5]. Other workers increased **N** by reflecting ions to give multiple passes through a QMF. A resolution of 11000 for *m/z* 20 at 50% peak width definition was obtained [1]. Brubaker and Tull, investigated the transmission efficiency and resolution of a QMF as a function of ion source aperture size and frequency of excitation; the ion source exit aperture defines the area of illumination of the QMF and is usually a fraction of the inscribed QMF field radius ($r_0$) [6]. It was concluded that higher resolution is obtained with small aperture size and higher frequency. However, higher frequencies reduce the mass range and also an electronic drive with a variable frequency option increases the instrument cost significantly compared with single frequency electronic device. For operation of QMF in stability zone 3, Hiroki *et al* performed computer simulations, and determined the relationship at the upper tip $\boldsymbol{R = 1.7N^2}$ and at the lower tip $\boldsymbol{R = 0.69N^2}$ [1]. The same simulations showed $\boldsymbol{R = N^2/10.9}$ for the stability zone 1, which is in reasonable agreement with the calculation of Paul *et al* [3]. Konenkov and Kratenko found $\boldsymbol{R = 0.7N^2}$ [7], Titov found $\boldsymbol{R = 1.7N^2}$ and Du *et al* measured at 50% peak width definition as $\boldsymbol{R = 1.4N^2}$ [8].

This chapter reports a study using a computer model to simulate a Quadrupole Mass Filter instrument under different operating conditions for Mathieu stability zones 1 and 3. The investigation considers the factors which limit the maximum resolution ($R_{max}$) that can be obtained for a given QMF for a particular value of scan line. Previously QMF resolution (R) has been found to be dependent on number (N) of radio frequency (rf) cycles experienced by the ions in the mass filter, according to $\mathbf{R = N^n/K}$, where *n* and *K* are the constants. However, this expression does not predict the limit to QMF resolution observed in practice and is true only for the linear regions of the performance curve for QMF operation in zone 1 and zone 3 of the stability diagram. In this chapter the saturated regions of the performance curve for QMF operation in zone 1 has been modeled. Also by careful calculations of the detail of the

stability tip of zone 1, a relationship was established between $R_{max}$ and percentage *U/V* ratio. For QMF operation in zone 3 the modeled expression simulates well the linear and saturated regions of the performance curve for a range of operational conditions.

### 7.2 The performance curve

The performance of the QMF, was measured in a series of experiments performed by Holme *et al* [4], and reproduced by Dawson (1976) is summarized as a simple relationship shown in Figure 7.1 [1, chapter 6]. The relationship takes account of the whole range of variation of ion injection energy (*Ez*) and mass. As seen from the figure the agreement between ***N*** and ***R*** becomes worse with increasing resolution. It was concluded that the factors responsible for this deviation from being linear were:

I. Mechanical misalignment in either source or quadrupole lens assembly, contamination of electrode surfaces by surface insulating layers or imperfections in the electrical supplies to the rods.
II. Inability to inject a significant number of ions into the quadrupole at high values of **dc/rf** voltage ratio.
III. Imperfect analysis in the quadrupole lens due either to its finite length or to the errors in field due to approximating a hyperbolic profile with round rods.

The performance curve shown in Figure 7.1 has been modeled using the numerical model described in chapter 4 for a range of operating conditions, and the following sub-sections explain in detail the results obtained.

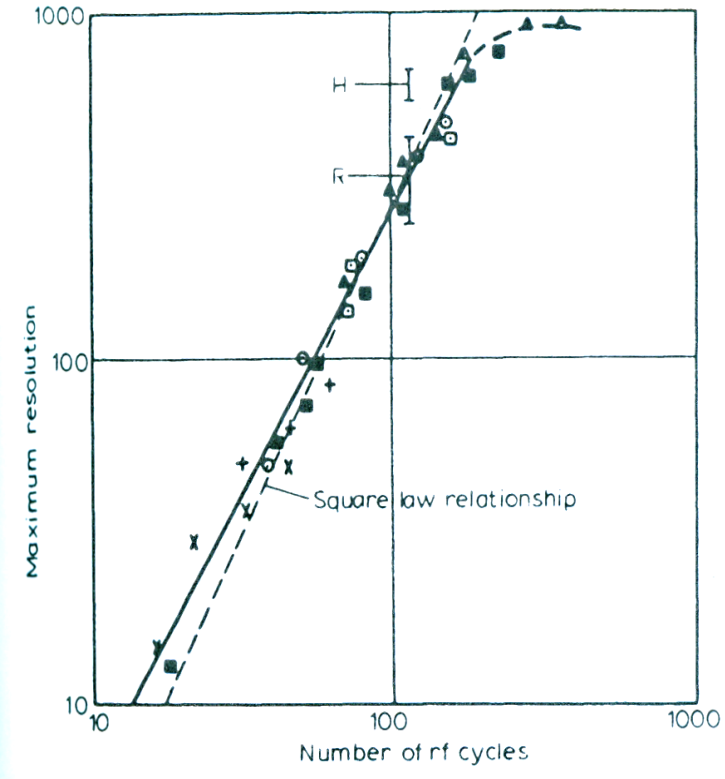


Figure 7.1: Dependence of Resolution on Number of rf cycles (Copyright Dawson, 1976).

### 7.3 Calculations of the details of the stability tip

To calculate and plot the details of the stability diagram tip, a program which is a direct conversion of the corresponding Fortran program in Zhang and Jin [9], was used [10]. The program generates the boundaries of the stable and unstable areas of the Mathieu stability diagram in a discretized form. These values are then imported into a Matlab Program, which plots the full Mathieu stability diagram. The scan line is then drawn over the Mathieu equation and the points of intersection with the Mathieu Stability boundaries can be detected ($\Delta q$: the width of the intersection of the operating scan line with the stability zone 1). By altering the active area of the graph and the scan line different scan line stability zone

combinations can be plotted. Figure 7.2 shows how the calculations were made at the tip using Matlab.

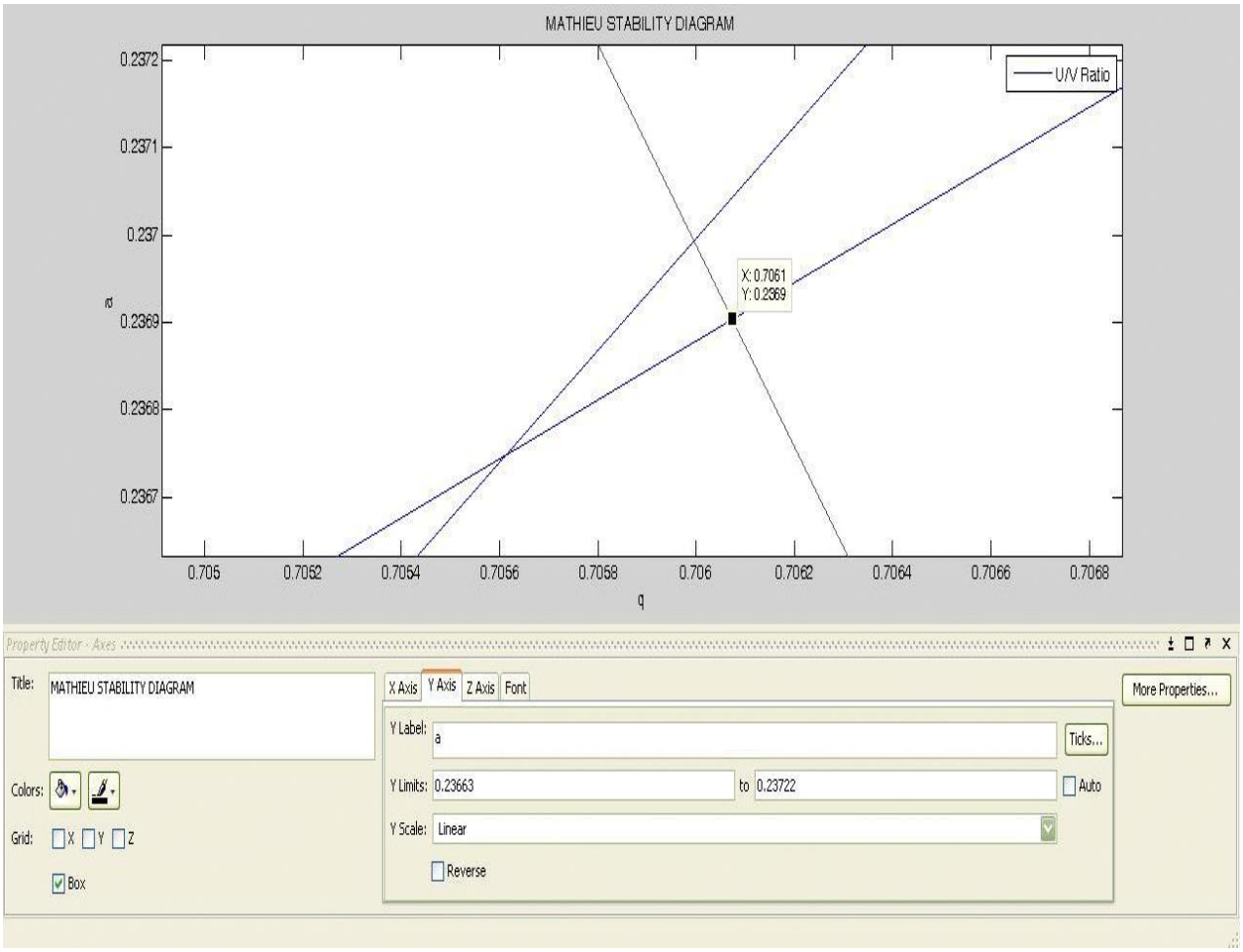


Figure 7.2: Matlab plot showing how $\Delta q$ is calculated at a particular value of scan line.

### 7.4 Performance of a QMF operating in stability zone 1

All the simulations use 300 steps across the mass range with $5 \times 10^5$ ions injected and traced at each mass step. Mass peaks for $^{40}Ar^{+}$ are generated for a hyperbolic quadrupole mass filter with inscribed radius (field radius) of 0.9 mm. The frequency of the rf voltage used in the simulation was 3.686 MHz and the input ion energy ($E_z$) was chosen as 5 $eV$. The ion source

radius ($r_{ie}$) was selected as 0.5 mm and the exit radius (detector radius) was chosen as 1.8 mm. The length of the mass filter was varied in order to vary the number of rf cycles the ion experiences. It is assumed in the model that the QMF control setting $U/V$=100% corresponds to the peak of the stability diagram (i.e., $a$ = 0.23699 and $q$ = 0.706 for zone 1). No account of fringing fields at the entrance or exit of the mass filter has been considered, and the initial velocities in the $x$ and $y$ directions are zero.

Figure 7.3a shows the dependence of resolution on number of rf cycles at $U/V$ ratios 99.9%, 99.95%, 99.99%, and 99.998%. For the linear region of each curve the results satisfy the previously reported experimental relationship between resolution and number of rf cycles [1], $R = N^n/K$, and the values of $n$ and $K$ at different $U/V$ ratios obtained via OriginPro 8.5 (Curve fitting software) [11] are shown in Table 7.1. As observed from Table 7.1 the values of $n$ and $K$ are in accord with values previously determined for a range of experimental measurements [1, chapter 6] with the precise values of $n$ and $K$ dependent upon the value of $U/V$ ratio. It can be seen from Figure 7.3a that in all cases as the number of rf cycles increases, resolution increases with a finite slope and then saturates. To test whether this was a true result or an artifact of the program, the same instrumental conditions were simulated using different computing parameters. However, even after decreasing the mass range, increasing the number of steps up to 1200 and the number of ions to $1 \times 10^8$; and integrating with fine settings (i.e. small integration intervals, so as to increase the Runge-Kutta time step size) the same results were obtained. It was concluded that results were not due to the computer model parameters or the method, but rather represented a feature of ion motion in an ideal quadrupole field. Figure 7.3b shows a computed mass spectrum for $^{40}Ar^+$, $M$ is the mass of the given spectral peak and $\Delta M$ is the width of the mass peak measured at 10% of its height.

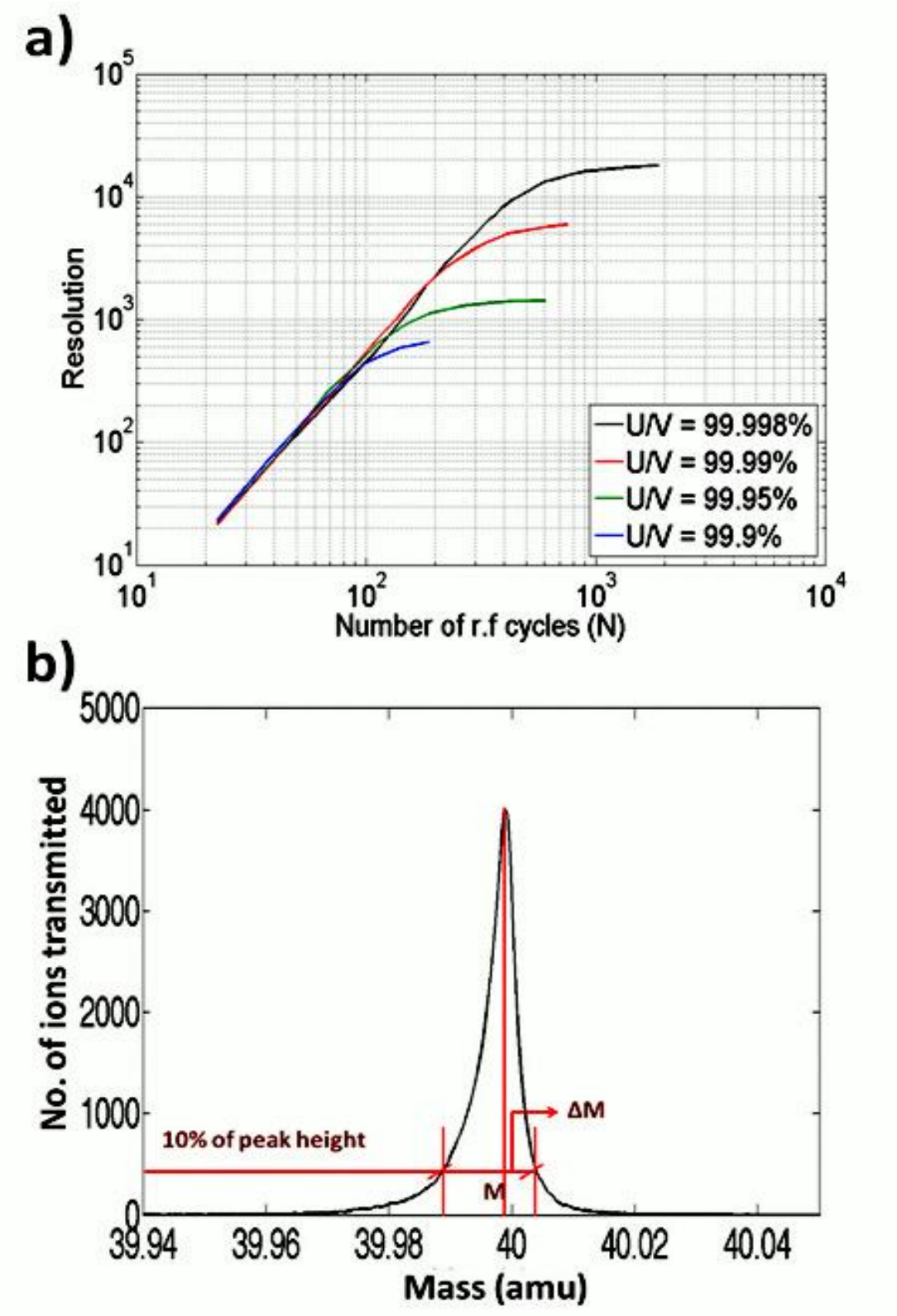


Figure 7.3: (a) The dependence of resolution on the number of rf cycles for stability zone 1 at different *U/V* ratios; predicted by QMS-hyperbolic; (b) A model of a mass spectrum for $^{40}Ar^{+}$.

**Table 7.1 : Values of *n* and *K* at different *U/V* ratios (Zone 1 operation)**

| ***U/V* ratio** | ***n*** | ***K*** |
|---|---|---|
| 99.9% | 1.954 | 16.155 |
| 99.95% | 1.954 | 15.84 |
| 99.99% | 2.02 | 20.981 |
| 99.998% | 2.08 | 28.02 |

For $U/V < 100\%$, it can be concluded that there is finite theoretical limit to resolution for a particular value of instrument operating point set by the *U/V* ratio (scan line), as at that particular point $\Delta q$ cannot go beyond a certain minimum obtainable value. This is because the intersection of the scan line with the stability diagram will give a minimum obtainable value of $\Delta q$ and correspondingly $\Delta M$. The Mathieu stability diagram for zone 1 with the intersection of the scan line at two operating points is shown in Figure 7.4.

Figure 7.4a shows the Mathieu stability diagram for zone 1 with the intersection of the scan line at 100%; whereas Figure 7.4b shows the intersection at $U/V < 100\%$. At 100% $\Delta q$ should be ideally zero; whereas, at $U/V < 100\%$ $\Delta q$ has a certain finite non zero value. Intersection of the scan line below the tip (Figure 7.4b) increases the pass-band and in turn limits the resolution of a QMF to a finite maximum value which is given by ($R_{max} = q/\Delta q = 0.706/\Delta q$) for a given mass even if the number of rf cycles is increased by increasing the length or frequency or by decreasing ion energy.

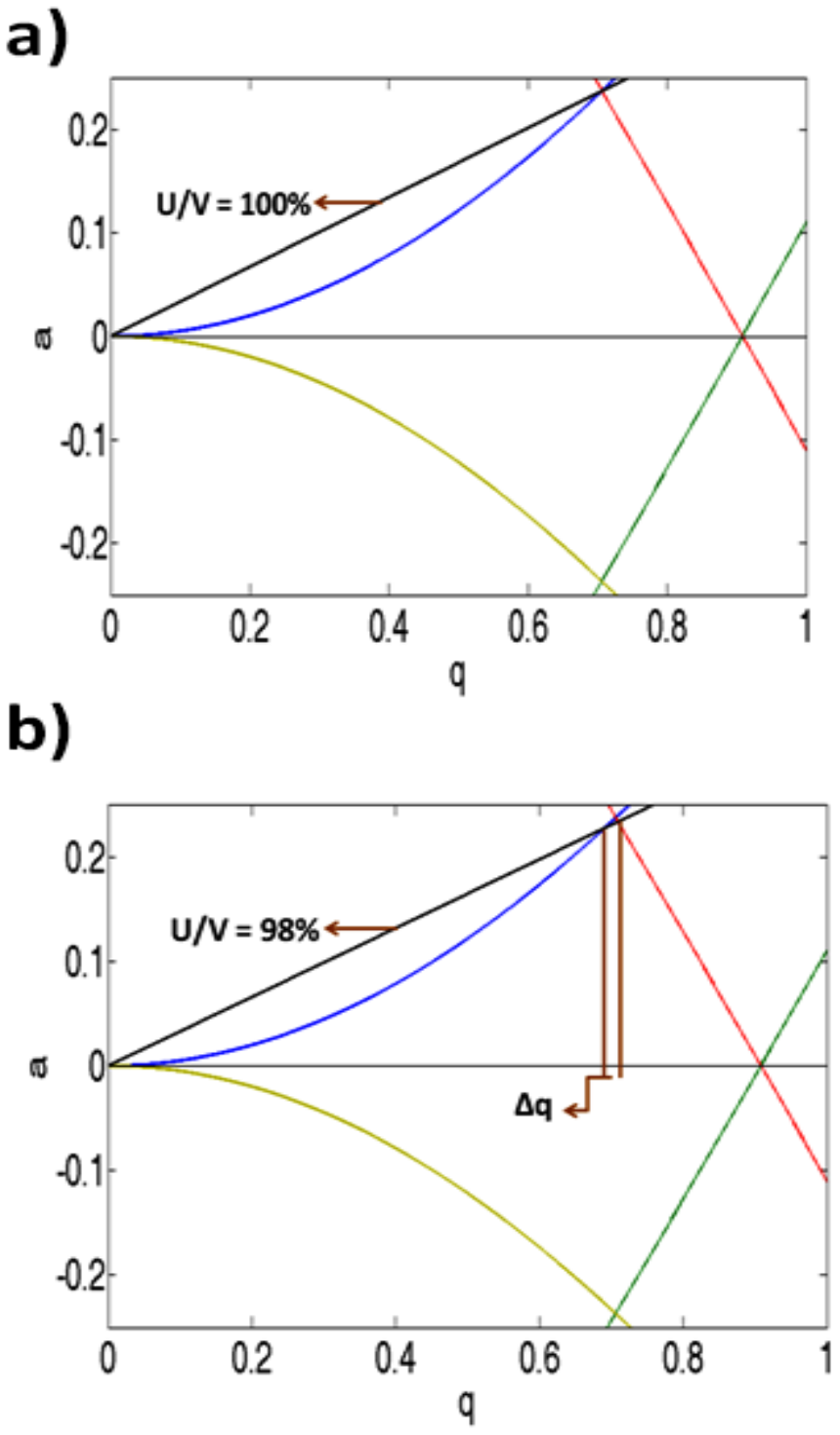


Figure 7.4: (a) The Mathieu stability diagram for zone 1 with the intersection of the scan line at 100%; (b) The Mathieu stability diagram for zone 1 with the intersection of the scan line at *U/V* <100%.

For the saturation regions of the performance curves, observed in practice [1] and modeled in Figure 7.3a, a good representation is given by a function of the form ($R = a - bc^N$); where a, b and c are constants. Figure 7.5 (square symbols) shows the relationship between *N* and *R* obtained using QMS-hyperbolic and a fitted curve to the data (red line) using OriginPro 8.5 for *U/V* ratio 99.99%. The value of the coefficient of determination (COD) termed as $R_c^2$ was found to be 0.9985, indicating a good regression fit between the curves ($R_c^2$ of 1 indicates that the regression line perfectly fits the data). The value of Adj. $R_c^2$ (a modification of $R_c^2$ that adjusts for the number of independent terms in a model) was found to be 0.9981. The values of the parameters *a*, *b* and *c* depend upon the *U/V* ratio used in the QMS-hyperbolic simulations. The same approach can be applied to model all the curves of Figure 7.3a and the corresponding Table 7.2 shows the values of the parameters *a*, *b*, *c* with their standard error (SE), and also the coefficient of determination $R_c^2$ at different *U/V* ratios.

**Table 7.2 Values of parameters a, b, c and COD's, for QMF operation in zone 1.**

| Variables | *U/V* 99.9% | *U/V* 99.95% | *U/V* 99.99% | *U/V* 99.998% |
|---|---|---|---|---|
| a | 725.80 | 1425.35 | 6093 | 17946 |
| b | 1516.28 | 2882.27 | 12237.96 | 36598.97 |
| c | 0.98278 | 0.98846 | 0.99441 | 0.99666 |
| SE for 'a' | 6.82 | 7.78 | 73.20 | 103.88 |
| SE for 'b' | 49.84 | 258.72 | 867.44 | 1268.58 |
| SE for 'c' | 0.000560675 | 0.00060428 | 0.000341121 | 0.0000893829 |
| COD- $R_c^2$ | 0.9994 | 0.999 | 0.9985 | 0.9977 |
| Adj. $R_c^2$ | 0.9991 | 0.9987 | 0.9981 | 0.9974 |
| a/b Ratio | 0.48 | 0.495 | 0.493 | 0.49 |

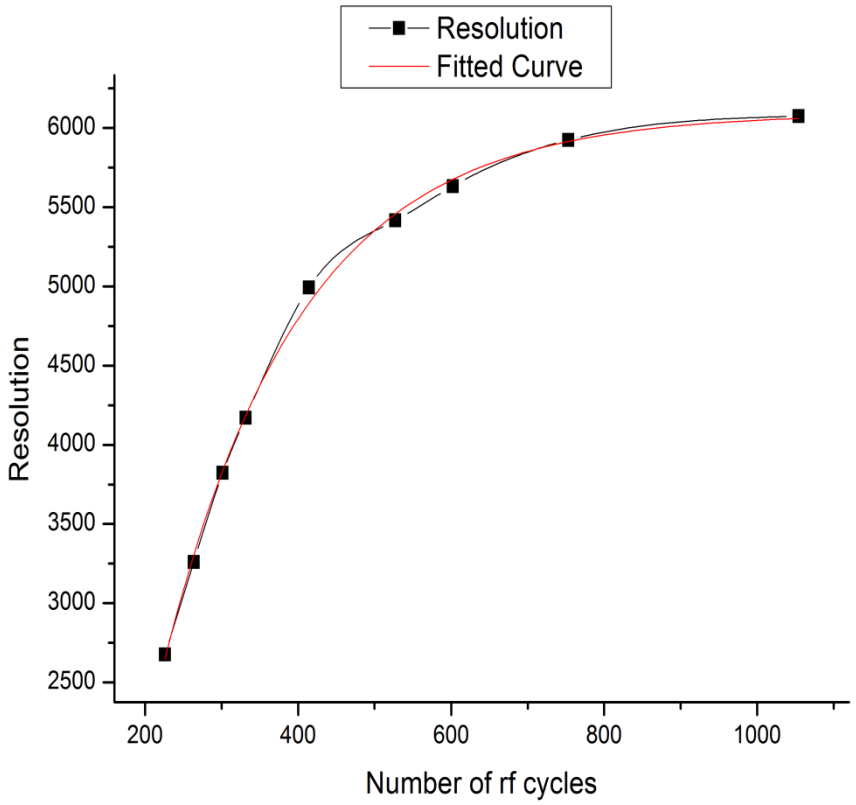


Figure 7.5: The dependence of resolution on number of rf cycles for the saturation region of the performance curve for stability zone 1 at $U/V$ = 99.99% (fit obtained using Origin 8.5).

From the values obtained it is observed in all cases that the parameters $a$ and $b$ have a constant ratio of approximately 0.49. Moreover the value of parameter $a$ is found to be approximately $q/\Delta q$, except for $U/V$ = 99.998%, and this discrepancy will be explained later in the chapter. By substituting these observations in the functional relationship determined from the curve fit, and for simplicity considering the ratio of $a/b$ as 0.5, then for the saturation region of the performance curve, $R$ can be related to $N$ using $\boldsymbol{R = q(1 - 2c^N)/\Delta q}$. It was previously thought that the saturation in the performance curve was as a result of imperfections in QMS manufacturing [1]. Simulations using QMS-hyperbolic are for the case

of an ideal (but finite length) quadrupole field with zero mechanical misalignments. The saturation behaviour in resolution observed by Holme *et al* [4] with increasing *N* is thus seen to be the feature of the QMF and therefore not necessarily due to mechanical deficiencies in QMF manufacture.

### 7.5 Dependence of ultimate maximum resolution on U/V ratio

By careful calculations of the details of the stability tip, the dependency between $\Delta q$ and scan line (*U/V* ratio) is obtained as shown in Figure 7.6. As expected, $\Delta q$ decreases linearly with increasing *U/V* ratio. A good mathematical relationship between $\Delta q$ and *U/V* ratio can be represented as $\Delta q = 0.933\text{-}0.00933U/V$. By substituting the value of $\Delta q$ in $R_{max} = q/\Delta q$, a relationship between the maximum resolution $R_{max}$ for a particular scan line (*U/V* ratio in percentage) is established and given by: $\boldsymbol{R_{max} = q/(0.9330\text{-}0.00933U/V).}$ Figure 7.7a shows the comparison of maximum resolution obtained in the simulations (i.e. the saturation region of the performance curve) and the $R_{max}$ calculated for the ideal case using the Mathieu Stability diagram at different *U/V* ratios. From Figure 7.7a the maximum resolution increases with increasing *U/V* ratio, and as scan line approaches the tip (*U/V* = 100%) it starts to increase dramatically towards the singularity at 100%. Moreover, it can be seen from Figure 7.7a, as the *U/V* ratio increases the discrepancy between maximum resolution obtained from simulations (i.e. the saturation region of the performance curve) and from the calculations of the idealized case (stability diagram) increases. The discrepancy between maximum resolution obtained from the saturation region of the performance curve and from the stability diagram at low values of *U/V* ratios (99.9-99.97%) is shown in the inset of Figure 7.7a. The discrepancy is low at lower *U/V* ratios. . The large discrepancy at high values of *U/V* ratios can be explained with the help of Figure 7.4b and Figure 7.3b. Figure 7.4b also shows how

the maximum resolution for a particular value of scan line is determined from the Mathieu Stability diagram (*q/Δq)*; whereas, Figure 7.3b shows the mass spectrum obtained by the numerical simulation, and how the resolution *R* can be calculated by using the equation $R=M/\Delta M$, where $\Delta M$ is the width of the mass peak measured at 10% of its height. Ideally (i.e. from stability diagram considerations) the shape of a mass spectral peak should be trapezoidal. However the simulation is for finite field radius and finite length and there are differences since:

(i) Some ions which are theoretically unstable are transmitted in the simulation because of the slow increase in the ion trajectory envelope with distance along the QMF.

(ii) Similarly some ions which are theoretically stable are lost because the ion trajectory envelope is so high that they collide with the electrode if the QMF has finite field radius.

However, the trend observed is similar to idealized model, and only at high *U/V* ratios is there a discrepancy in the maximum resolution, since a slight change in $\Delta M$ or $\Delta q$ will change the resolution by a large amount. In practice $\boldsymbol{R_{max}}$ will be determined by the accuracy (percentage tolerances) of the QMF driving voltages at this point. State-of-the-art electronics to date can achieve percentage tolerances between ±0.1% and ±0.5% for the rf amplitude. For direct voltages it is currently possible to achieve ±0.1% or better. Other practical limiting factors for the electronics include operating conditions (i.e. temperature range etc). Moreover, in practice operation at maximum obtainable resolution is also determined by the minimum measureable signal current on the detector. Figure 7.7b shows the variation of resolution and percentage transmission with *U/V* ratio for a QMF operating at 188 rf cycles. As seen from Figure 7.7b the percentage transmission falls with

increasing *U/V* ratio and at 99.998% the percentage transmission is 0.399% of the total ions injected into the QMF.

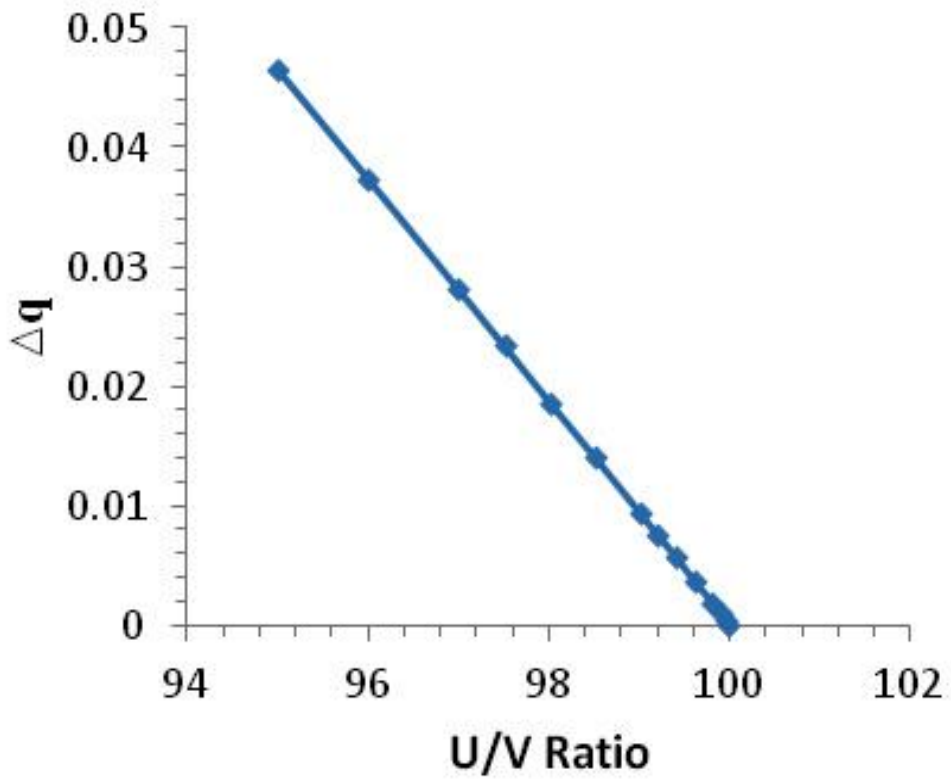


Figure 7.6: Variation of $\Delta q$ with *U/V* ratio for stability zone 1.

Using the QMS-hyperbolic the 5.82 meters long QMF reported by Von Zhan [6] was simulated. At an operating point for stability zone 1 with a *U/V* ratio of 99.998%, and *N*= 415 an instrument resolution of around 17000 at 50% peak width definition was predicted using the QMS2 model which matches well the reported experimental results.

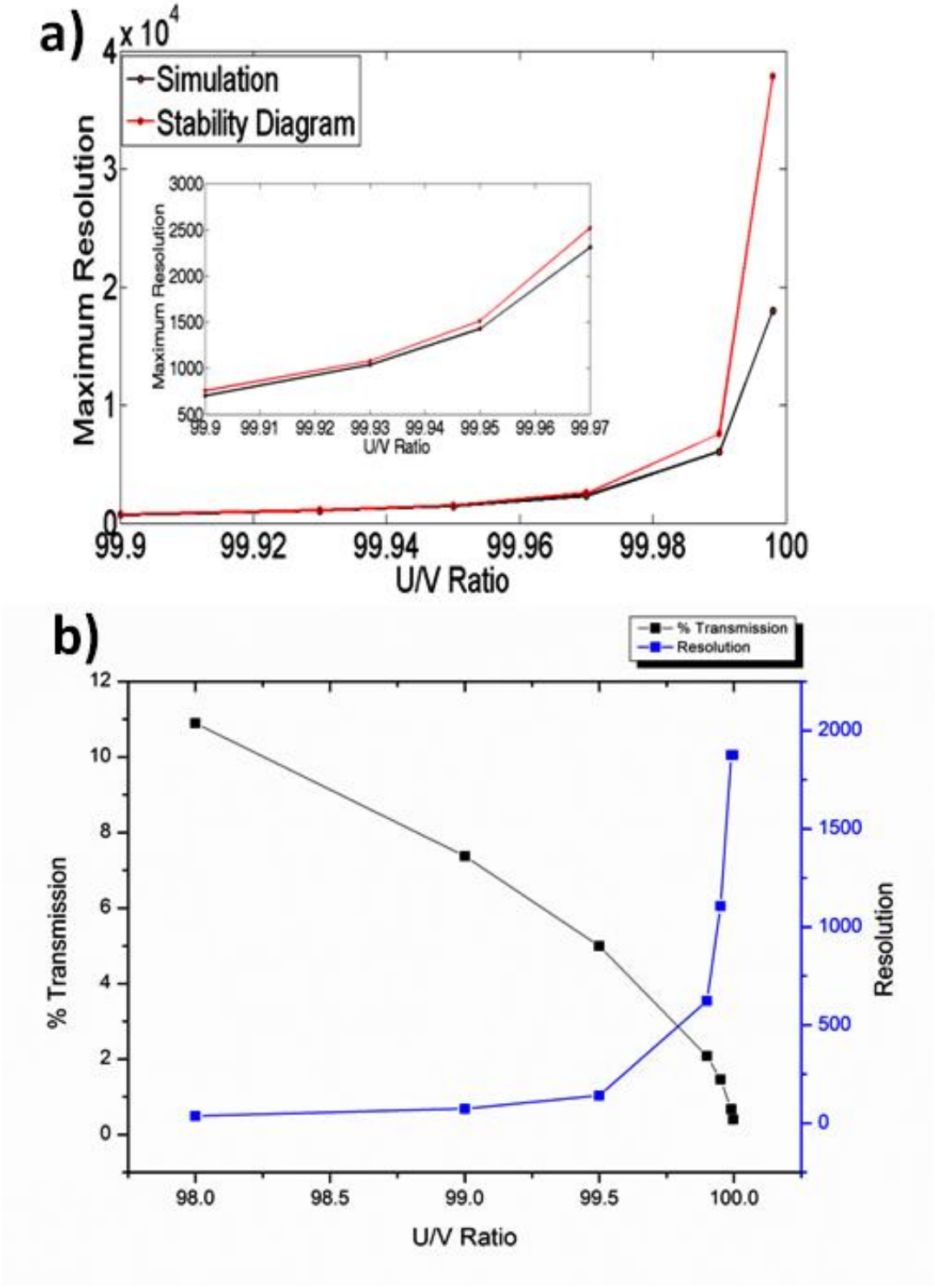


Figure 7.7: (a) Comparison of maximum resolution obtained in the simulations and the $R_{max}$ calculated for the ideal case using the Mathieu Stability diagram at different *U/V* ratios, inset $R_{max}$ Vs *U/V* ratio from (99.9-99.97%); (b) The variation of resolution and percentage transmission with *U/V* ratio for stability zone 1.

### 7.6 Performance of a QMF operating in stability zone 3

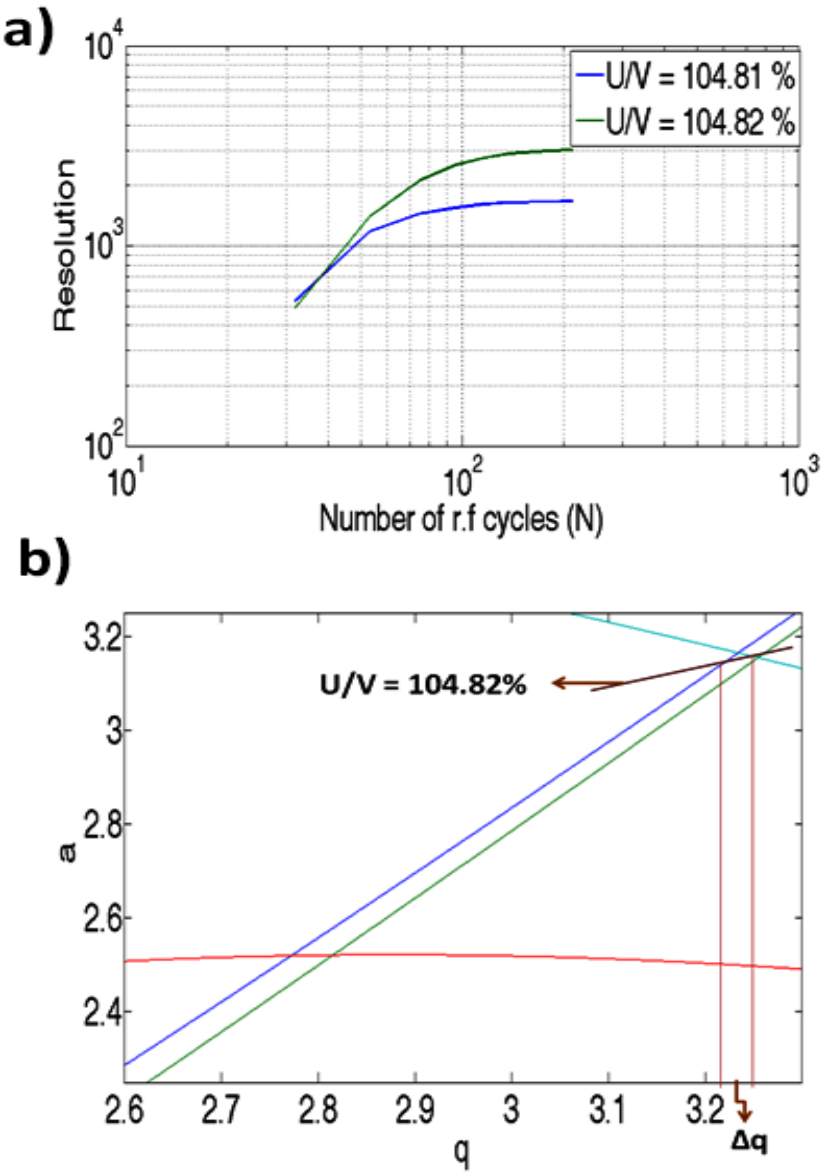


Figure 7.8: (a) The dependence of resolution on the number of rf cycles for stability zone 3 at different *U/V* ratios; predicted by QMS-hyperbolic; (b) The Mathieu stability diagram for zone 3 with the intersection assumed at *U/V* =104.82%.

Simulations of QMF performance in zone 3 were also carried out using QMS-hyperbolic. In this case each simulation used 150 steps across the mass range, with $9 \times 10^5$ ions injected and traced at each point. Here, the operating point at 100% corresponds to the *U/V* ratio at $q$ = 3.0

and $a$ = 2.8 which is near the centre of the stability zone 3. With increasing *U/V* ratio the scan line approaches the upper left tip of stability zone 3. Figure 7.8a shows the dependence of maximum resolution on number of rf cycles at two different *U/V* ratios 104.81% and 104.82%. It can be seen from the Figure 7.8a that as the number of rf cycles increases, resolution increases with a finite slope and then the curve showing the dependence starts to saturate. Comparing Figure 7.8a with Figure 7.3a, the behavior for QMF operation in zone 3 is similar to that obtained in zone 1 but the predicted saturation is more pronounced in the case of zone 3 operation (i.e. occurs at a lower number of rf cycles).

For zone 3 the values of $n$ and $K$ at *U/V* ratio 104.82% are 2.17 and 4.22 respectively and for *U/V* 104.81% are 1.56 and 0.43 respectively. These values are similar to those obtained experimentally by Konenkov and Kratenko [7]. It is noticeable that for zone 3 fewer rf cycles are needed to achieve a given resolution compared to stability zone 1. As seen from Figure 7.8b the intersection of the scan line (assumed as 104.82%) below the tip limits $\Delta q$ and in turn limits the resolution of a QMF to a maximum value for a given mass even if number of rf cycles are increased. Figure 7.9 (square symbols) shows the relationship between $N$ versus $R$ for stability zone 3 obtained using QMS-hyperbolic and a fitted curve to the data (red line) using OriginPro 8.5. A good representation of the performance curve is given by $\boldsymbol{R = a - bc^N}$, where a, b and c are constants the values of which depend upon the *U/V* ratio. The value of the coefficient of determination $R_c^2$ was found to be 0.9965 and the value of Adj. $R_c^2$ was found to be 0.9959, indicating a good regression fit between the curves. Table 3 shows the values of the parameters $a$, $b$, $c$ with their standard error, and also the coefficient of determination $R_c^2$ at different *U/V* ratios. For QMF operation in stability zone 3 (as for zone 1) it can be also be concluded that the predicted saturation behaviour of resolution with increasing $N$ is a feature of the QMF.

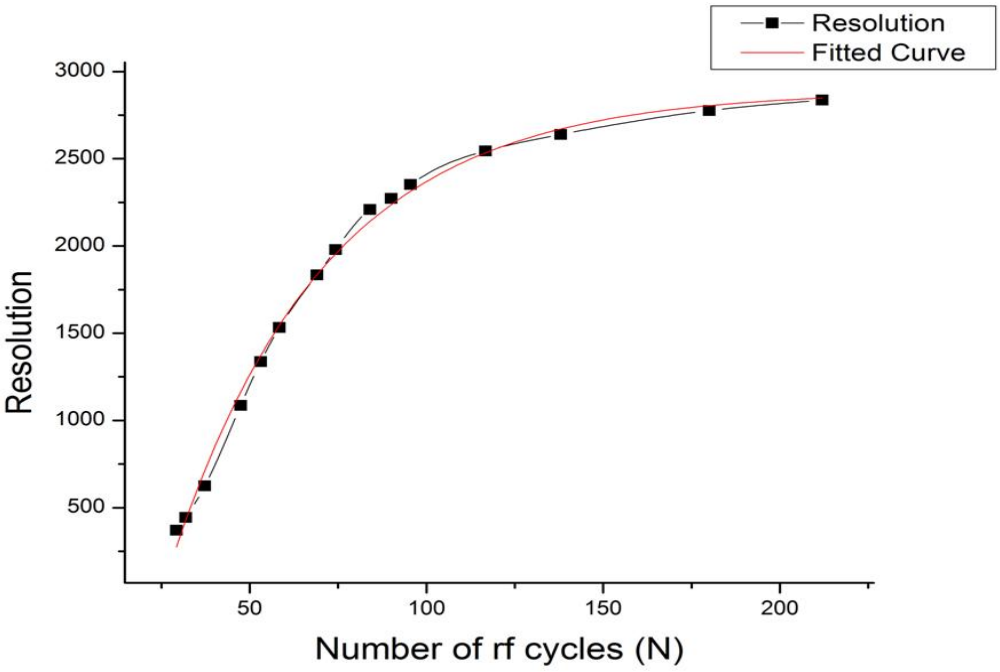


Figure 7.9: The dependence of resolution on number of rf cycles for stability zone 3, at *U/V* = 104.82% (fit obtained using Origin 8.5).

**Table 3 Values of parameters a, b, c and COD's, for QMF operation in zone 3.**

| Variables | *U/V* 104.81% | *U/V* 104.82% |
|---|---|---|
| a | 1662.19 | 2887.83 |
| b | 3898.46 | 5100.54 |
| c | 0.9618 | 0.9773 |
| SE for 'a' | 6.74 | 36.37 |
| SE for 'b' | 143.07 | 226.50 |
| SE for 'c' | 0.00105 | 0.00117 |
| COD- $R_c^2$ | 0.9993 | 0.9965 |
| Adj. $R_c^2$ | 0.9990 | 0.9959 |

### 7.7 Performance of a QMF operating under stability zone 1 with magnetic field applied

Figure 7.10 shows the dependence of resolution on number of rf cycles without and with an axial magnetic field applied. The ion energy has been varied in order to vary the number of rf cycles. For simulations without the magnetic field the value of *n* was found to be 2.08 and that of *K* to be about 28.02. For simulations with $B_z$ = 0.03 T, the value of *n* was found to be 2.18 and that of *K* to be about 40. In line with the previous simulations the performance curve shown in the figure is expected to saturate at high number of rf cycles as seen from Figure 7.3a.

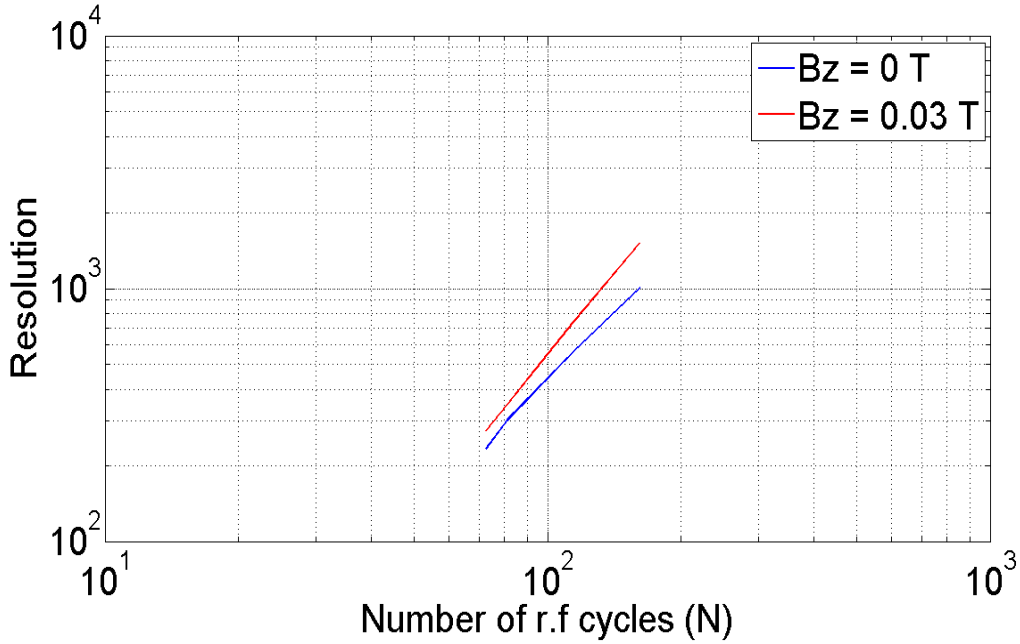


Figure 7.10: The dependence of resolution on number of rf cycles with and without an applied axial magnetic field (*Bz* = 0.03 T) for stability zone 1.

These results clearly indicate that the predicted performance of the QMF increases in the presence of an axial magnetic field. A detailed investigation of the effect of an axial magnetic field on the performance of QMS has been described before in Chapter 5. However, investigation of the performance plots showing the dependence of resolution on number of rf cycles with and without a transverse magnetic field applied for stability zone 1 is not possible as the optimum *U/V* ratio is different in the presence of magnetic field in transverse direction (*Bx*) as discussed in Chapter5.

### 7.8 Performance of a QMF operating under stability zone 3 with magnetic field applied

Figure 7.11 shows the dependence of resolution on number of rf cycles with and without an applied transverse magnetic field for the case of zone 3 operation. For simulations without the magnetic field and for the linear region of the curve, the value of *n* was found to be 2.17 and that of *K* to be about 4.22. For simulations with $B_x$ = 0.0015 T, the value of *n* was found to be 2.44 and that of *K* to be about 11.53. These results clearly indicate that the predicted performance of the QMF operating in stability zone 3 improves in the presence of a transverse magnetic field. Moreover, as can be observed from Figure 7.11, that the percentage increase in resolution with magnetic field increases as number of rf cycles increases.

Figure 7.12 shows the dependence of maximum resolution on number of rf cycles with and without an applied axial magnetic field. For simulations without the magnetic field and for the linear region of the curve, the value of *n* was found to be 2.17 and that of *K* to be about 4.22. For simulations with $B_z$ = 0.0015 T, the value of *n* was found to be 2.4 and that of

*K* to be about 11.2. These results clearly indicate that the predicted performance of the QMF operating in stability zone 3 also improves in the presence of an axial magnetic field.

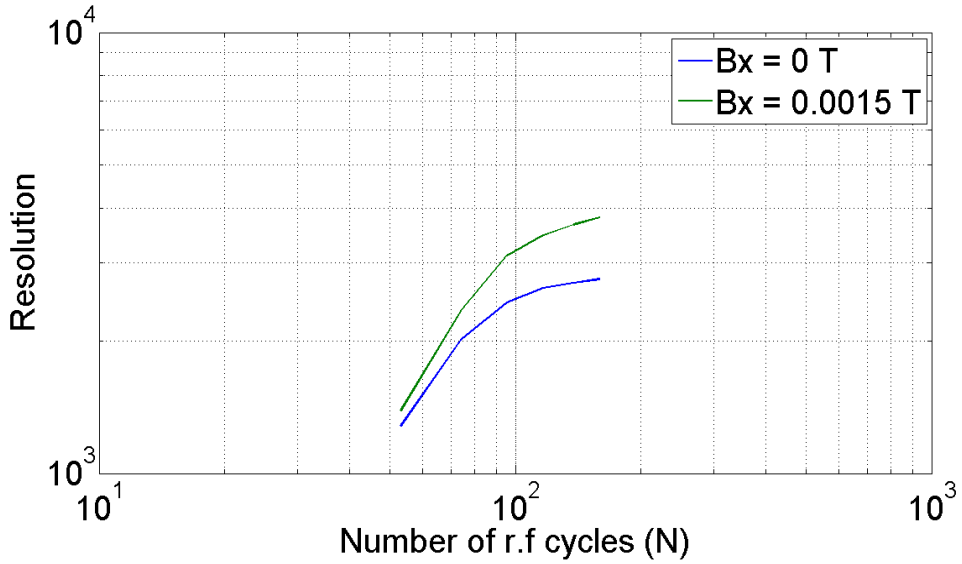


Figure 7.11: The dependence of resolution on number of rf cycles with and without an applied transverse magnetic field (*Bx* = 0.0015 T) for stability zone 3.

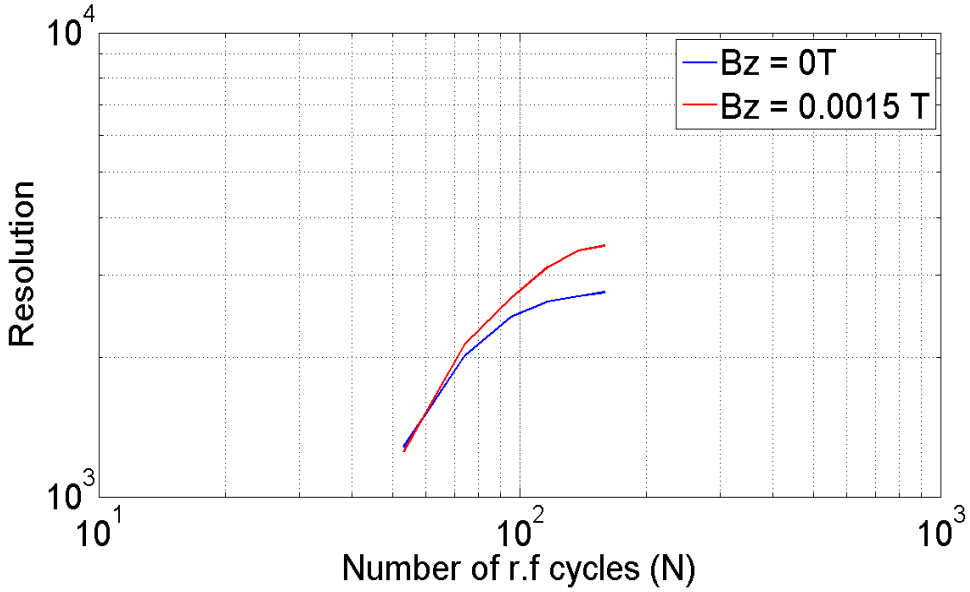


Figure 7.12: The dependence of resolution on number of rf cycles with and without an applied axial magnetic field (*Bz* = 0.0015 T) for stability zone 3.

## 7.9 Conclusions

Simulation results showing the performance of the QMF operating in stability zone 1 and zone 3 have been presented. The dependence of resolution R on number N of rf cycles experienced by the ions in the mass filter have been examined at different operating points. It has been observed that as the number of rf cycles increases, resolution increases with a finite slope and then the curve showing dependence starts to saturate. This is attributed to the fact that for a QMF there is a finite theoretical limit to its resolution for a particular value of operating point (scan line), since at that particular point $\Delta q$ cannot go beyond a certain minimum value.

For stability zone 1 and for the linear region of the performance curve, QMF resolution has been found to be dependent on number of radio frequency cycles, according to $\mathbf{R = N^n/K}$, however for the saturated region of the curve (observed in practice and here modeled), QMF resolution has been found to be dependent on $N$ according to $\boldsymbol{R = q(1 - 2c^N)/\Delta q}$. Also a relationship has been established between maximum resolution $R_{max}$ and percentage $U/V$ ratio, given by $\boldsymbol{R_{max} = q/(0.9330\text{-}0.00933U/V)}$. For QMF operation in zone 3 the expression $\boldsymbol{R = a - bc^N}$ simulates well the linear and saturated regions of the performance curve for a range of operational conditions, where a, b and c are constants.

In the case with magnetic field the increase in performance is ascribed to the modification of the ion motion in the mass filter by the magnetic field and the effects may be explained in each case by considering the additional Lorentz force produced by ion motion in the magnetic field.

## References


1. Dawson, P.H.; *Quadrupole mass spectrometry and its applications*, Elsevier: Amsterdam 1976.
2. Douglas, D.J. Linear quadrupoles in mass spectrometry. *Mass Spectrometry Reviews*. 2009, *28*, 937-960.
3. Paul, W.; Reinhard, H.P.;Von, Z.U. Das elektrische massenfilter asl massenspektrometer and isotopentrenner. *Z Phys*. 1958, 152, 143-182.
4. Holme, A.E.; Thatcher, W.J.; Leck, J.H. An investigation of the factors determining maximum resolution in a quadrupole mass spectrometer. *Journal of Physics **E:** Scientific Instruments.* 1972, *5*, 429-433.
5. Von Zahn, U. Prazisions-massenbestimmungen mit dem elekrischen massenfilter. *Zeitschrift fur Physik.* 1962, *168*, 129-142.
6. Brubaker, W.M.; Tuul, J. Performance studies of a quadrupole mass filter. *The review of scientific instruments*. 1964, *35 (8)*, 1007-1010.
7. Konenkov, N.V.; Kratenko, V.I. Characteristics of a quadrupole mass filter in the separation mode of a few stability regions. *International Journal of Mass Spectrometry and Ion Processes*. 1991, *108*, 115-136.
8. Du, Z.; Douglas, D. J.; Konenkov N. Elemental Analysis with Quadrupole Mass Filters Operated in Higher Stability Regions. *J. Anal. At. Spectrom.* 1999, *14*(8), 1111–1119.
9. Zhang S.C.; Jin J.M. Computations of Special Functions, Wiley: New York, 1996.
10. Hogan, T. *Private communication*.
11. http://www.originlab.com/index.aspx?go=Products/OriginPro

# Chapter 8

# Conclusions and Future Work

The main aim of this project was to improve the performance of the QMS and to investigate the factors influencing the resolution of a QMF for operation in stability zones 1 and 3.The commercially available QMS instruments generally provide limited features and usually operate in stability Zone 1. QMS simulation using suitable software offers many advantages and plays a very important role in a study of well-defined application requirements. A software model can also help in identifying the application solution for a process problem at a reduced cost and cycle time.

In this work, experimental results for a QMS instrument showing an increase in resolution when a static magnetic field is applied along the mass filter length for operation in stability zone 1 is presented. This enhanced resolution observed experimentally has been simulated theoretically using QMS-hyperbolic. The effects may be explained by considering the fact that, in the presence of the magnetic field in addition to the alternating quadrupole field an ion experiences Lorentz force which modifies its motion. This results in rejection of ions in the low mass tail and/or high mass tail depending on the orientation of magnetic field giving increased resolution for a set of operating parameters. Also, a comprehensive simulation study has been carried out to show the effects of different input parameters such as variation of ion energy, drive frequency and electrode length under the influence of both ***axial*** and ***transverse*** magnetic field. High resolutions (R > 3000) are predicted for QMFs of

length 200 mm as a result of the applied magnetic field which allows wider instrument application.

Simulation studies have been carried out using the software to show the possibilities of achieving enhanced resolution under the influence of static magnetic field in both ***axial*** and ***transverse*** directions for QMF operation in stability zone 3. The QMS-Hyperbolic computer simulation program predicted achieving a better resolution for the qualitative and quantitative identification of low mass isotopes in a process environment which require a resolution greater than 930. High resolutions (R > 3500) measured at 10% peak width definition are predicted under the influence of ***transverse*** magnetic field for a HT and $D_2$ mixture with a QMF of length 200 mm, such high resolutions for low mass isotopes were never reported before. For a QMF of length 100 mm, for Argon the analysis also predicted resolution (R > 5000) as a result of the applied ***transverse*** magnetic field and (R > 3000) as a result of the applied ***axial*** magnetic field. These features suggest potential of wider applications than hitherto for such QMS instruments e.g. applications include identification of low mass isotopes in the mass range (1-6 *amu*), as this issue is of some importance in the nuclear industry for protecting of personnel involved in handling of radioactive material.

Moreover, in this work Quadrupole mass filter instrument was simulated under different operating points for Mathieu stability zones 1 and 3. The maximum resolutions ($R_{max}$) that can be obtained for a given QMF for a particular value of scan line have been investigated. In this work, the saturated regions of the performance curve for QMF operation in zone 1 were modeled according to $\boldsymbol{R = q(1 - 2c^N)/\Delta q}$, where c is a constant and $\Delta q$ is the width of the intersection of the operating scan line with the stability zone 1, measured at *q*-axis of the Mathieu stability diagram. Also by careful calculations of the detail of the stability

tip of zone 1, the following relationship was established between $R_{max}$ and percentage *U/V* ratio: $\boldsymbol{R_{max} = q/(0.9330-0.00933U/V)}$. For QMF operation in zone 3 the expression $\boldsymbol{R = a - bc^N}$ simulates well the linear and saturated regions of the performance curve for a range of operational conditions, where a, b and c are constants.

Future research will be involved with modeling, design, fabrication and experimental study of the performance of a QMF with static magnets incorporated inside the *x* electrodes of the mass filter to see the effects on sensitivity and resolution for operation in stability zones 1 and 3. Also the research can be taken further by studying the effect of magnetic field on the performance of linear ion trap analyzer. With good results this may develop new analytical methods for quadrupole mass spectrometry using QMF or linear ion traps and may offer many potential applications which have yet to be explored.

# Appendix A

## Matlab Script for generation of stability diagram

```
Clear all;
load temp;      %Read in arrays

agraph_min = -10; %Defines a min value for diagram
agraph_max = 10; %Defines a max value for diagram
qgraph_min = 0;   %Defines q min value for diagram
qgraph_max = 10;  %Defines q max value for diagram

%Generate zone1 tip point

i=1
while ax0val(i)<by1val(i)
   i=i+1;
end
z1atip = -ay0val(i);
z1qtip = q_val(i);
while by1val(i)>0
   i=i+1;
end
z1abase=0;
z1qbase=q_val(i);

%Generate zone2 corner points

%Intersection of ay1 with q axis
%because of symmetry of ay1 and ax1 only
%need to calculate for one
%The while overshoots value by count of 1
%This is reasons for -1 in index of arrays
i=1;
while ay1val(i)>0
   i=i+1;
end

z2axy1 = ay1val(i-1);
```

```
z2qxy1 = q_val(i-1);
tempval   = ay1val(i-1);

%Intersection of by2 with q axis

i=1;
while by2val(i)>0
   i=i+1;
end

z2bxy2 = by2val(i-1);
z2qxy2 = q_val(i-1);
tempval   = by2val(i-1);

%Intersection of ax1 with by2

i=1;

while ax1val(i) < by2val(i)
   i=i+1;
end

z2amax = by2val(i-1);
z2qmax = q_val(i-1);
tempval   = by2val(i-1)- ax1val(i-1);

 %Generate zone3 corner points

%Calculate a0 intersection points
i=1;
   while (ax0val(i))<(ay1val(i))
      i=i+1;
   end
   z3amin=ax0val(i);
   z3qamin=q_val(i);
   while ax0val(i)<by2val(i)
      i=i+1;
   end
   z3amax=ax0val(i);
   z3qamax=q_val(i);

%Calculate b1 intersection points
i=1;
  while (bx1val(i))<(ay1val(i))
```

```
      i=i+1;
  end
  z3bmin=bx1val(i);
  z3qbmin=q_val(i);
  while bx1val(i)<by2val(i)
      i=i+1;
  end
  z3bmax=bx1val(i);
  z3qbmax=q_val(i);


 %Generate scan line

 Res = 98;        %Instrument resolution in percentage ie 100% = tip of the selected stability
zone

 a_tip = z1atip;    %Use this for zone 1 scan line
 q_tip = z1qtip;    %Use this for zone 1 scan line

i = 1;
 while i < scan+1
      sl(i) = ((a_tip * q_val(i)/q_tip)* Res)/100;    %generate scan line array
      i = i+1;
 end




%% Create figure
figure1 = figure(...
 'FileName','C:\MATLAB_SV701\work\MCN\MATHIEU STABILITY DIAGRAM.bmp',...
 'PaperOrientation','landscape',...
 'PaperType','a4letter');
 'PaperPosition',[0.6345 0.6345 26.29 19.72],...
 'PaperSize',[29.68 20.98],...
%% Create axes
axes = axes('Parent',figure1);
axis(axes,[qgraph_min qgraph_max agraph_min agraph_max]);
title(axes,'MATHIEU STABILITY DIAGRAM');
xlabel(axes,'q');
ylabel(axes,'a');
box(axes,'on');
hold(axes,'all');
```

```
%% Create mutliple lines using matrix input to plot

plot(q_val,ax0val,q_val,bx1val,q_val,ay1val,q_val,by2val,q_val,ax1val,q_val,ay0val,q_val,b
y1val,q_val,bx2val,q_val,0,'b',q_val,sl,'b');
hleg = legend('U/V Ratio');
set(hleg, 'NorthEast');
%%Save figure
saveas(gcf,'MATHIEU_DIAGRAM_FULL.bmp');
%saveas(gcf,'MSD_3_COL_Z3-1.fig');
```

# Appendix B

# QMS-Hyperbolic Integration setting Code

```
#include "stdafx.h"
#include "Tabs_Bld.h"

#ifdef _DEBUG
#undef THIS_FILE
static char THIS_FILE[]=__FILE__;
#define new DEBUG_NEW
#endif

int Set_H_Bld(double *H_v, int *MxStps, double Qlen, double VzNom, int Md, double Freq)
{
 int     er = 0;

 /* Md sets step resolution, codes 0 to 3, very coarse to fine
     To be used to create number of steps in quad using VERY approx
       23 steps per cycle for very coarse        42 steps per cycle for coarse
       68 steps per cycle for medium             98 steps per cycle for fine
     but value adjusted so not exactly an integer number */
 switch (Md)
  {
    case 0: *H_v = Pi/23.1;
            break;
    case 1: *H_v = Pi/42.1;
            break;
    case 2: *H_v = Pi/68.1;
            break;
    case 3: *H_v = Pi/98.1;
            break;
   default: er = 1;
  }
 *MxStps = int(Qlen*D_Pi*Freq/(VzNom*(*H_v))); // safe max steps
 if (*MxStps > MaxStp_C)
  {
    if ((*MxStps-MaxStp_C) < (0.25*MaxStp_C))
```

```
        {
          *MxStps = MaxStp_C;
          er = 99;
        }
       else er = 6;
    }
  return(er);
}

int Read_ARC_Bld(double *Nom_En_v, CString ArcFil, CString *Sna, CString *Stx1,
CString *Stx2)
{
  int  Idx_v=0;
  ifstream  ft;
  ft.open(Path_C+ArcFil,ios::in|ios::nocreate);
  if (ft.fail()) Idx_v = 2;
  else
    {
      char ch;
      int i,j;
      char buffer[500];
      char nu[20];
      char *st;
      ch = ' ';  i = 0;
      do
        {
          buffer[i] = ch;
          ft.read((char *)&ch,1);
        } while ((ch != EOF) && (i++ <500));
       i = 0;
       while (buffer[i] != 10) i++;   i++;
       while (buffer[i] == 32) i++;   j = 0;
       while (((buffer[i] >= '0') && (buffer[i] <= '9')) || (buffer[i] == '.'))
        {
          nu[j] = buffer[i];   i++;  j++;
        }
      nu[j] = '!';
      *Nom_En_v = strtod(nu, &st);          // got mass number
      while (buffer[i] != 10) i++;   i++;
      while (buffer[i] != 10) i++;   i++;
      while (buffer[i] != 10) i++;   i++;
      *Sna="";  *Stx1 = "";  *Stx2 = "";
      while (buffer[i] != 10)
        { *Sna = *Sna + buffer[i];  i++;}   i++;
```

```
      while (buffer[i] != 10)
        { *Stx1 = *Stx1 + buffer[i];  i++;}   i++;
      while (buffer[i] != 10)
        { *Stx2 = *Stx2 + buffer[i];  i++;}   i++;
    }
  return(Idx_v);
}
```

# Appendix C

# Publications

### Journal

1. Syed, S.U.A.H.; Hogan. T.J.; Gibson, J.R.; Taylor, S. Factors influencing the QMF resolution for operation in stability zones 1 and 3. *J Am Soc Mass Spectrom*. 2012.
2. Syed, S.U.A.H.; Sreekumar, J.; Gibson, J.R.; Taylor, S. QMS in the third stability zone with a transverse magnetic field applied. *J Am Soc Mass Spectrom*. 2011, 22, 1381-1387.
3. Syed, S.U.A.H.; Sreekumar, J.; Brkic, B.; Gibson, J.R.; Taylor, S. Effect of an axial magnetic field on the performance of a Quadrupole Mass Spectrometer. *J Am Soc Mass Spectrom*. 2010, 21, 2070-2076.
4. Syed, S.U.A.H.; Maher, S.; Gibson, J.R.; Taylor, S. A new quadrupole mass filter with a transverse magnetic field applied. *(In preparation for submission).*

### Conference

1. Syed, S.U.A.H.; Brkic, B.; Taylor, S. Portable mass spectrometry for environmental, medical and security applications. *JEMI Technical Meeting*. September 2011. Liverpool, UK.
2. Maher, S.; Syed, S.U.A.H.; Sreekumar, J.; Gibson, J.R.; Taylor, S. Performance enhancement for miniature QMS through application of a magnetic field. *The 8th*

*Harsh Environment Mass Spectrometry (HEMS) Workshop*. September 2011. St. Pete Beach, Florida, USA.

3. Syed, S.U.A.H.; Gibson, J.R.; Taylor, S. Resolution enhancement of a QMS using an applied magnetic field. *32nd BMSS Annual Meeting.* September 2011. Cardiff, UK.
4. Syed, S.U.A.H.; Brkic, B.;Sreekumar, J.; Gibson, J.R.; Taylor, S. Performance of an RGA with a transverse magnetic field applied to the mass filter. *The 9th RGA Users Meeting*. February 2010, Daresbury Laboratory, Warrington, UK.
5. Syed, S.U.A.H.; Maher, S.; Gibson, J.R.; Taylor, S. Performance of QMS operating in stability zones 1 and 3 under the influence of magnetic field. *Accepted. BMSS*. Alderley Edge. UK (2012).
6. Maher, S. U; Syed, S.U.A.H.; Taylor, S. Mapping the stability diagram of a QMS with an applied magnetic field. *Accepted. ASMS*. Vancouver, Canada (2012).
7. Syed, S.U.A.H.; Maher, S.; Gibson, J.R.; Taylor, S. Quadrupole Mass Spectrometer under the infuelnce of magnetic field. *Accepted. IOP/IET Mass Spectrometry Meeting*. Liverpool, UK (2012).